Negative microfilm 63–415
received from university

O'KANE, Daniel Francis, 1933–
AN INVESTIGATION OF TERNARY SEMICONDUCTING COMPOUNDS.

University of Michigan, Ph.D., 1962
Engineering, chemical

University Microfilms, Inc., Ann Arbor, Michigan

AN INVESTIGATION OF TERNARY SEMICONDUCTING COMPOUNDS

By

Daniel Francis O'Kane

A dissertation submitted in partial fulfillment
of the requirements for the degree of
Doctor of Philosophy in the
University of Michigan
1962

Doctoral Committee:

Associate Professor Donald R. Mason, Chairman
Professor Lee O. Case
Professor Ernst Katz
Professor Guiseppe Parravano

ACKNOWLEDGMENTS

The author would like to express his sincere appreciation to Professor Donald R. Mason for his guidance and assistance during the course of this research.

Acknowledgment is also due to the Linde Company, Division of the Union Carbide Corporation, and the Standard Oil Foundation of Indiana for their fellowships, and to the Borg-Warner Educational Foundation for its aid. The Department of Chemical and Metallurgical Engineering provided partial support for this study. The financial assistance from the Texas Instruments Corporation is especially appreciated.

Expressions of thanks are also due to the numerous students, Messrs. Ping-Wang Chiang, B. M. Kulwicki, E. K. Parrott, G. A. Schmitt, and P. H. Smith, who assisted with various phases of the research.

AN INVESTIGATION OF TERNARY SEMICONDUCTING COMPOUNDS

Daniel Francis O'Kane

ABSTRACT

Certain pseudo-binary phase diagrams were investigated in order to locate congruently and peritectically melting ternary compounds, and the electrical and thermal properties of some of the compounds were measured and interpreted. The pseudo-binary phase diagrams were composed of binary compounds with the chemical formulae $In_2VI^b_3$ and either $I^b_2VI^b$ or II^bVI^b. The group I^b elements were silver and copper, the group II^b elements were cadmium, zinc and mercury, and the group VI^b elements were selenium and tellurium. The properties measured were transformation temperatures, electrical conductivity, Hall effect, Seebeck coefficient, and thermal conductivity.

The pseudo-binary phase diagrams for the $CdSe-In_2Se_3$ system and the $ZnTe-In_2Te_3$ system have been established. In addition, partial phase diagrams are given for the $Ag_2Se-In_2Se_3$ system and the $Ag_2Te-In_2Te_3$ system. Summaries of the transformation temperatures observed by differential thermal analysis are given for some compositions in the $Cu_2Te-In_2Te_3$ and the $Cu_2Se-In_2Se_3$ systems.

Two congruently melting compounds, $AgIn_3Te_5$ and $Ag_2In_8Se_{13}$, were found as a result of the phase diagram studies. Polycrystalline samples of these compounds and the peritectic compound $CdIn_2Se_4$ were prepared by zone refining. Zone leveling was used to prepare the three peritectic compounds in the $CdTe-In_2Te_3$ pseudo-binary system.

Some of the semiconducting properties, such as electrical conductivity, Hall effect, and Seebeck coefficient, were determined for $CdIn_2Se_4$, the three peritectic compounds from the $CdTe-In_2Te_3$ system, $AgIn_3Te_5$, and $Ag_2In_8Se_{13}$. The energy gap values obtained from the electrical measurements were 1.1 eV for $AgIn_3Te_5$, 1.51 eV for $Ag_2In_8Se_{13}$, 1.02 eV for $CdIn_8Te_{13}$, and 1.38 eV for the β-phase

(45 mole % CdTe - 55 mole % In_2Te_3) and 1.17 eV for the δ-phase (9 mole % CdTe - 91 mole % In_2Te_3) materials from the CdTe-In_2Te_3 system. The Hall electron mobilities of $CdIn_8Te_{13}$, $AgIn_3Te_5$, and $Ag_2In_8Se_{13}$ were all near 200 cm^2/volt-second at 300° K.

The electrical conductivity of $Ag_2In_8Se_{13}$ was about 10^{-7} mho/cm. at 300° K. This value could be changed to about 10 mho/cm. by heating the compound above 500° C in an inert atmosphere. The change could be partially reversed by heat treating $Ag_2In_8Se_{13}$ in a selenium atmosphere.

The thermal conductivities of the β-phase material (45 mole % CdTe - 55 mole % In_2Te_3), $AgIn_3Te_5$, and $Ag_2In_8Se_{13}$ were approximately 0.011 watts/cm. °C near 300° K.

TABLE OF CONTENTS

	Page
ACKNOWLEDGMENTS	ii
ABSTRACT	iii
LIST OF TABLES	viii
LIST OF FIGURES	ix
LIST OF APPENDICES	xiii
INTRODUCTION	1
LITERATURE SURVEY	3
THEORY	5
A. Electrical Conductivity and Hall Effect	5
1. General Formulae for Electrical Conductivity and Hall Effect	6
2. Electrical Conductivity and Hall Effect Formulae for Extrinsic Semiconductors	6
3. Electrical Conductivity and Hall Effect Formulae for Intrinsic Semiconductors	7
B. Seebeck Coefficient	10
1. Seebeck Coefficient in the Extrinsic Range	10
2. Seebeck Coefficient in the Intrinsic Range	11
C. Thermal Conductivity	12
D. Thermoelectric Figure of Merit	15
EXPERIMENTAL PROCEDURES	16
A. Sample Preparation	16
B. Differential Thermal Analysis Measurements	18
C. Chemical Analysis	20
D. Electrical Measurements	21
E. Thermal Conductivity	22
SEMICONDUCTING PROPERTIES OF $CdIn_2Se_4$	23
A. Literature Review	23
B. Results of Differential Thermal Analysis and Electrical Measurements	24

TABLE OF CONTENTS (Cont'd)

Page

1. Differential Thermal Analysis 24

2. Results of Electrical Measurements on $CdIn_2Se_4$ . . . 30

SEMICONDUCTING PROPERTIES OF PERITECTIC COMPOUNDS FROM THE PSEUDO-BINARY SYSTEM OF $CdTe-In_2Te_3$ 34

A. Introduction 34

B. β-phase Material 34

C. γ-phase Material 37

D. δ-phase Material 41

E. Discussion of the Semiconducting Properties of Materials from the $CdTe-In_2Te_3$ System 46

THE PHASE DIAGRAM BEHAVIOR OF THE PSEUDO-BINARY SYSTEM OF $Ag_2Te-In_2Te_3$ AND THE SEMICONDUCTING PROPERTIES OF $AgIn_3Te_5$ 53

A. Introduction 53

B. Literature Review 53

C. Phase Diagram Study 54

1. Differential Thermal Analysis Results 54

2. Discussion of the Differential Thermal Analysis Results 57

D. Semiconducting Properties of $AgIn_3Te_5$ 59

1. Results of Electrical and Thermal Measurements . . . 59

2. Discussion of the Semiconducting Properties of $AgIn_3Te_5$ 75

THE PHASE DIAGRAM BEHAVIOR OF THE PSEUDO-BINARY SYSTEM OF $Ag_2Se-In_2Se_3$ AND THE SEMICONDUCTING PROPERTIES OF $Ag_2In_8Se_{13}$ 77

A. Introduction 77

B. Literature Review 77

C. Phase Diagram Study 78

1. Differential Thermal Analysis 78

2. Discussion of Differential Thermal Analysis Results . 82

TABLE OF CONTENTS (Cont'd)

	Page
D. Semiconducting Properties of $Ag_2In_8Se_{13}$	84
1. Results of Electrical and Thermal Measurements	84
2. Apparent Irreversible Effect in $Ag_2In_8Se_{13}$	101
3. Discussion of the Semiconducting Properties of $Ag_2In_8Se_{13}$	105
THE PHASE DIAGRAM BEHAVIOR OF THE PSEUDO-BINARY SYSTEM OF ZnTe-In_2Te_3	108
A. Introduction	108
B. Literature Review	108
C. Results of Differential Thermal Analysis Measurements	108
OTHER PSEUDO-BINARY SYSTEMS	113
A. Introduction	113
B. Literature Review	113
C. The Cu_2Se-In_2Se_3 Pseudo-binary System	113
D. The Cu_2Te-In_2Te_3 Pseudo-binary System	114
E. Pseudo-binary Systems Containing Mercury	117
SUMMARY OF RESULTS	118
CONCLUSIONS	120
APPENDICES	121
BIBLIOGRAPHY	146

LIST OF TABLES

Table		Page
I.	Properties of Ternary Compounds	4
II.	Summary of Differential Thermal Analysis Measurements for the Pseudo-binary Phase Diagram of $CdSe-In_2Se_3$	27
III.	Electrical Properties of Peritectic Materials from the $CdTe-In_2Te_3$ System	36
IV.	Hall Coefficient as a Function of Temperature for the γ-phase in the $CdTe-In_2Te_3$ System	39
V.	Hall Coefficient as a Function of Temperature for the δ-phase in the $CdTe-In_2Te_3$ System	47
VI.	Summary of Differential Thermal Analysis Measurements for the Pseudo-binary Phase Diagram of $Ag_2Te-In_2Te_3$	56
VII.	Summary of Electrical Properties of $AgIn_3Te_5$	65
VIII.	Hall Coefficient of $AgIn_3Te_5$ as a Function of Temperature	66
IX.	Summary of Differential Thermal Analysis Measurements for the Pseudo-binary Phase Diagram of $Ag_2Se-In_2Se_3$	80
X.	Summary of Electrical Properties of $Ag_2In_8Se_{13}$	90
XI.	Hall Coefficient of $Ag_2In_8Se_{13}$ as a Function of Temperature	91
XII.	Summary of Differential Thermal Analysis Measurements for the Pseudo-binary Phase Diagram of $ZnTe-In_2Te_3$	110
XIII.	Summary of Differential Thermal Analysis Measurements for the Pseudo-binary Phase Diagram of $Cu_2Se-In_2Se_3$	114
XIV.	Summary of Differential Thermal Analysis Measurements for the Pseudo-binary Phase Diagram of $Cu_2Te-In_2Te_3$	116
XV.	Summary of Semiconducting Properties for the Ternary Compounds	119

LIST OF FIGURES

Figure		Page
1.	Phase Diagram for the Cd Te-In_2Te_3 System	19
2.	Differential Thermal Analysis Heating and Cooling Curves for the Cd Se-In_2Se_3 System	25
3.	Differential Thermal Analysis Heating and Cooling Curves for Sample Number 083, $CdIn_2Se_4$	28
4.	Phase Diagram for the Cd Se-In_2Se_3 System	29
5.	Logarithm of Electrical Conductivity vs. Reciprocal Absolute Temperature for Sample Number 083, $CdIn_2Se_4$.	31
6.	Seebeck Coefficient vs. Absolute Temperature for Sample Number 083, $CdIn_2Se_4$.	32
7.	Logarithm of Electrical Conductivity vs. Reciprocal Absolute Temperature for β-phase Material, Sample Number 137, from the Cd Te-In_2Te_3 System	35
8.	Logarithm of Electrical Conductivity vs. Reciprocal Absolute Temperature for the γ-phase Material, Sample Numbers 150(4), 151(4), and 169(2), from the Cd Te-In_2Te_3 System	38
9.	Logarithm of $\lvert R_H T^{3/2} \rvert$ vs. Reciprocal Absolute Temperature for the γ-phase Material, Sample Numbers 150(4) and 151(4), from the Cd Te-In_2Te_3 System . . .	40
10.	Logarithm of Hall Mobility vs. Logarithm of Absolute Temperature for the γ-phase Material, Sample Numbers 150(4) and 151(4), from the Cd Te-In_2Te_3 System . . .	42
11.	Seebeck Coefficient vs. Absolute Temperature for the γ-phase Material, Sample Numbers 150(4) and 151(4), from the Cd Te-In_2Te_3 System	43
12.	Seebeck Coefficient vs. Reciprocal Absolute Temperature for the γ-phase Material, Sample Numbers 150(4) and 151(4), from the Cd Te-In_2Te_3 System	44

LIST OF FIGURES (Cont'd)

Figure		Page
13.	Logarithm of Electrical Conductivity vs. Reciprocal Absolute Temperature for the δ-phase Material, Sample Number 169(3), from the Cd Te-In_2Te_3 System.	45
14.	Logarithm of $\lvert R_H T^{3/2} \rvert$ vs. Reciprocal Absolute Temperature for the δ-phase Material, Sample Number 169(3), from the Cd Te-In_2Te_3 System	48
15.	Logarithm of Hall Mobility vs. Logarithm of Absolute Temperature for the δ-phase Material, Sample Number 169(3), from the Cd Te-In_2Te_3 System	49
16.	Seebeck Coefficient vs. Absolute Temperature for the δ-phase Material, Sample Number 169(3), from the Cd Te-In_2Te_3 System	50
17.	Seebeck Coefficient vs. Reciprocal Absolute Temperature for the δ-phase Material, Sample Number 169(3), from the Cd Te-In_2Te_3 System	51
18.	Differential Thermal Analysis Heating and Cooling Curves for the Ag_2Te-In_2Te_3 System	55
19.	Partial Phase Diagram for the Ag_2Te-In_2Te_3 System .	58
20.	Logarithm of Electrical Conductivity vs. Reciprocal Absolute Temperature for Sample Number 181, Zone Refined from 30 mole % Ag_2Te - 70 mole % In_2Te_3 . .	60
21.	Logarithm of Electrical Conductivity vs. Reciprocal Absolute Temperature for Ag In_3Te_5, Sample Numbers 735, 194, and 206	62
22.	Logarithm of Electrical Conductivity vs. Reciprocal Absolute Temperature for Ag In_3Te_5, Sample Numbers 217 and 238.	64
23.	Logarithm of $\lvert R_H T^{3/2} \rvert$ vs. Reciprocal Absolute Temperature for Ag In_3Te_5, Sample Numbers 206, 217(2), 238(1C), and 238(4A)	68

LIST OF FIGURES (Cont'd)

Figure		Page
24.	Logarithm of Hall Mobility vs. Logarithm of Absolute Temperature for $AgIn_3Te_5$, Sample Numbers 238(1C) and 238(4A)	70
25.	Seebeck Coefficient vs. Absolute Temperature for $AgIn_3Te_5$, Sample Numbers 735, 217(1), 217(2), 238(1C), and 238(4A)	71
26.	Seebeck Coefficient vs. Reciprocal Absolute Temperature for $AgIn_3Te_5$, Sample Numbers 217(1), 217(2), 238(1C), and 238(4A)	72
27.	Thermal Conductivity vs. Absolute Temperature for $AgIn_3Te_5$, Sample Number 206	74
28.	Differential Thermal Analysis Heating and Cooling Curves for the Ag_2Se-In_2Se_3 System	79
29.	Partial Phase Diagram for the Ag_2Se-In_2Se_3 System .	83
30.	Logarithm of Electrical Conductivity vs. Reciprocal Absolute Temperature for $Ag_2In_8Se_{13}$, Sample Numbers 199(4), 199(5B), 211(1A), 211(1B), 211(3B), and 211(7).	85
31.	Logarithm of Electrical Conductivity vs. Reciprocal Absolute Temperature for $Ag_2In_8Se_{13}$, Sample Numbers 215(2A), 215(2B), 215(5), 225(A), 225(B), and 736 . .	87
32.	Apparent Irreversible Change in the Electrical Conductivity of $Ag_2In_8Se_{13}$, Sample Number 215(1C) After Heating to a High Temperature	88
33.	Logarithm of $\lvert R_H T^{3/2} \rvert$ vs. Reciprocal Absolute Temperature for $Ag_2In_8Se_{13}$, Sample Numbers 211(1A), 211(1B), 211(7), 215(2B), 215(5), 225(A), and 225(B) .	94
34.	Logarithm of Hall Mobility vs. Logarithm of Absolute Temperature for $Ag_2In_8Se_{13}$, Sample Numbers 225(B) and 211(7)	96

LIST OF FIGURES (Cont'd)

Figure		Page
35.	Seebeck Coefficient vs. Absolute Temperature for $Ag_2In_8Se_{13}$, Sample Numbers 211 (1A), 211 (3B), 225 (A), and 736	97
36.	Seebeck Coefficient vs. Reciprocal Absolute Temperature for $Ag_2In_8Se_{13}$, Sample Numbers 211 (1A), 211 (3B), and 225 (A)	98
37.	Thermal Conductivity vs. Absolute Temperature for $Ag_2In_8Se_{13}$, Sample Number 225	100
38.	Electrical Conductivity Changes in $Ag_2In_8Se_{13}$	106
39.	Differential Thermal Analysis Heating and Cooling Curves for the ZnTe-In_2Te_3 System	109
40.	Phase Diagram for the ZnTe-In_2Te_3 System	112
41.	Differential Thermal Analysis Measuring System	126
42.	Electrical Circuit Used for Measuring the Electrical Conductivity, Hall Effect, and Seebeck Coefficient of the Semiconducting Compounds	131
43.	Sample Holder and Measuring System for the Determination of the Electrical Conductivity, Hall Effect, and Seebeck Coefficient of the Semiconducting Compounds	133
44.	Equipment Used for Measuring Thermal Conductivity	139
45.	Measurement and Control Circuits for the Thermal Conductivity Apparatus	141

LIST OF APPENDICES

		Page
I.	PREPARATION OF SAMPLES	121
	A. Introduction	121
	B. Raw Materials	121
	C. Etching Procedure	121
	D. Preparation of Samples for Differential Thermal Analysis and Zone Refining	122
	E. Zone Refining	123
II.	DIFFERENTIAL THERMAL ANALYSIS	125
III.	CHEMICAL ANALYSIS	127
IV.	ELECTRICAL CONTACTS	129
V.	MEASUREMENTS OF HALL EFFECT, ELECTRICAL CONDUCTIVITY, AND SEEBECK COEFFICIENT	130
	A. Electrical Circuit	130
	B. Electrical Samples	130
	C. Sample Holder and Container	132
	D. Measuring Procedures	134
	1. Hall Effect	134
	2. Electrical Conductivity	135
	3. Type of Current Carrier	135
	E. Sample Calculations	135
	1. Calculation of the Hall Coefficient	135
	2. Calculation of the Electrical Conductivity	136
	3. Calculation of the Seebeck Coefficient	137
VI.	THERMAL CONDUCTIVITY	138
	A. Description of Equipment	138
	B. Calibration and Operation	142
	C. Sample Calculation of Thermal Conductivity	145

INTRODUCTION

The purpose of this work was to investigate pseudo-binary phase diagrams in order to locate congruently and peritectically melting ternary semiconducting compounds and to measure and interpret the electrical and thermal properties of some of the compounds. The pseudo-binary phase diagrams were composed of binary compounds with the chemical formulae $In_2VI_3^b$ and either $I_2^bVI^b$ or II^bVI^b. The group I^b elements were silver and copper, the group II^b elements were cadmium, zinc, and mercury, and the group VI^b elements were selenium and tellurium. All these compounds should be semiconductors, as predicted from structure studies made by Hahn, et. al.[1, 2] and rules delineated by Mooser and Pearson[3]. The properties measured were transformation temperatures, electrical conductivity, Hall effect, Seebeck coefficient (also sometimes referred to as thermoelectric power), and thermal conductivity.

Initial work was centered on the preparation and evaluation of the properties of ternary compounds in the homologous series $I^bInVI_2^b$ and $II^bIn_2VI_4^b$. In order to prepare homogeneous samples, it was necessary to have some knowledge of the ternary phase diagrams in which the compounds appear. These ternary compounds represent a linear combination of two binary constituents, each of which has semiconducting properties. One constituent can be represented by the formula $In_2VI_3^b$ and the other constituent either as $I_2^bVI^b$ or as II^bVI^b. Since each of the binary constituents is a pure chemical component, adequate equilibrium relationships can be obtained by investigating only the pseudo-binary plane which joins them in the ternary system.[4] This is not true in general, but appears to be valid in these systems.

Differential thermal analysis (DTA) can be used to determine the solid-liquid transformations of a mixture or compound as a function of temperature. In conjunction with X-ray results, the phase diagram behavior of the system can be delineated and the conditions established which are necessary for the preparation of high purity compounds. For a

congruently melting compound, the melting point is obtained readily from DTA measurements. For a peritectic compound, the peritectic decomposition temperature can be measured as well as the extent of the solid-liquid region above the decomposition temperature. Solid-solid transitions can also be detected with DTA provided the latent heat associated with the transition is sufficiently large to be observed on the measuring equipment.

If a congruently melting compound exists in a phase diagram, DTA can provide an estimate of its composition and melting point. Zone refining can be used to produce the compound if the starting composition of the sample is close to the compound and the structure of the phase diagram is favorable. After the composition of the compound is known, zone refining principles developed by Pfann[5] can be applied to obtain high purity samples of the compound. For peritectic compounds, the zone leveling techniques described by Mason and Cook[6] can be used to provide samples of the compound.

The samples obtained by zone refining will usually be polycrystalline, but of sufficient purity to provide information on the intrinsic electrical properties of the semiconducting compound. Electrical conductivity measurements as a function of temperature will indicate the energy gap of the compound as long as certain simplifying assumptions are valid. Hall effect data in the intrinsic region will also provide an estimate of the energy gap, and in the extrinsic range, it is sometimes possible to measure the majority carrier concentration. For high purity samples, the decrease of the Seebeck coefficient in the intrinsic range will be dependent on the ratio of the electron to hole mobility.

If the thermal conductivity of the semiconductor compound is known along with the electrical conductivity and the Seebeck coefficient, the thermoelectric figure of merit can be calculated. This term provides a means of estimating the potential application of the semiconductor in thermoelectric devices. Simon[7] presented a means of obtaining the optimum thermoelectric figure of merit without an extensive study of impurity effects.

LITERATURE SURVEY

Hahn, et. al.[1, 2] made structure studies on all the following pseudo-binary systems which were investigated in this work: Ag_2Te-In_2Te_3; Ag_2Se-In_2Se_3; Cu_2Te-In_2Te_3; Cu_2Se-In_2Se_3; $HgTe$-In_2Te_3; $HgSe$-In_2Se_3; $CdTe$-In_2Te_3; $CdSe$-In_2Se_3; $ZnTe$-In_2Te_3; and $ZnSe$-In_2Se_3. He reported lattice parameters for selected compositions in each system and defined the existence of compounds with the compositions $I^bInVI^b_2$ and $II^bIn_2VI^b_4$, all of which were found to have chalcopyrite structures. Beyond this point, he made no effort to speculate on the appearance of the pseudo-binary phase diagrams or to ascertain whether these compounds melt congruently or peritectically.

Woolley, et. al.[8, 9] investigated the $CdTe$-In_2Te_3 and $ZnTe$-In_2Te_3 phase diagrams using only X-ray analysis techniques. For the $CdTe$-In_2Te_3 system, these results do not agree with those found by Mason, et. al.[10] who reported the phase diagram for $CdTe$-In_2Te_3 on the basis of DTA and X-ray measurements.

Energy gap values have been reported for the compositions characterized by the formula $II^bIn_2VI^b_4$. Busch, Mooser, and Pearson[11] reported energy gaps of 0.6 eV for $HgIn_2Se_4$, 0.9 eV for $CdIn_2Te_4$, 1.4 eV for $ZnIn_2Te_4$, and 2.6 eV for $ZnIn_2Se_4$ from electrical resistivity data. Busch, Junod, and Schade[12] obtained an energy gap of 1.25 eV from electrical measurements on single crystal $HgIn_2Te_4$. Optical energy gaps of 0.86 eV for $HgIn_2Te_4$, 0.86 eV for $ZnIn_2Te_4$, 0.92 eV for $CdIn_2Te_4$, and 1.3 eV for $CdIn_2Se_4$ were measured by Peters.[13] The optical energy gap of $CdIn_2Te_4$ was reported as 1.08 eV by Edwards and O'Kane.[14] Hall[15] found an energy gap of 1.14 eV for $ZnIn_2Te_4$ from electrical resistivity measurements. The optical energy gap of $ZnIn_2Te_4$ was measured as 1.15 eV by Newman.[16] The optical energy gap of $CdIn_2Se_4$ was reported as 1.45 eV by Kolomiets and Mal'kova.[17] The energy gap measurements on the compounds are summarized in Table I.

In the case of the $I^bInVI^b_2$ compounds, there are only two sources of published energy gap values. Austin, Goodman, and Pengelly[18] re-

TABLE I

Properties of Ternary Compounds

Compound	Maximum Transition Temperature °C	Energy Gap, eV	
		Electrical Measurements	Optical Measurements
$CuInSe_2$	990 ± 10 (20) 990 (18) 990 (19)	1.07 (19)	0.92 (18)
$AgInSe_2$	780 ± 10 (20) 1000 (18) 775 (19)	1.18 (19)	1.18 (18)
$ZnIn_2Se_4$	980 ± 10 (20)	2.6 (11)	
$CdIn_2Se_4$	915 ± 5 (20)	1.3 (17)	1.45 (17) 1.3 (13)
$HgIn_2Se_4$	830 ± 10 (20)	0.6 (11)	
$CuInTe_2$	790 ± 10 (20) 700 (18) 780 (19)	0.95 (19)	0.95 (18)
$AgInTe_2$	680 ± 10 (20) 675 (18) 680 (19)	0.93 (19)	0.96 (18)
$ZnIn_2Te_4$	800 ± 5 (20)	1.14 (15) 1.4 (11)	1.15 (16) 0.86 (13)
$CdIn_2Te_4$	785 ± 2 (20)	0.9 (11)	1.08 (14) 0.92 (13)
$HgIn_2Te_4$	708 ± 2 (20)	1.25 (12)	0.86 (13)

ported optical energy gaps of 0.92 eV for $CuInSe_2$, 0.95 eV for $CuInTe_2$, 1.18 eV for $AgInSe_2$, and 0.96 eV for $AgInTe_2$; these measurements were made on zone refined samples. Zhuze, Sergeeva, and Strum[19] reported energy gaps of 1.07 eV for $CuInSe_2$, 0.95 eV for $CuInTe_2$, 1.18 eV for $AgInSe_2$, and 0.93 eV for $AgInTe_2$ using electrical resistivity measurements.

Both these teams of investigators measured the maximum solid-liquid transition temperature of each composition. These are shown in Table I along with values reported by Mason and O'Kane.[20]

THEORY

In this section the various formulae are developed which must be used to interpret the experimental measurements. The electrical conductivity and Hall effect are discussed first, followed by the Seebeck coefficient and the thermal conductivity. Methods for measuring these properties have been developed and discussed by Lindberg,[21] Putley,[22] and LaBotz,[23] and are discussed in more detail in the section on experimental procedures and in the appendices.

Electrical Conductivity and Hall Effect

The electrical conductivity is a measure of the number of current carriers and the ease with which they move in the presence of an electric field. The Hall effect occurs when a magnetic field is applied perpendicular to an electric field. A potential is induced which is perpendicular to both the magnetic field and the electric current. In some cases, the Hall effect serves to define the magnitude of the factors which make up the electrical conductivity.

The generalized formulae for the electrical conductivity and Hall coefficient are presented first followed by expressions which are applicable when the semiconductor is extrinsic in the lower temperature region and intrinsic at higher temperatures.

General Formulae for Electrical Conductivity and Hall Effect

The expressions for electrical conductivity and Hall effect are given by:

(1) $\sigma = qn\mu_n + qp\mu_p$

and

(2) $$R_H = - \frac{n(\mu_{H,n}/\mu_n)\mu_n^2 - p(\mu_{H,p}/\mu_p)\mu_p^2}{q(n\mu_n + p\mu_p)^2}$$

where σ = electrical conductivity, mho/cm.

R_H = Hall coefficient, $cm.^3$/coulomb

n = concentration of electrons in the conduction band, electrons/$cm.^3$

p = concentration of holes in the valence band, holes/$cm.^3$

μ_n = drift mobility of electrons, $cm.^2$/volt-second

μ_p = drift mobility of holes, $cm.^2$/volt-second

$\mu_{H,n}$ = Hall mobility for electrons, $cm.^2$/volt-second

$\mu_{H,p}$ = Hall mobility for holes, $cm.^2$/volt-second

q = electron charge, 1.602×10^{-19} coulombs/electron

The ratio of Hall mobility to drift mobility depends on the scattering mechanism and the shape of the energy surfaces in momentum space. Equation (2) can be written as

(3) $$R_H = - \beta\left\{\frac{n\mu_n^2 - p\mu_p^2}{q(n\mu_n + p\mu_p)^2}\right\}$$

where β is the ratio of the Hall mobility to drift mobility. For spherical energy surfaces and scattering by thermal vibrations, β is equal to $3\pi/8$. In the case of impurity scattering, β is 1.93.

Electrical Conductivity and Hall Effect Formulae for Extrinsic Semiconductors

At low temperatures the number of electrons excited to acceptor levels or excited from donor levels far exceeds the number of electrons

thermally excited from the valence band to the conduction band. If only one type of carrier is present in this temperature region, the expression for the Hall coefficient reduces to

(4) $R_H = -\beta(1/qn)$

for n-type semiconductors, and

(5) $R_H = +\beta(1/qp)$

for p-type semiconductors.

If the ionization energy of an impurity level is considerably less than the width of the band gap, all the impurity levels will be ionized before the intrinsic region is reached. Since both donor and acceptor levels are usually present, the observed charge carrier concentration is the difference $N_d - N_a$, where N_d is the concentration of donor levels and N_a is the concentration of acceptor levels.

Smith[24] shows that a plot of the natural logarithm of carrier concentration versus the reciprocal absolute temperature will have a slope of $E_d/2k$, where E_d is the distance between the donor level and the conduction band, and k is the Boltzman constant. This assumes that N_a is very small. When the temperature dependence of the electron mobility is $T^{-3/2}$ (lattice scattering), E_d can be obtained from the slope of the plot of natural logarithm of electrical conductivity against reciprocal absolute temperature. The derivation is similar to that shown for the determination of energy gap from electrical conductivity data in the intrinsic range.

Electrical Conductivity and Hall Effect Formulae for Intrinsic Semiconductors.

In the intrinsic region, $n = p = n_i$, where n_i is the intrinsic carrier concentration. Equation (1) can then be written as

(6) $\sigma = n_i q(\mu_n + \mu_p)$

If the electron mobility is considerably larger than the hole mobility, then Equation (6) can be written as

(7) $\sigma \cong n_i q \mu_n$

Since

$$(8) \quad n_i = \frac{2(2\pi mkT)^{3/2}}{h^3} \left(\frac{m_n^* m_p^*}{m^2} \right)^{3/4} \exp(-E_g/2kT)$$

where

m = free electron mass

h = Planck constant, 6.624×10^{-27} erg-second

m_n^* = effective mass of electrons

m_p^* = effective mass of holes

T = absolute temperature, $^{\circ}K$

Equation (7) can be expressed as

$$(9) \quad \sigma = q \frac{2(2\pi mkT)^{3/2}}{h^3} \left(\frac{m_n^* m_p^*}{m^2} \right)^{3/4} \left[\exp(-E_g/2kT) \right] \mu_n$$

If the product of the effective masses is constant and the electron mobility is proportional to $T^{-3/2}$ (which would presume that lattice scattering is the predominant mechanism), then

$$(10) \quad \sigma = A \exp(-E_g/2kT)$$

where

A = a constant

If the assumption is now made that

$$(11) \quad E_g = E_{g_o} + aT$$

where

E_{g_o} = energy gap at $0^{\circ}K$

a = the temperature dependence of the energy gap

then

$d \log_{10} \sigma / d(1/T)$ is equal to $-E_{g_o} / 4.606k$

If n_i is substituted for n and p in Equation (3), the Hall coefficient in the intrinsic range becomes

$$(12) \qquad R_H = -\beta \left\{ \frac{\mu_n^2 - \mu_p^2}{q n_i (\mu_n + \mu_p)^2} \right\}$$

and

$$(13) \qquad R_H = \frac{-\beta}{q n_i} \left(\frac{b-1}{b+1} \right)$$

where b = the ratio of electron mobility to hole mobility. Combining Equation (8) with Equation (13), the Hall coefficient is then

$$(14) \qquad R_H = -\frac{\beta}{q} \left(\frac{b-1}{b+1} \right) \frac{h^3}{2(2\pi mkT)^{3/2} (m_n^* m_p^* / m^2)^{3/4}} \exp(+E_g / 2kT)$$

or

$$(15) \qquad R_H T^{3/2} = (\text{constant}) \exp(+E_g / 2kT)$$

if the effective mass ratio is constant and the mobility ratio is constant or large compared to one. If the change in energy gap with temperature can be represented by Equation (11), then the slope of $\log_{10} R_H T^{3/2}$ vs. $1/T$ will provide the value of $E_{g_o} / 4.606\,k$.

When the electron mobility is considerably larger than the hole mobility, Equation (13) reduces to

$$(16) \qquad R_H = \frac{-\beta}{q n_i}$$

Combining this with the expression for the electrical conductivity in Equation (7), the result is

$$(17) \qquad \mu_n = \frac{-1}{\beta} (R_H \sigma)$$

or

$$(18) \qquad \mu_{H,n} = -(R_H \sigma)$$

The Hall mobility, $\mu_{H,n}$, is usually written as a function of temperature, such as

$$(19) \qquad \mu_{H,n} = BT^{\gamma}$$

where

B = a constant

γ = a constant

The value of γ is dependent on the scattering mechanism, and for lattice scattering is equal to -1.5. From the Hall coefficient and electrical conductivity data in the intrinsic range, the temperature dependence of the Hall mobility can be obtained.

Seebeck Coefficient

The Seebeck coefficient results from the diffusion of electrons and holes inside a material when a thermal gradient is present and the electric current flow is zero. In semiconductors the Seebeck coefficient may be a factor of 100 to 1,000 higher than that of a metal, such as platinum, which is used in the measuring circuit. This means that it is usually not necessary to distinguish between the absolute Seebeck coefficient and the Seebeck coefficient relative to the metal.

The Seebeck coefficient, which can vary rapidly with temperature, is strongly dependent on the impurity concentration. Expressions will be shown for the Seebeck coefficient in both the extrinsic and intrinsic ranges. All measurements of this property were made above room temperature and relative to platinum.

Seebeck Coefficient in the Extrinsic Range

In the extrinsic range, the Seebeck coefficient, α, is given by Putley[22] as

$$(20) \qquad \alpha = -\frac{k}{q}\left[(p + 5/2) - E_f/kT\right]$$

where p = a constant which is dependent on the scattering mechanism

E_f = the Fermi level, eV

and

$$(21) \quad E_f = kT \ln \frac{nh^3}{2(2\pi m^* kT)^{3/2}}$$

For the case of acoustic lattice scattering, the Seebeck coefficient is

$$(22) \quad \alpha = \pm \frac{k}{q} (2 - E_f/kT)$$

and for impurity scattering,

$$(23) \quad \alpha = \pm \frac{k}{q} (4 - E_f/kT)$$

If the scattering mechanism is known, then it is possible to determine the Fermi level. When the carrier concentration is also known from the Hall data, the effective mass of the charge carriers can be obtained from Equation (21).

Seebeck Coefficient in the Intrinsic Range

Johnson[25] developed an expression for the Seebeck coefficient of an intrinsic semiconductor in terms of the mobility ratio, energy gap, temperature dependence of the energy gap, and the ratio of electron effective mass to hole effective mass.

In an intrinsic semiconductor, $n = p$ and the equilibrium condition described by Equation (8) applies. Assuming classical statistics and a mean free path independent of energy, the Seebeck coefficient is

$$(24) \quad \alpha = -\frac{k}{q(nb+p)} \left\{ 2(nb-p) - nb \ln \frac{nh^3}{2(2\pi m_n^* kT)^{3/2}} + p \ln \frac{ph^3}{2(2\pi m_p^* kT)^{3/2}} \right\}$$

Combining Equations (8) and (24), the result is

$$(25) \quad \alpha = -\frac{k}{q} \left\{ \left(\frac{b-1}{b+1}\right) (E_g/2kT) + \frac{2(b-1)}{(b+1)} + \frac{3}{4} \ln (m_n^*/m_p^*) \right\}$$

If the energy gap is a linear function of temperature as shown in equation (11), then

$$(26)\quad \alpha = -\frac{k}{q}\left(\frac{b-1}{b+1}\right)\left\{\left(E_{g_o}/2kT\right) + \frac{a}{2k} + 2 + \frac{3}{4}\,\frac{(b+1)}{(b-1)}\,\ln\left(m_n^*/m_p^*\right)\right\}$$

By plotting the Seebeck coefficient against the reciprocal of the absolute temperature, the slope, m, and the intercept, c, of the equation

$$(27)\quad \alpha = \frac{m}{T} + c$$

can be determined. Now,

$$(28)\quad m = -\frac{k}{q}\left(\frac{b-1}{b+1}\right)\left(\frac{E_{g_o}}{2k}\right)$$

Using the value of the energy gap obtained from electrical measurements, the mobility ratio, b, can be solved. The intercept, c, is equal to

$$(29)\quad c = -\frac{k}{q}\left\{\left(\frac{b-1}{b+1}\right)\left(\frac{a}{2k} + 2\right) + \frac{3}{4}\,\ln\left(m_n^*/m_p^*\right)\right\}$$

As a first approximation for the effective mass ratio, the following expression can be used:

$$(30)\quad b = \left(m_p^*/m_n^*\right)^{5/2}$$

Equation (30) applies for semiconductors with spherical energy bands in the temperature region where lattice scattering predominates. If this is valid, then the temperature dependence of the energy gap, a, can be solved for in Equation (29).

Thermal Conductivity

Thermal conductivity is a measure of the ease of transport of energy in the form of heat, Q, when a temperature gradient exists. If the energy flows through a unit cross section in unit time when a temperature gradient dT/dX is applied, then the thermal conductivity is

$$(31)\quad \lambda_{th} = \frac{Q}{(dT/dX)}$$

Heat can be conducted through a solid either by vibration of the crystal lattice or by charge carriers. In semiconductors below 700°K where radiation effects are negligible (Ioffe,[26] p. 287), the total thermal conduc-

tivity may be expressed as

(32) $\lambda_{th} = \lambda_{ph} + \lambda_e$

where

λ_{ph} = phonon component of thermal conductivity

λ_e = electronic component of thermal conductivity

In most semiconductors the lattice scattering or phonon component is considerably greater than the electronic component. The phonon contribution to thermal conductivity is given by

(33) $\lambda_{ph} = Cv\delta/3$

where

C = specific heat per unit volume, gm. cal./cm.^{3} ^oK

v = velocity of sound, cm./sec.

δ = phonon mean free path, cm.

Above the Debye temperature, the phonon thermal conductivity is proportional to T^{-1}, until amorphism effects become significant.

Putley[22] (p. 75) shows that the application of the Wiedemann-Franz-Lorentz ratio, $\lambda_e/\sigma T$, in the case where classical statistics hold, results in

(34) $\lambda_e = 2\left(\frac{k}{q}\right)^2 \sigma T$

Deviations from this relationship occur when intrinsic conduction begins and both electrons and holes participate in the diffusion process. In the case of joint diffusion of electrons and holes, bipolar diffusion, Ioffe[27] gives the following expression for the electronic component of thermal conductivity:

(35) $\lambda_e = 2\left(\frac{k}{q}\right)^2 T(\sigma_+ + \sigma_-) + 2(2)\left(\frac{k}{q}\right)^2 T\left\{\frac{\sigma_+\sigma_-}{\sigma_+ + \sigma_-}\left(E_g/2kT + 2 + r\right)\right\}^2$

where σ_+ = hole component of the electrical conductivity, pqu_p

σ_- = electron component of the electrical conductivity, nqu_n

r = the exponent in the expression for the mean free path of the free carriers as a function of their temperature

For the case of atomic lattices, r = 0, and a high electron to hole mobility ratio, Equation (34) reduces to

$$\lambda_e = 2\left(\frac{k}{q}\right)^2 T\left\{\sigma_- + 2\sigma_+\left(\frac{E_g}{2kT} + 2\right)^2\right\} \tag{36}$$

or

$$\lambda_e = 2\left(\frac{k}{q}\right)^2 T\,\sigma_-\left\{1 + \frac{2}{b}\left(\frac{E_g}{2kT} + 2\right)^2\right\} \tag{37}$$

Still another process that can lead to an increase in thermal conductivity is the diffusion of hole-electron pairs, excitons, from the hot region of the solid to the cold region with a liberation of the energy initially needed for the excitation. The exciton concentration is a function of the temperature and the excitation energy; and, it is not necessary to be in the intrinsic temperature range for exciton generation.

The thermal conduction resulting from excitons is given by Ioffe[27] as

$$\lambda_{exc} = \left(\frac{k}{q}\right)^2 \sigma T\left(\frac{N}{n}\right)\left(\frac{U}{u}\right)\left[\frac{E_{exc}}{kT} + 2\right]^2 \tag{38}$$

where

N = exciton concentration

$U = \frac{q}{kT} D$ (D is the exciton diffusion coefficient)

E_{exc} = exciton energy

Since the exciton diffusion coefficient, the exciton concentration, and the exciton energy are unknown quantities, it is not possible to establish the contribution of this term to the total thermal conductivity unless all other components can be separated from the experimental data.

Ioffe[27] also points out that there may be an interaction of phonons with holes and electrons or excitons which would result in an entrainment of phonons.

Thermoelectric Figure of Merit

The criterion used to describe the performance of a semiconductor in thermoelectric applications is the figure of merit which is given by the equation:

$$(39) \qquad Z = (\sigma \alpha^2) / \lambda_{th}$$

In a semiconductor, λ_{th} as a first approximation is independent of carrier concentration. However, both σ and α are dependent on the carrier concentration. The optimum figure of merit is usually obtained with a carrier concentration near $10^{19}/cm^3$. A large effective mass, a high mobility, and a small thermal conductivity are considered among the requirements for a good thermoelectric material.

It is possible to estimate the maximum thermoelectric figure of merit for a particular semiconductor from the curves derived by Simon[7]. This requires a knowledge of electrical conductivity, Seebeck coefficient, and thermal conductivity for an extrinsic sample.

EXPERIMENTAL PROCEDURES

This section describes the experimental procedures used for the preparation of samples and the measurement of the electrical and thermal properties. More detailed descriptions can be found in the appendices.

Sample Preparation

All samples were prepared from the elements with purities of 99.99+ % or 99.999+ %. Stoichiometric quantities of the elements were sealed in fused silica tubes which had been evacuated to 5×10^{-5} mm. Hg or lower. A digital temperature programming unit described by Hozak, Cook, and Mason[28] was used for the heating cycles. After fusion, each sample for differential thermal analysis (DTA) was ground to a powder and rebottled in an evacuated 10 mm. inside diameter fused silica tube with a concentric 4 mm. inside diameter fused silica tube in the bottom to accommodate a thermocouple. In almost all cases, this was followed by annealing the sample for one week at about 600°C before making the DTA measurements.

Zone refining was usually done on 60 gram samples in sealed, evacuated, 10 mm. inside diameter fused silica tubes with a length of 12 inches. The zone refiner was operated at a zone travel rate of 3/4 inches per hour with a 1-1/2 inch liquid zone. Zone leveling was done at 0.3 inches per hour on most peritectic compounds. The number of zone refining passes used depended on the compound. The $Ag_2In_8Se_{13}$ samples, on the average, had 11 passes, and the $AgIn_3Te_5$ samples had anywhere from 1 to 13 passes. In a number of cases, the 99.999+ % tellurium was zone refined before being used to make the $AgIn_3Te_5$ samples. A more detailed description of the sample preparation technique is given in Appendix I.

Zone refining was used to prepare polycrystalline samples of the congruently melting compounds $Ag_2In_8Se_{13}$ and $AgIn_3Te_5$, and the barely peritectic compound $CdIn_2Se_4$ for electrical measurements. However, satisfactory samples of the congruently melting compound $HgIn_2Te_4$ could not be obtained.

High purity samples of $Ag_2In_8Se_{13}$ were readily obtained by zone refining the compound in sealed, evacuated fused silica tubes. In most cases, $AgIn_3Te_5$ was found to cause cracking of the tubes during zone refining, apparently as a result of wetting of the fused silica by the liquid or a very slight reaction with it. However, a few samples of zone refined $AgIn_3Te_5$ were prepared in sealed, evacuated fused silica tubes.

Two samples of $AgIn_3Te_5$ were zone refined by sealing the compound in evacuated 10 mm. tubes which were then sealed in evacuated 16 mm. tubes. The inner fused silica tube acted as a boat for the compound. In both cases the inner tube cracked, but zone refining was continued without oxidation of the compound. The resulting ingot was multiphase. This was entirely unexpected, since the compound melts congruently and there was no evidence of significant vapor transport of the most volatile component, tellurium.

This same type of multi-phase ingot was obtained when a carbon boat was used inside an evacuated 16 mm. fused silica tube as a container for the compound during zone refining. Since little is known about the nature of the pseudo-binary phase diagram in the region of 25 mole % Ag_2Te - 75 mole % In_2Te_3 ($AgIn_3Te_5$), the multi-phase behavior cannot be explained at this time.

Forty-two samples of $HgIn_2Te_4$ were prepared in the course of a study of zone refining variables. An attempt was made to use these samples for this investigation; however, only one sample was found to be free of microcracks after polishing the surface of the sample. The one mechanically sound ingot proved to be multi-phase, despite the fact that the starting composition, $HgIn_2Te_4$, was congruently melting and there was no evidence of vapor transport. This phenomenon appears to be similar to that encountered with $AgIn_3Te_5$ under certain zone refining conditions.

Attempts were made to prepare the peritectic compounds $CdIn_2Se_4$, $CdIn_2Te_4$, and $ZnIn_2Te_4$ using zone leveling techniques described by

Mason and Cook.[6] In order to precipitate the peritectic compound from solution during zone leveling, the liquid must have a substantially different composition which is in equilibrium with solid at the solidification temperature.

Zone leveling of ingots with starting compositions of 47 mole % CdSe - 53 mole % In_2Se_3 did not result in the desired separation of the peritectic compound $CdIn_2Se_4$. The same was true of zone leveling carried out on an ingot of 50% CdSe - 50% In_2Se_3 having a liquid zone of 30% CdSe - 70% In_2Se_3.

By zone refining an ingot of $CdIn_2Se_4$ in the normal manner, the peritectic compound was formed without inclusions of a second phase. This was possible because the peritectic decomposition point of this compound is close to the liquidus curve, and the liquidus curve extends over a relatively wide temperature range. However, the degree of purification, as indicated by electrical measurements, seemed to be very poor.

For the case of the CdTe - In_2Te_3 pseudo-binary system investigated by Thomassen and Mason[10] and shown in Figure 1, the peritectic compounds used in these studies were obtained by zone leveling ingots with initial compositions of 90 mole % In_2Te_3, and 83 mole % In_2Te_3.

Two attempts were made to obtain the peritectic compound $ZnIn_2Te_4$ by zone leveling. The composition 47 mole % ZnTe and 53 mole % In_2Te_3 was zone leveled; however, after three passes, the sample tube cracked. There also was a considerable amount of vapor transport during the zone leveling operation. The second sample was made by zone leveling an ingot with a liquid zone of 30 mole % ZnTe and the remainder of the ingot contained 50 mole % ZnTe at the start. This ingot had better mechanical properties; but, it was multi-phase.

Differential Thermal Analysis Measurements

The differential thermal analysis measurements were made in a furnace with approximately linear heating and cooling rates of $2\text{-}1/2^{\circ}$ C

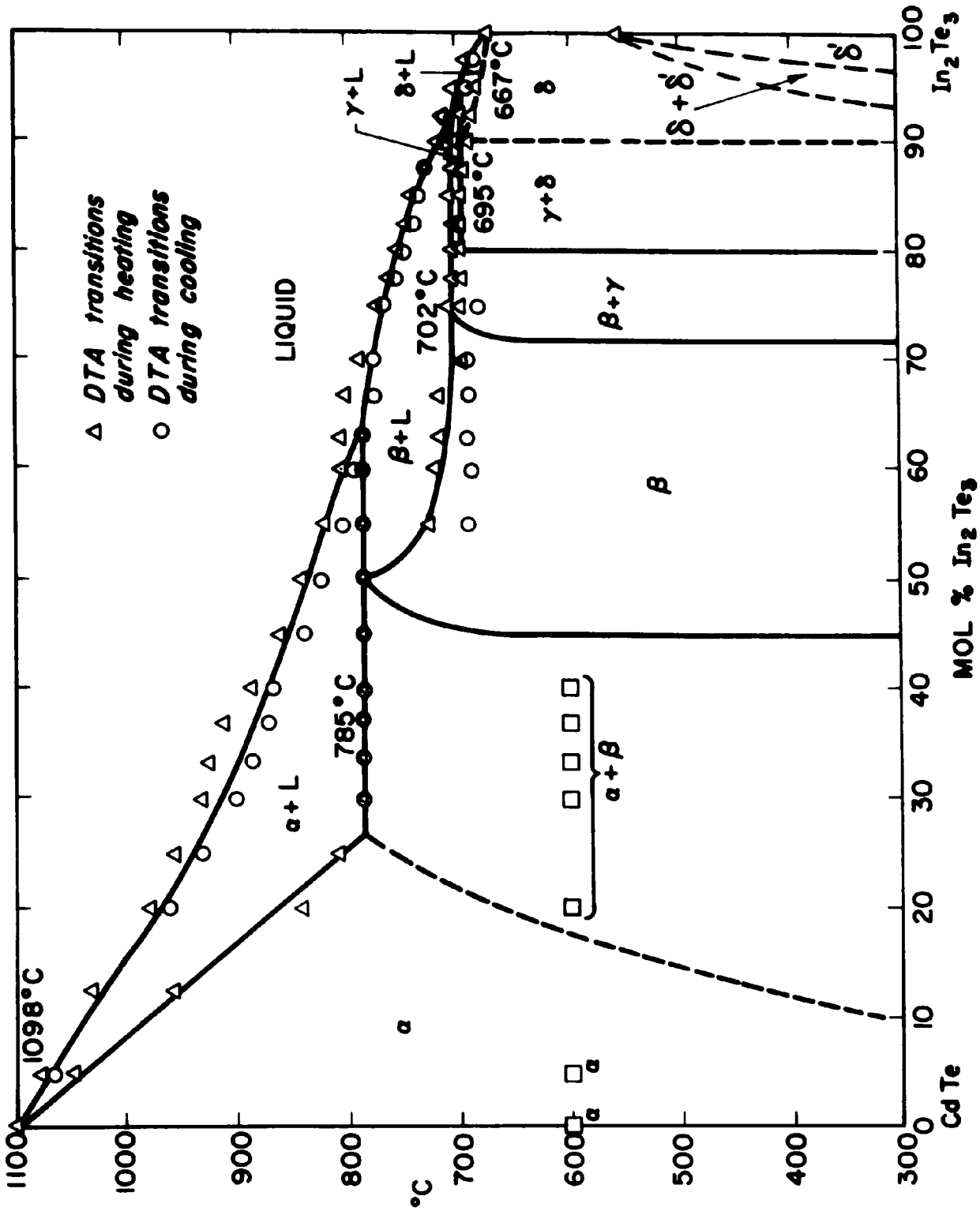


Figure 1. Phase Diagram for the CdTe-In_2Te_3 System.

per minute. The differential temperature between the sample and the reference material, such as indium, was recorded along with the sample temperature on an X-Y recorder. Solid-solid transitions and melting temperatures were obtained between 25°C and 1300°C. The complete measuring system is shown in Appendix II, Figure 41.

The equipment was used to determine the characteristics of the heating and cooling curves for various compositions in the following pseudo-binary phase diagrams: Ag_2Te - In_2Te_3; Ag_2Se - In_2Se_3; Cu_2Te - In_2Te_3; Cu_2Se - In_2Se_3; CdSe - In_2Se_3; and ZnTe - In_2Te_3.

Chemical Analysis

The chemical analysis scheme was initially designed to analyze for Cd, In and Te, which are contained in the compounds formed in the CdTe - In_2Te_3 pseudo-binary system. When a calibration of X-ray data for a large number of compositions in this system was available, it was no longer necessary to rely on the chemical analysis procedure. The analysis was used to identify the congruently melting compound found in the Ag_2Te - In_2Te_3 pseudo-binary phase diagram. A more detailed description of the development of the analytical procedures is contained in Appendix III.

Experiments with the compound $CdIn_2Te_4$ showed that tellurium could be precipitated with sulfur dioxide after the compound was dissolved in nitric acid and the excess acid vaporized off using a hot water bath. The tellurium precipitate was washed with ether and dried at 50°C in vacuum. When the filtrate was treated with ammonia, the indium precipitated as $In(OH)_3$ and was dried in air at 600°C to form In_2O_3. The cadmium remaining in solution was then precipitated with 8-hydroxyquinoline (oxine). The cadmium oxine precipitate was dried under vacuum at 40°C and weighed.

The Ag-In-Te ternary compound was dissolved in nitric acid, the excess acid vaporized, and sulfur dioxide added. This resulted in coprecipitation of the silver and tellurium which were dried in vacuum at

50°C and weighed. Indium was precipitated from the filtrate with ammonia as $In(OH)_3$ and dried in air at 600°C to form In_2O_3. The assumption was then made and later justified that the compound was in the pseudo-binary system composed of Ag_2Te and In_2Te_3. In this case, knowing the weight of indium permits the calculation of the mole % In_2Te_3 and, hence, the mole % Ag_2Te.

Electrical Measurements

Rectangular blocks, approximately 0.7 x 0.2 x 0.1 inches, were cut from the zone refined ingots. The specimens were polished with Linde B powder, etched, examined microscopically, repolished, and then cleaned in an ultrasonic washer. After placing the specimen in a lavite holder, platinum wires (30 or 32 gauge) were fused to the ends and along the sides of the sample. A 30-gauge differential thermocouple of chromel-alumel was placed at the ends of the sample for measurement of the Seebeck coefficient.

The apparatus used for the electrical conductivity, Hall effect, and Seebeck coefficient measurements is described in Appendix V, and shown in Figures 42 and 43. The temperature differential across the sample was controlled by adjusting the power input to the heaters above and below the sample. The measurements were made in either a hydrogen or argon atmosphere maintained at a pressure of 2 pounds per square inch gauge. The hydrogen was passed through a "Deoxo" platinum catalyst to remove oxygen, and either a liquid nitrogen cold trap or molecular sieves to remove water. The argon (99.995%) was passed through a dry ice cold trap before entering the measuring system.

The electrical conductivity and Hall effect were measured using direct current and a magnetic field of 2100 gauss. Electrical conductivity readings were taken in both current directions in order to eliminate the Seebeck potential. Hall effect measurements required reversing both the magnetic field and electric current directions. This eliminated the potentials resulting from non-alignment of the Hall probes, the Nernst effect,

and the Righi-Leduc effect. However, it does not remove the Ettingshausen effect which is generally small in relation to the Hall voltage.

Thermal Conductivity

A dynamic calorimeter described by LaBotz[23] was used to measure the thermal conductivity of $Ag_2In_8Se_{13}$ and $AgIn_3Te_5$. A more detailed discussion of the apparatus, along with figures showing the measuring system and control circuits, is given in Appendix VI.

The thermal conductivity is measured by placing the sample between two copper blocks, one of which has a resistance heater attached to it and serves as a heat source. The second copper block acts as a heat sink and is thermally isolated from the surrounding system. A constant power input is supplied to the heat source, and this causes a fairly constant rate of temperature increase in the blocks and a constant temperature differential across the sample. Under steady state conditions it is possible to calculate the thermal conductivity from a measurement of the dimensions of the sample, the temperature drop across the sample and the rate of temperature rise of the sink. The heat capacity of the sink is known and, hence, the amount of heat flowing through the sample.

The test specimens of $AgIn_3Te_5$ and $Ag_2In_8Se_{13}$ were obtained by melting zone refined material in evacuated, 18 mm. fused silica tubes and slowly cooling the compounds to obtain crystal growth. One inch long sections were cut and polished for the thermal conductivity measurements. Holes, .020 inches in diameter, were cut in the sample with an ultrasonic cutter for the placement of thermocouples.

SEMICONDUCTING PROPERTIES OF $CdIn_2Se_4$

Literature Review

Before presenting the results of this investigation, a review will be given of the published data on the crystal structure of compositions within the pseudo-binary phase diagram composed of CdSe-In_2Se_3, and the semiconducting properties of $CdIn_2Se_4$. Hahn, et. al.[2] published crystal structure results on the compound $CdIn_2Se_4$ along with lattice parameter values at the points 10, 20, 33, 43, 50, 57, 67, 80, 90, and 100% CdSe in the pseudo-binary phase diagram of CdSe-In_2Se_3. They obtained only one lattice parameter over the range 10 to 67% CdSe, and its value was almost constant at $a = 5.80 \pm 0.01$ kX.

Kolomiets and Mal'kova[17] also made X-ray lattice parameter measurements on this system, and reported a region of homogeneous alloys of ordered sphalerite structure between approximately 45 and 60% CdSe. At 66.7% CdSe and 33.3% CdSe, the structure was sphalerite, but ordering lines were absent. The 83.3% CdSe composition had a hexagonal structure. The samples were prepared by slowly cooling (100° C per hour) the melt to 800°C and then furnace cooling. There is no indication that the X-ray samples were annealed.

Kolomiets and Mal'kova[17] made electrical conductivity measurements in a vacuum system on cast samples of $CdIn_2Se_4$. An energy gap of 1.3 eV was obtained from the slope of the logarithm of the electrical conductivity versus reciprocal absolute temperature between about 440°C and 620°C. The electrical conductivity was substantially constant between room temperature and 250°C. The room temperature values of electrical conductivity varied between 1 mho/cm. and 500 mho/cm., and the Hall mobility was about 100 $cm.^2$/volt-second. The electron concentration ranged from $10^{17}/cm.^3$ to 5×10^{19}/cm. The optical energy gap was 1.45 eV; this compares with a value of 1.3 eV reported by Peters.[13]

Since the crystal structure of any ternary compounds formed in the pseudo-binary system of CdSe-In_2Se_3 will depend to some extent on

the binary compounds, CdSe and In_2Se_3, a brief review is given of the known properties of the two binary compounds.

Miyazawa and Sugaike[29] reported a hexagonal structure at room temperature for In_2Se_3. They obtained a sharp heat absorption at nearly 200°C from differential thermal analysis heating curves. On cooling, the transition occurred below 100°C. A high temperature modification of the crystal structure was reported by Hahn.[30] This is believed to occur in the region of 740 ± 20°C on the basis of the differential thermal analysis results of Mason and O'Kane.[20] Semiletov[31] claimed that In_2Se_3 had four crystal modifications: two hexagonal; a cubic; a monoclinic. In_2Se_3 has a melting point of 888°C and CdSe melts at 1258°C according to Mason and O'Kane.[20] Kolomiets and Mal'kova[17] report a hexagonal crystal structure for CdSe.

Results of Differential Thermal Analysis and Electrical Measurements

Differential Thermal Analysis

The differential thermal analysis (DTA) measurements serve two important purposes. They define the zone leveling conditions which could result in pure samples of any peritectic compound in the pseudo-binary phase diagram, and they provide an estimate of the appearance of the phase diagram. The complete picture of the phase diagram can only, if at all, be determined from a combination of DTA measurements, X-ray studies, and microscopic examination of a large number of samples. Since the primary purpose of this investigation was to obtain electrical samples, only a partial solution to the phase diagram behavior was obtained.

Eighteen different compositions in the pseudo-binary phase diagram of CdSe-In_2Se_3 were tested in the differential thermal analysis equipment. Heating and cooling curves for each composition are shown in Figure 2 for the following compositions: 100, 90, 80, 75, 70, 60, 55, 50, 45, 40, 35, 30, 25, 20, 15, 10, 5, and 0 mole % CdSe. All samples

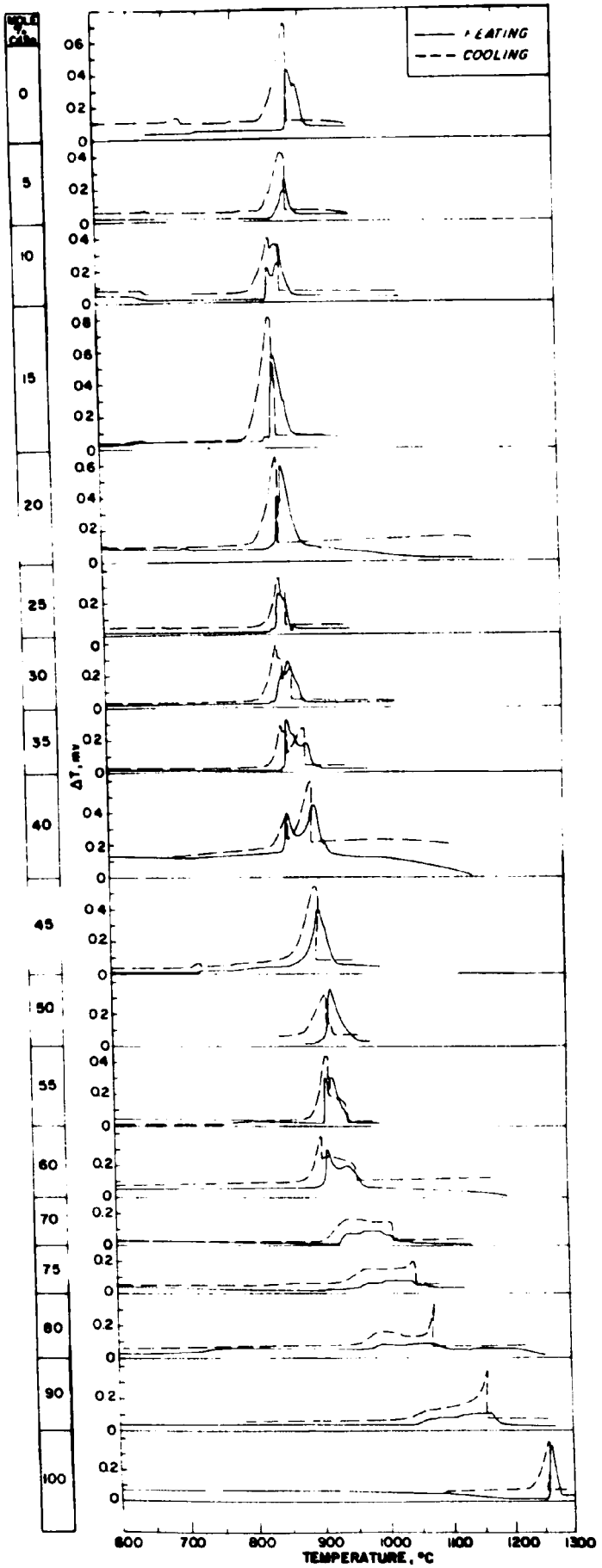


Figure 2. Differential Thermal Analysis Heating and Cooling Curves for the CdSe-In_2Se_3 System.

with the exception of the 50 and 20 mole % CdSe compositions, were cooled from the liquid state, after fusion of the elements, by quenching the sample tube either rapidly in air or in a water bath. Prior to the DTA measurements, the samples were usually annealed one week at about 600°C. Table II shows the exact annealing conditions for each sample and some of the liquidus, solid-liquid, and solid-solid transformation temperatures indicated by the DTA data. In many cases, there are overlapping transformations which make it impossible to estimate the temperature of transformation. Figure 3 shows the DTA measurements made on single phase material directly adjacent to the section of zone refined ingot number 083 used for electrical measurements.

The transformation temperature data in Table II give some indication of the complexity of the CdSe-In_2Se_3 system. An estimate of what the pseudo-binary phase diagram might look like is shown in Figure 4. A long liquidus line extends from 1258°C, the melting point of CdSe, to about 915°C at 46 mole % CdSe. The liquidus then proceeds down to 865°C, which is another peritectic temperature, and over to a eutectic at about 18 mole % CdSe and 855°C. A liquidus line extends from the eutectic point up to the melting point of the binary compound, In_2Se_3, at 888°C.

There are two peritectic compounds in the phase diagram: the first one is at 50 mole % CdSe, $CdIn_2Se_4$; and the second one may be in the region of 40 mole % to 35 mole % CdSe. The small transitions which occur only in some samples near 840°C in the low CdSe side of the phase diagram cannot be explained. The solid-solid transition in In_2Se_3 near 740°C seems to extend over to compositions containing up to 20 mole % CdSe in the phase diagram.

A more extensive investigation of the phase diagram of CdSe-In_2Se_3 would require X-ray studies over a wide range of compositions. This would necessitate extremely careful measurements, since the variation in lattice parameter between 10 mole % CdSe and 67 mole % CdSe was about 0.3% from the data of Hahn, et al.[2]

TABLE II

SUMMARY OF DIFFERENTIAL THERMAL ANALYSIS MEASUREMENTS FOR THE PSEUDO-BINARY PHASE DIAGRAM OF CdSe - In_2Se_3.

Sample Composition		Sample Number	Annealing Conditions After Rebottling Sample in DTA Tube	Differential Thermal Analysis Results			
Mole % CdSe	Mole % In_2Se_3			Liquidus Temp. °C	Transition Temp. °C	Liquidus Temp. °C	Transition Temp. °C
				Heating		Cooling	
100	0	705	None	1258		1258	
90	10	689	11 days at 705° C	1176	1044	1158	
80	20	644	7 days at 615° C	1094	973	1074	
75	25	720	5 days at 800° C, 3 days at 350° C	1050	947	1046	
70	30	695	6 days between 650° C and 700° C	1021	927	1012	
60	40	645	7 days at 600° C	967	911	957	903
55	45	727	7 days at 600° C	947	909	943	915
50	50	537	None		920	926	914
45	55	702	9 days at 590° C	929	866, 731	904	855, 729
40	60	643	7 days at 615° C, 1 day at 460° C, 1 day at 305° C	917	861	898	863
35	65	713	7 days at 590° C	902	861	889	863, 855
30	70	690	11 days at 650° C	890	865, 839	871	859, 852
25	75	711	7 days at 590° C	874	852, 843	865	858
20	80	661	None	885	854, 716	855	686
15	85	710	6 days at 590° C	876	851, 836, 650	854	661
10	90	693	7 days at 635° C	879	847	865	852, 667
5	95	721	7 days at 600° C	890	854	876	850, 676
0	100	676	5 days at 595° C	888	751, 210	885	731, 98

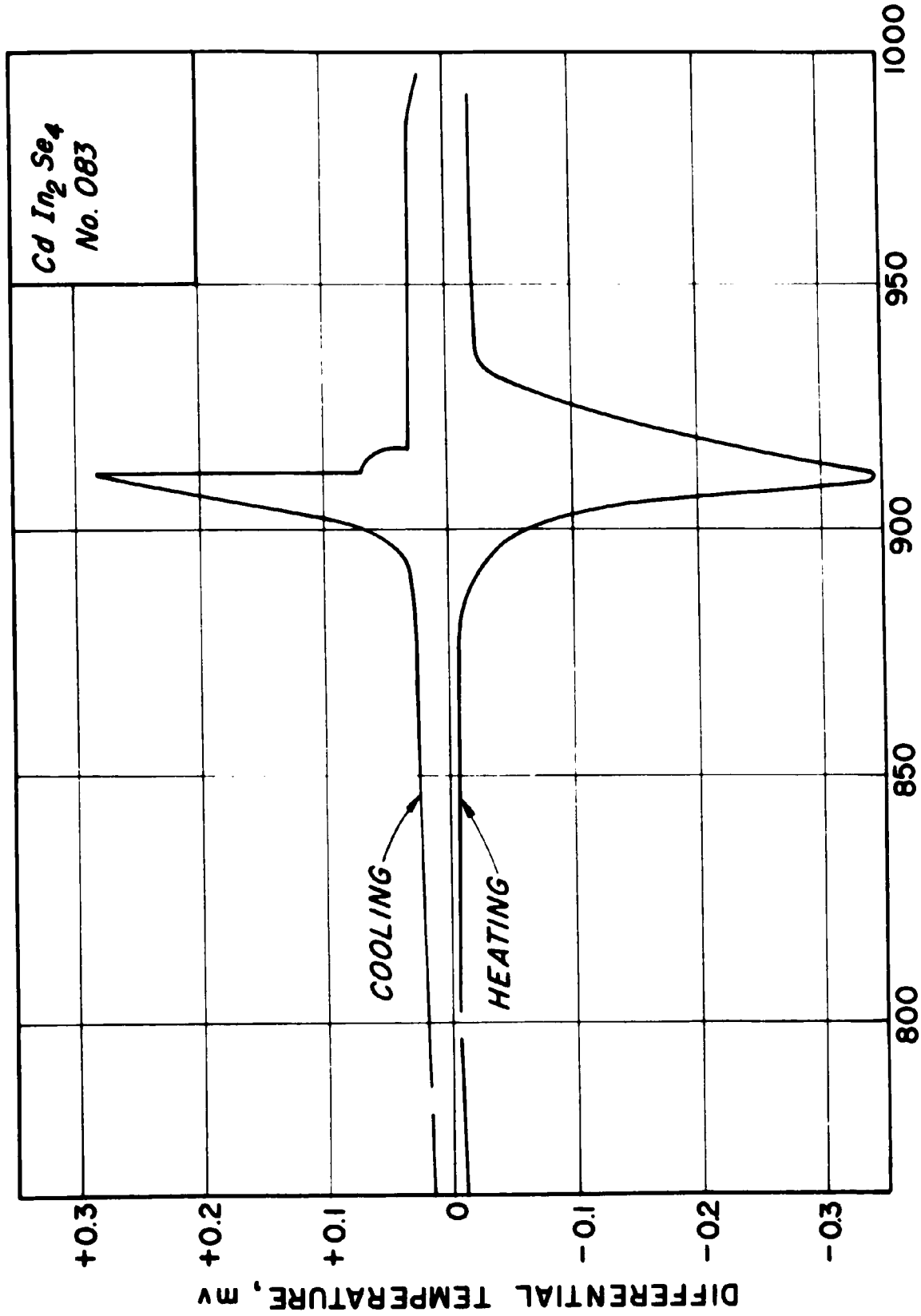


Figure 3. Differential Thermal Analysis Heating and Cooling Curves for Sample Number 083, $CdIn_2Se_4$.

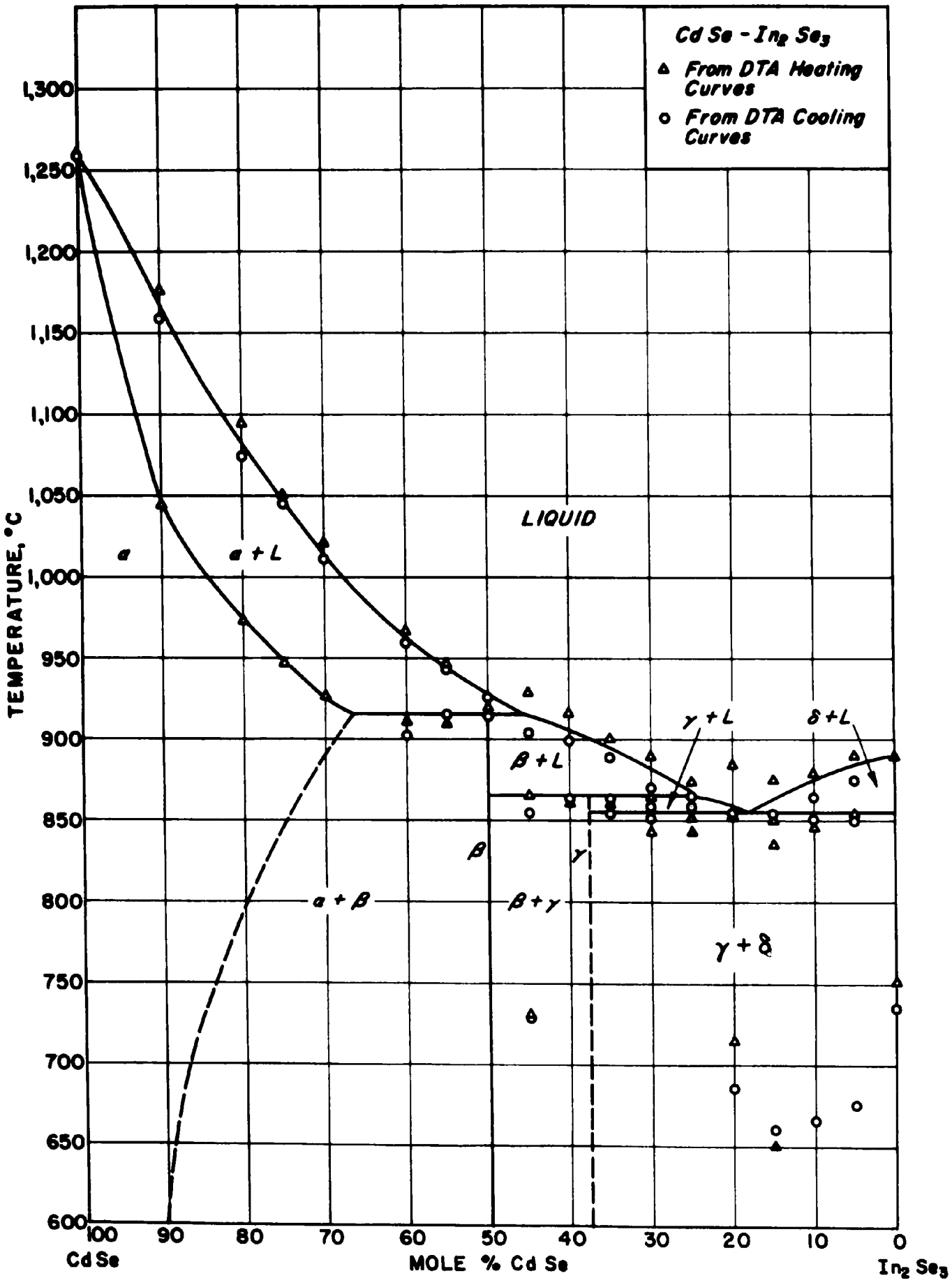


Figure 4. Phase Diagram for the CdSe-In_2Se_3 System.

Results of Electrical Measurements on $CdIn_2Se_4$

The peritectic compound $CdIn_2Se_4$ was separated without inclusions of a second phase in the central region of an ingot which was prepared by normal zone refining the composition 50 mole % CdSe and 50 mole % In_2Se_3. Electrical conductivity measurements were made in a hydrogen atmosphere between 22°C and 830°C on two sections of this ingot, number 083; a plot of $\log\sigma$ vs. $10^3/T$ is shown in Figure 5. Seebeck coefficient data between 49°C and 583°C are shown in Figure 6. The Hall coefficient was about 1.7 $cm.^3$/coulomb at 129°C. This value represents about the lower limit of detection for the measuring system so that the temperature dependence of the Hall coefficient was not measured. The electron Hall mobility at 129°C was 78 $cm.^2$/volt-second, and the electron concentration was $4 \times 10^{18}/cm.^3$

The electrical conductivity of $CdIn_2Se_4$, sample number 083(2A), which is shown in Figure 5, is relatively constant at about 47 mho/cm. between 22°C and 210°C. This indicates that the temperature dependencies of the electron concentration and electron mobility may counterbalance each other. The decrease in conductivity above 210°C can be accounted for by a decrease in electron mobility after complete ionization of some of the impurities. Above 640°C, it is uncertain if the behavior of the electrical conductivity is intrinsic. The slope of $\log\sigma$ vs. $10^3/T$ cannot be represented by a straight line which would make it possible to estimate the energy gap of the compound.

Section 2B of the same sample shows a constant electrical conductivity of about 34 mho/cm. between 20°C and 180°C. This is followed by a sharp decrease to 5 mho/cm. near 315°C, and a gradual increase of electrical conductivity with temperature. The Seebeck coefficient data on Section 2B, which was taken along with the electrical data and are shown in Figure 6, indicate that the compound is still extrinsic at 583°C.

One other sample of n-type $CdIn_2Se_4$ from a similar zone refined

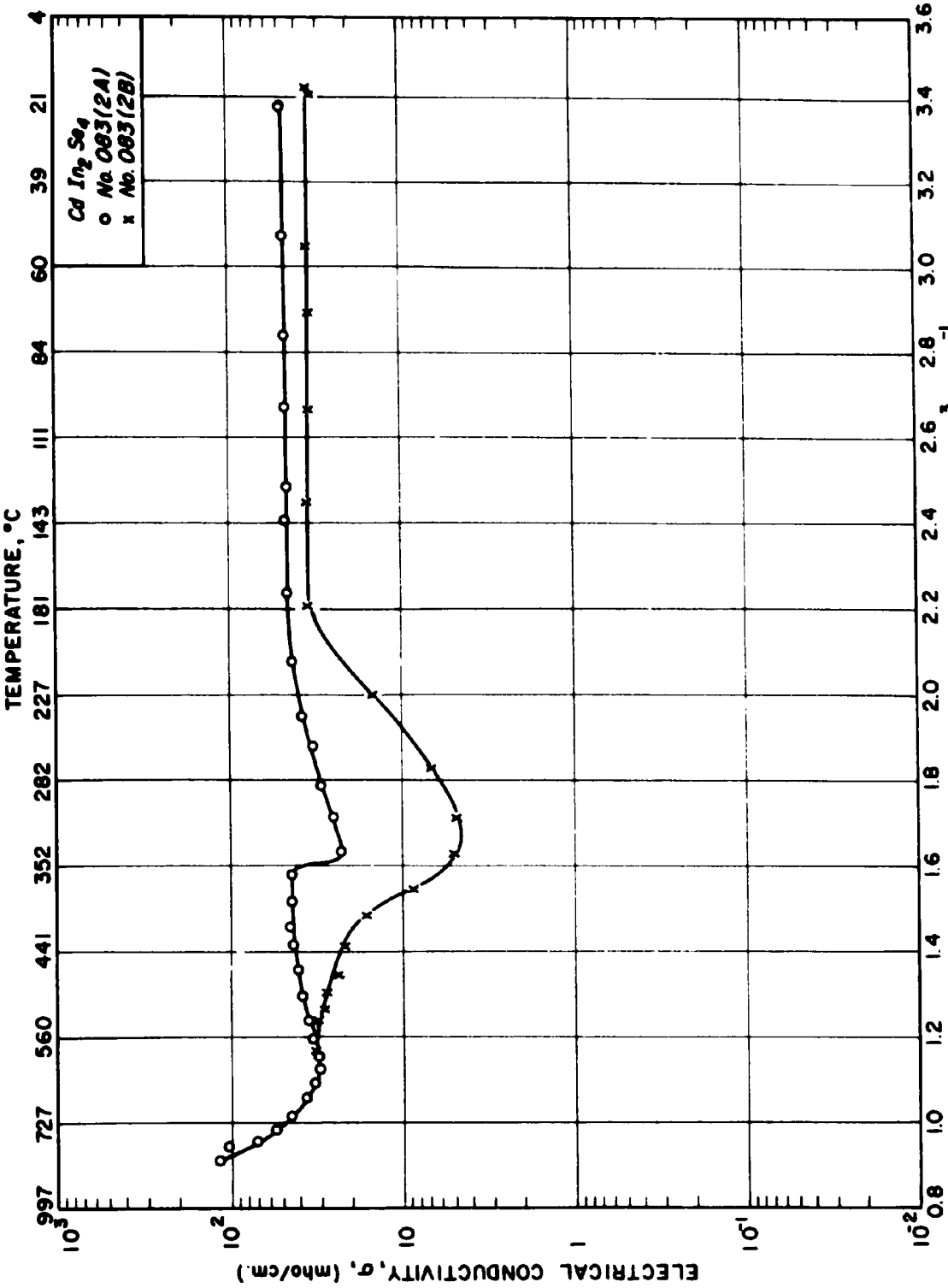


Figure 5. Logarithm of Electrical Conductivity vs. Reciprocal Absolute Temperature for Sample Number 083, $CdIn_2Se_4$.

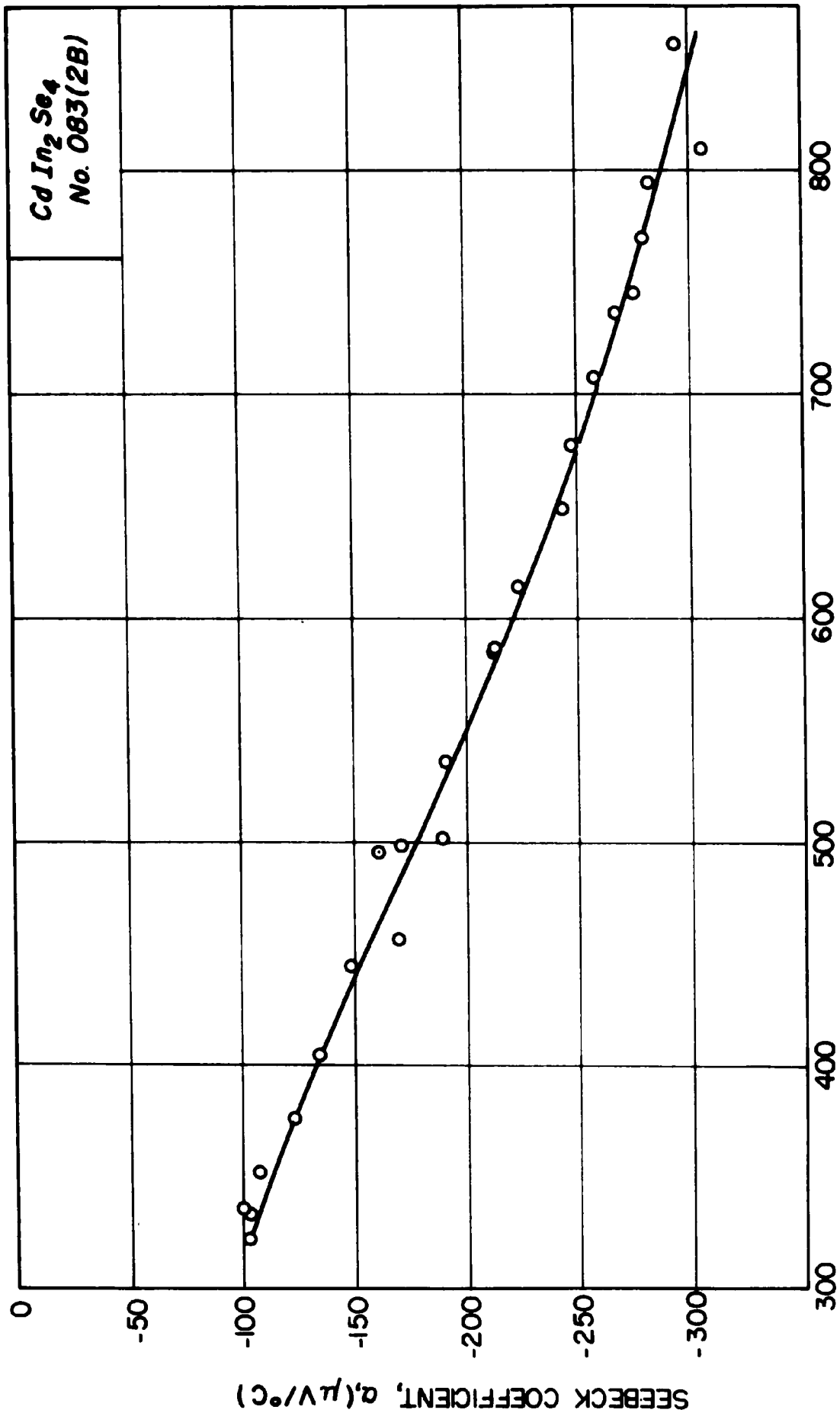


Figure 6. Seebeck Coefficient vs. Absolute Temperature for Sample Number 083, $CdIn_2Se_4$.

ingot, number 079, was tested for electrical conductivity at 20°C. Since the value was 90 mho/cm., no data was taken at higher temperatures. The results on sample number 083 showed that a higher purity (electrical conductivity) than that measured on number 079 would be necessary to determine the intrinsic properties of the compound $CdIn_2Se_4$. It is doubtful if pure samples can be obtained by normal zone refining. Zone leveling techniques offer the promise of pure samples, but the attempts made in this investigation were unsuccessful.

The results of this investigation confirmed the extrinsic electrical conductivity and Hall mobility results reported on $CdIn_2Se_4$ by Kolomiets and Mal'kova.[17] Intrinsic behavior was not observed in this work on electrical measurements, electrical conductivity and Seebeck coefficient, made up to 560°C. The electrical conductivity was almost constant between room temperature and about 200°C.

SEMICONDUCTING PROPERTIES OF PERITECTIC COMPOUNDS FROM THE PSEUDO-BINARY SYSTEM OF CdTe-In_2Te_3.

Introduction

Zone refining and zone leveling techniques were used to obtain samples of the β, γ, and δ-phases in the CdTe-In_2Te_3 system. The CdTe-In_2Te_3 phase diagram is shown in Figure 1; this represents the present interpretation of the phase diagram by D. R. Mason and is slightly modified from that given in reference 10. Electrical conductivity, Hall effect and Seebeck coefficient measurements were made on the γ and δ-phase materials. Electrical conductivity and thermal conductivity results are reported on the β-phase material. The compositions of the single phase materials were established by X-ray analysis and comparison of the lattice parameter measurements with previous measurements on samples throughout the phase diagram.

β-phase Material

Zone leveling of the composition 47 mole % CdTe-53 mole % In_2Te_3, sample number 137, resulted in the separation of single phase material which was identified by X-ray analysis as approximately 45 mole % CdTe-55 mole % In_2Te_3. In the phase diagram, this is the β-phase which has a chalcopyrite structure with a c/a ratio of 2.0.

Electrical conductivity measurements are shown in Figure 7 for two sections, A and B, of number 137. Below 100°C, the samples are p-type. The energy gap obtained from the intrinsic conductivity data above 474°C is 1.37 eV for section A and 1.38 eV for section B. These energy gap values are listed in Table III which summarizes the properties of the materials in the CdTe-In_2Te_3 system.

Thermal conductivity measurements on a section of sample number 137 resulted in values of 0.011 (±0.001) watts/cm°C between 60°C and 300°C. The thermal conductivity sample contained some second phase material; but it should give a reasonable indication of the actual thermal conductivity of the β-phase material.

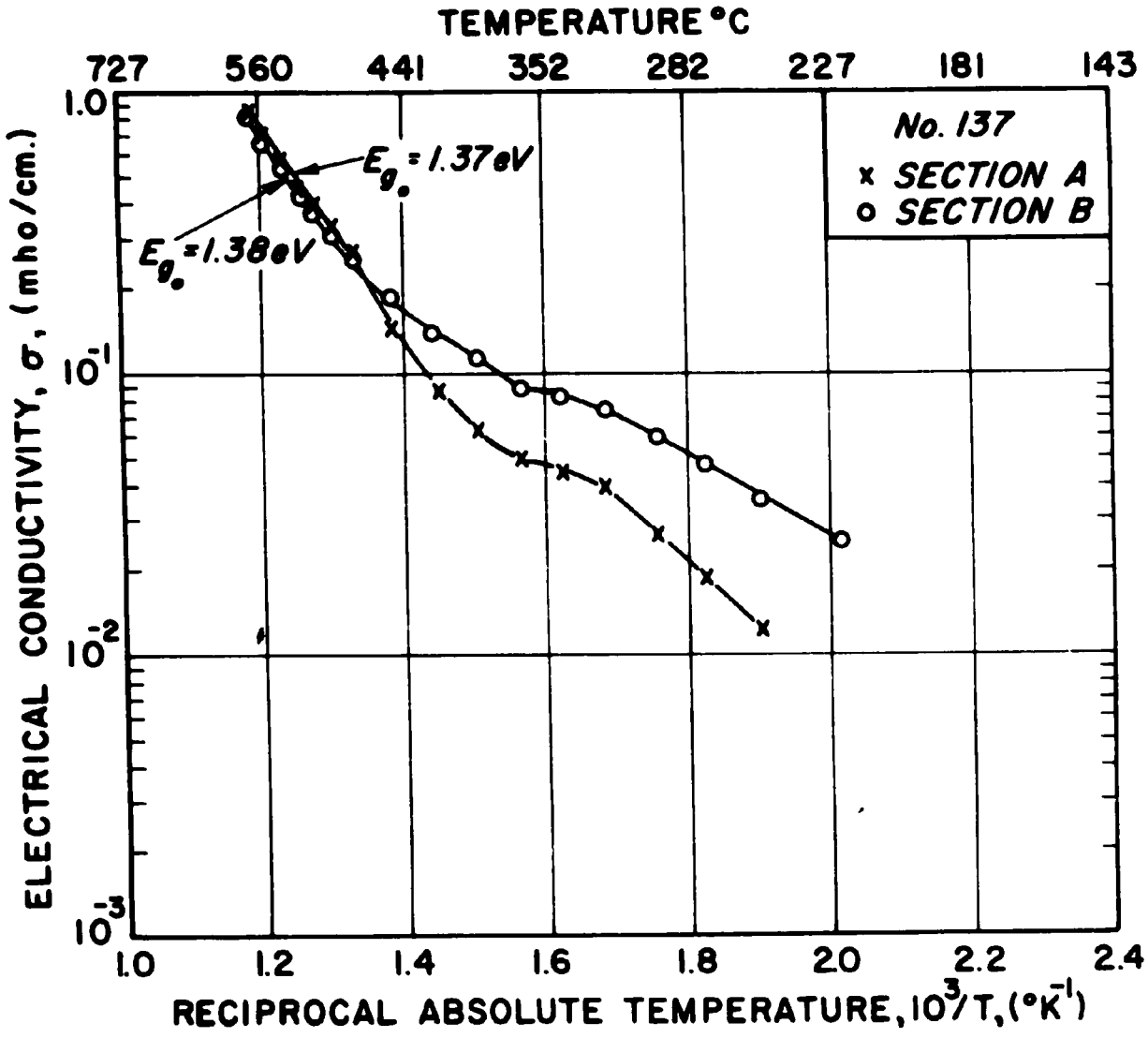


Figure 7. Logarithm of Electrical Conductivity vs. Reciprocal Absolute Temperature for β-phase Material, Sample Number 137, from the CdTe-In_2Te_3 System.

TABLE III

ELECTRICAL PROPERTIES OF PERITECTIC MATERIALS FROM THE CdTe - In_2Te_3 SYSTEM

Sample Number	Composition	Lattice Parameter a_o	Energy Gap ($\log \sigma$ vs. $10^3/T$)		Energy Gap ($\log R_H T^{3/2}$ vs. $10^3/T$)		Temperature Dependence of Hall Mobility $\mu_{H,n} = \mu_{300}(T/300)^{\gamma}$		
			E_{g_o}, eV	Temp. Range of Data	E_{g_o}, eV	Temp. Range of Data	μ_{300}	γ	Temp. Range of Data
137A	β-phase	6.217Å < a_o < 6.220Å	1.37	474°C to 567°C					
137B	β-phase	6.217Å < a_o < 6.220Å	1.38	475°C to 568°C					
169(2)	γ-phase	6.194Å	1.09	437°C to 581°C					
150(4)	γ-phase	6.185Å	0.98	234°C to 565°C	0.98	196°C to 491°C	140	-1.7	177°C to 491°C
151(4)	γ-phase	6.185Å	1.02	276°C to 567°C	1.10	335°C to 529°C	240	-2.1	335°C to 529°C
169(3)	δ-phase	6.177Å	1.18	331°C to 641°C	1.15	331°C to 479°C	80	-1.1	250°C to 479°C

γ-phase Material

The γ-phase, which is approximately 20 mole % CdTe-80 mole % In_2Te_3, $CdIn_8Te_{13}$, was obtained from regions of two zone leveled ingots which had an initial composition of 10 mole % CdTe-90 mole % In_2Te_3. The X-ray results on these regions, section 4 of sample 150 and section 4 of 151, showed a zinc blende type cubic structure with a lattice parameter, a_o, equal to 6.185 Å for both samples. Normal zone refining of ingot number 169, which had an initial composition of 17 mole % CdTe-83 mole % In_2Te_3, also produced some γ-phase material (section 2) with a lattice parameter, a_o of 6.194 Å and some weak diffraction lines which were not characteristic of a cubic structure. The difference in lattice parameter values between number 169(2) and the two exactly identical samples, 150(4) and 151(4), may be accounted for by a slight difference in composition of less than 1%, and by ordering.

The electrical conductivity data for samples 150(4), 151(4), and 169(2) are shown in Figure 8. The energy gaps obtained from the slope of the log σ vs. $10^3/T$ data are: 0.98 eV for 150(4); 1.02 eV for 151(4); and 1.09 eV for 169(2). Both 150(4) and 151(4) are intrinsic before 280°C, whereas 169(2) has a high impurity level as evidenced by the characteristics of the conductivity data. At low temperatures, 169(2) is p-type and in the region of 250°C it is n-type. Intrinsic conduction does not appear below about 440°C. The results obtained from electrical conductivity measurements on the γ-phase material are listed in Table III.

The results of Hall coefficient measurements on samples (150(4) and 151(4) are shown in Table IV. The energy gaps calculated from the slope of the log $R_H T^{3/2}$ vs. $10^3/T$ data in Figure 9 are 0.98 eV for 150(4) and 1.10 eV for 151(4). This is in adequate agreement with the values obtained from electrical conductivity data. At the lowest temperatures for which intrinsic Hall coefficient data are available on the γ-phase, the carrier concentrations, n_i, obtained from Equation (13) are $4 \times 10^{14}/cm^3$ at 196°C for 150(4) and $8 \times 10^{15}/cm^3$ at 335°C for 151(4).

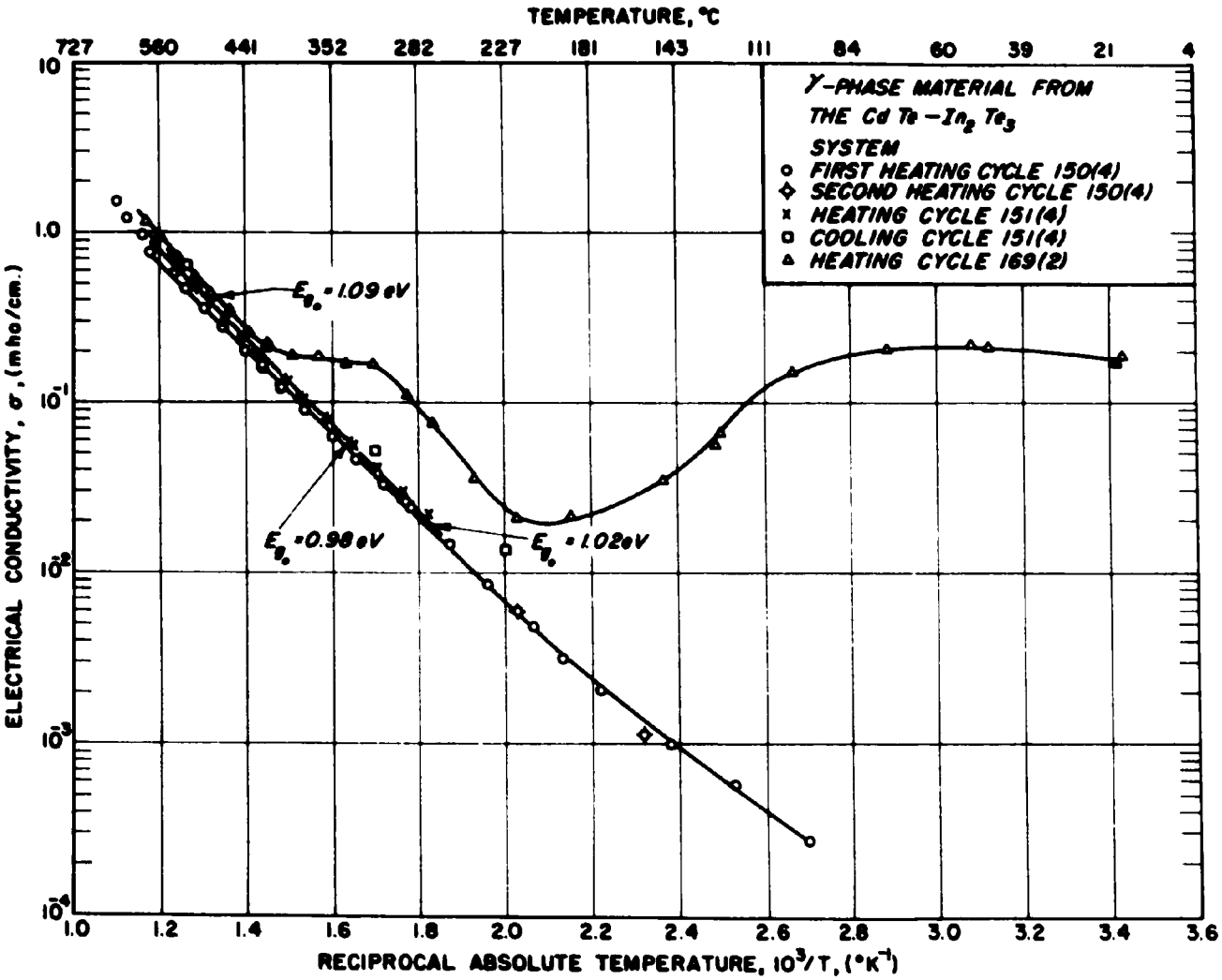


Figure 8. Logarithm of Electrical Conductivity vs. Reciprocal Absolute Temperature for the γ-phase Material, Sample Numbers 150 (4), 151 (4), and 169 (2), from the CdTe-In_2Te_3 System.

TABLE IV.

HALL COEFFICIENT AS A FUNCTION OF TEMPERATURE

FOR THE γ-PHASE IN THE CdTe-In_2Te SYSTEM

Sample Number 150(4)		Sample Number 151(4)	
Temperature T, °K	Hall Coefficient R_H, cm^3/coulomb	Temperature T, °K	Hall Coefficient R_H, cm^3/coulomb
450	-26000	609	-1090
451	-30500	608	-838
470	-19200	630	-605
470	-17500	630	-518
484	-12200	654	-534
484	-11400	654	-380
509	-5730	670	-327
509	-6630	670	-323
534	-3280	697	-223
535	-3520	698	-208
561	-1930	714	-163
561	-2010	715	-157
581	-1530	739	-127
581	-1580	739	-114
604	-775	756	-92.0
604	-1050	756	-89.7
625	-621	777	-68.0
625	-657	777	-66.4
650	-590	802	-51.0
650	-615	802	-45.6
674	-258		
673	-318		
696	-198		
696	-206		
714	-140		
713	-141		
740	-103		
740	-112		
764	-75.7		
764	-81.3		

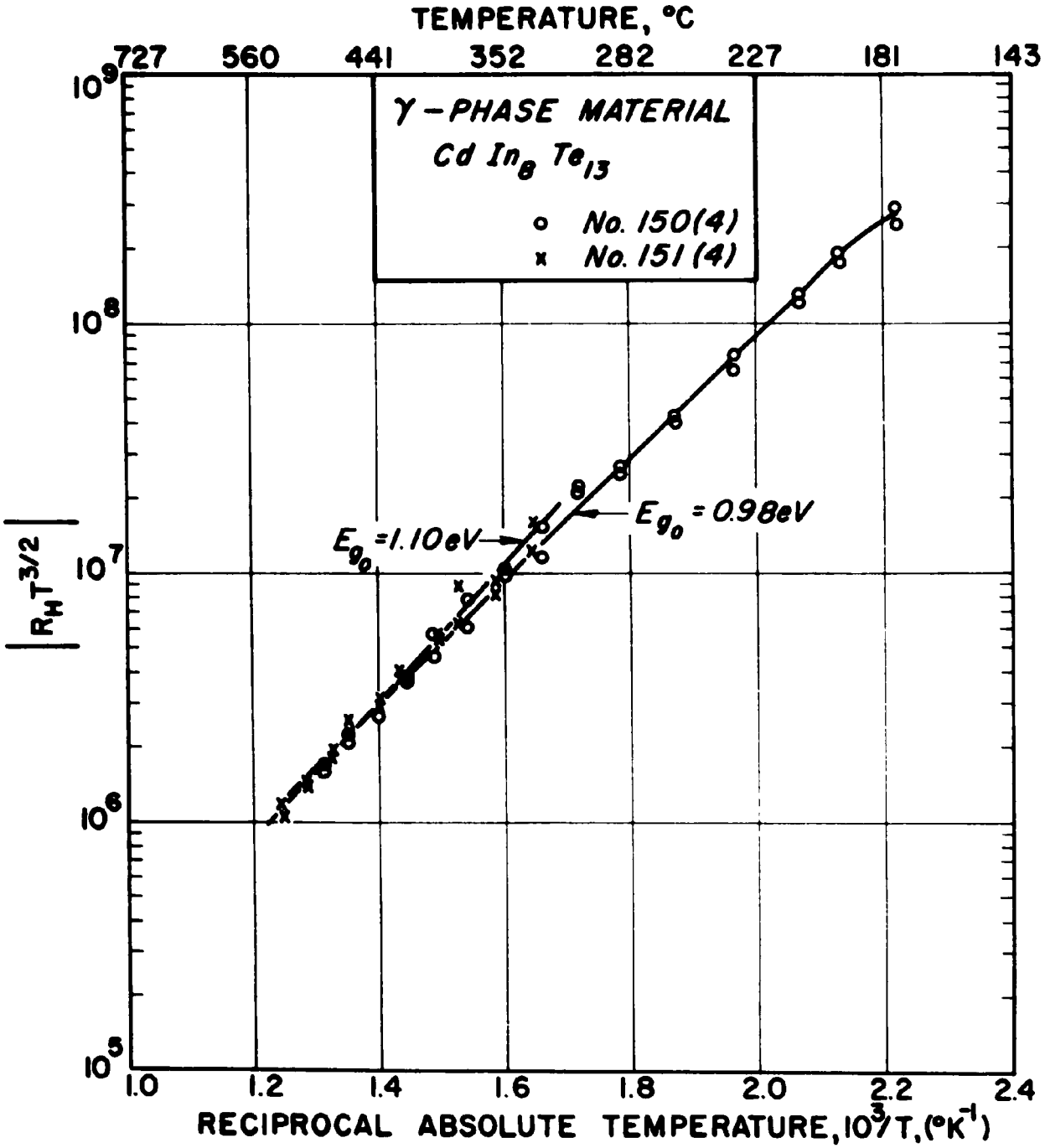


Figure 9. Logarithm of $|R_H T^{3/2}|$ vs. Reciprocal Absolute Temperature for the γ-phase Material, Sample Numbers 150 (4) and 151 (4), from the CdTe-In_2Te_3 System.

The Hall mobility, which is designated as $|R_H\sigma|$ or as $\mu_{H,n}$, is plotted as a function of the logarithm of absolute temperature for 150(4) and 151(4) in Figure 10. The temperature dependence of the Hall mobility in the expression $\mu_{H,n} \propto T^{\gamma}$ was -1.7 for 150(4) and -2.1 for 151(4); the standard deviations of the γ values were 0.11 and 0.25 units for 150(4) and 151(4), respectively. An alternate expression for the Hall mobility temperature dependence is $\mu_{H,n} = \mu_{300}(T/300)^{\gamma}$. If the Hall mobility data can be extrapolated to 300°K, then μ_{300} represents the mobility of the material at 300°K. The values of μ_{300} are 140 cm^2/v sec. for 150(4) and 240 cm^2/v sec. for 151(4).

Seebeck coefficient data as a function of temperature for 150(4) and 151(4) are plotted in Figure 11. Both samples are intrinsic above 250°C. The plot of Seebeck coefficient against reciprocal absolute temperature shown in Figure 12 was used to determine the value of m in Equation (27), $\alpha = m/T + c$, which permits the calculation of the electron-to-hole mobility ratio, b, from Equation (28). This assumes that the spherical energy band approximation is valid and that lattice scattering predominates. The values of m were -878 mv and -547 mv for 150(4) and 151(4), respectively; however, these values result in a negative mobility ratio which implies that the theory does not hold. It is clear from the Seebeck coefficient data that the electron mobility is larger than the hole mobility in the intrinsic conduction temperature range.

δ-phase Material

The single phase material from section 3 of zone refined ingot number 169 was found to have a lattice parameter, a_o, of 6.177 Å which means the material is in the δ-phase with a composition of about 9 mole % CdTe-91 mole % In_2Te_3. This phase has a zinc blende type cubic structure.

Electrical conductivity results on sample number 169(3) are shown in Figure 13. The energy gap calculated from the slope of log σ vs. $10^3/T$ in the intrinsic region above 330°C was 1.18 eV. The Hall

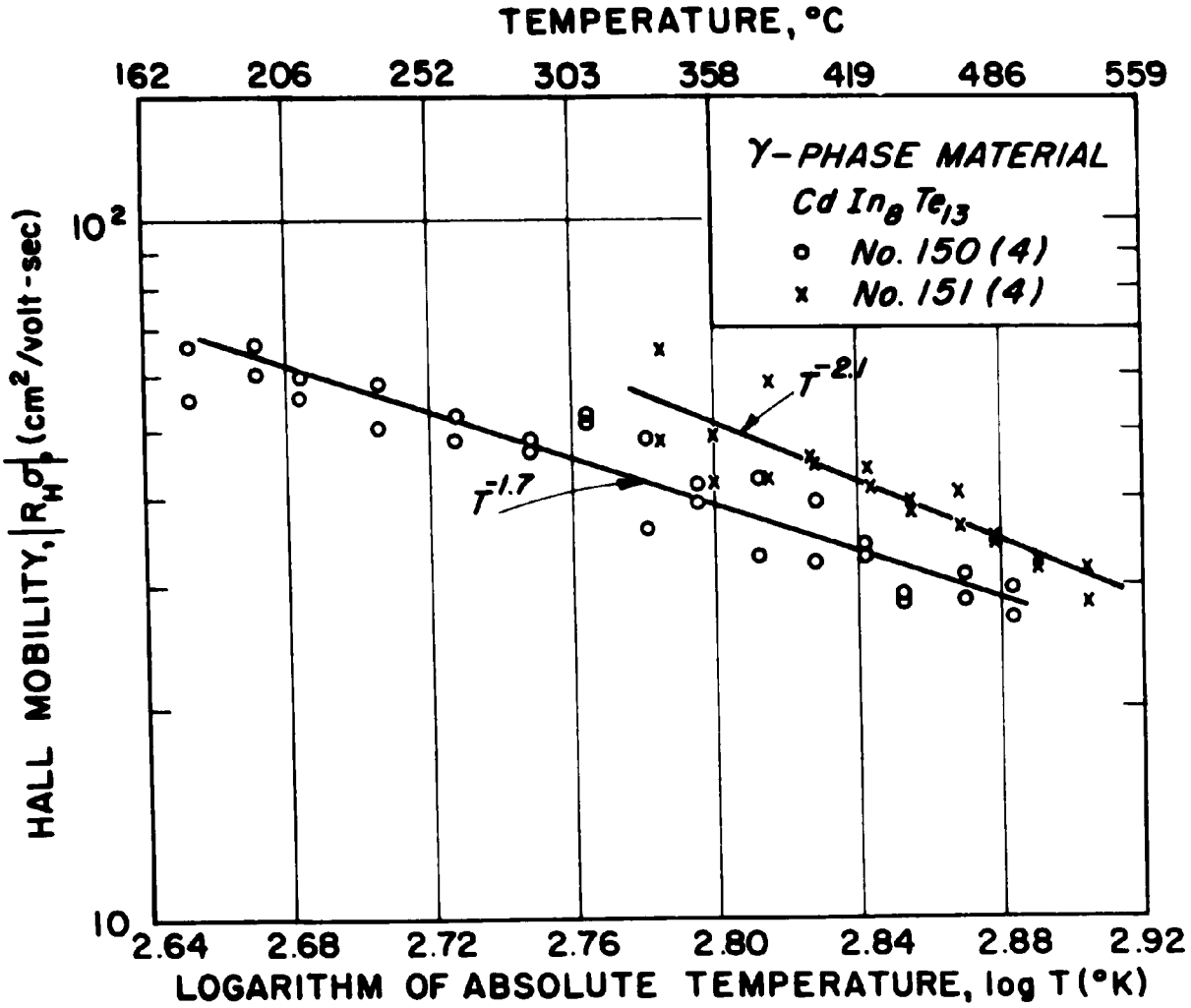


Figure 10. **Logarithm of Hall Mobility vs. Logarithm of Absolute Temperature for the γ-phase Material, Sample Numbers 150 (4) and 151 (4), from the $CdTe-In_2Te_3$ System.**

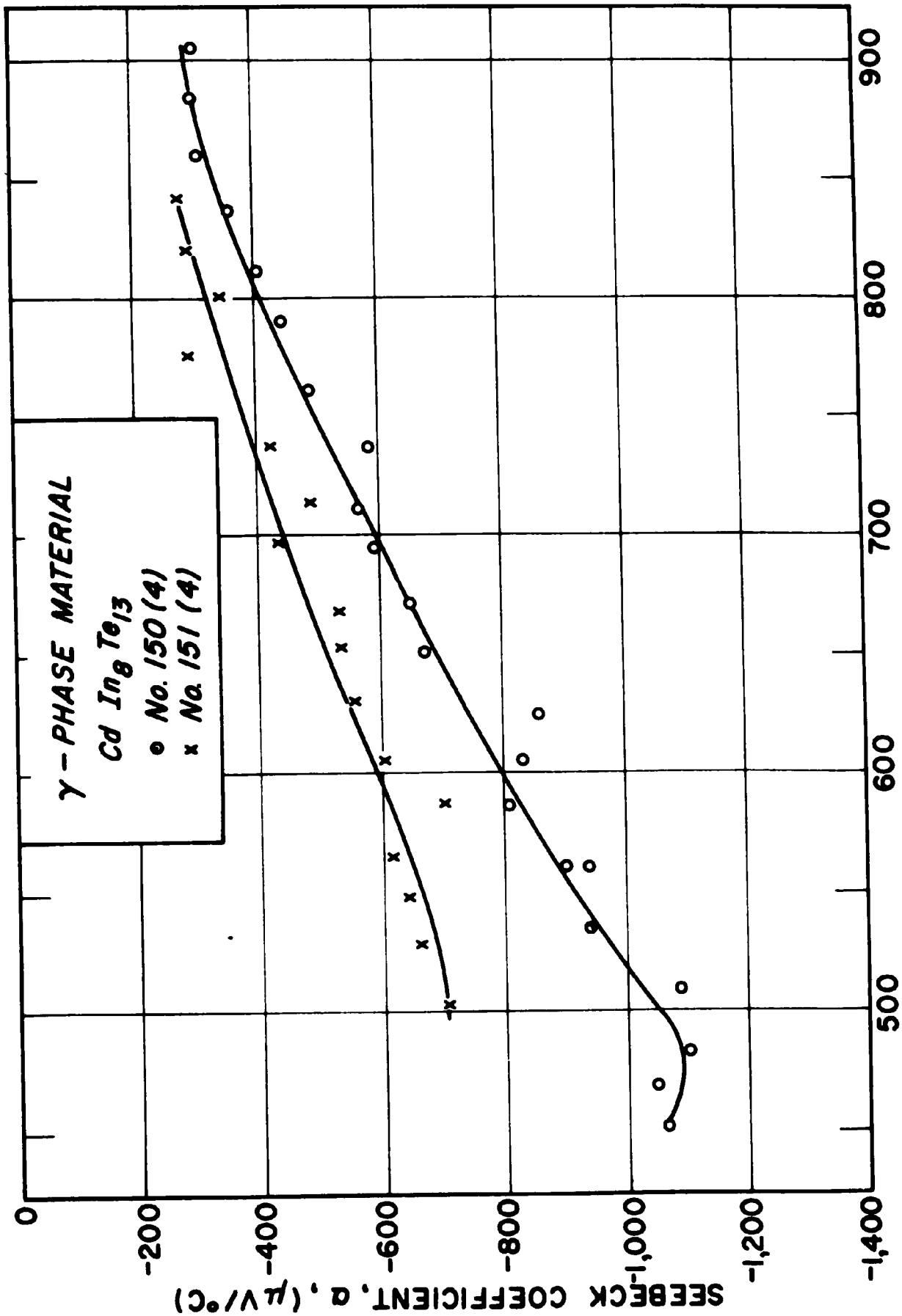


Figure 11. Seebeck Coefficient vs. Absolute Temperature for the γ-phase Material, Sample Numbers 150 (4) and 151 (4), from the CdTe-In_2Te_3 System.

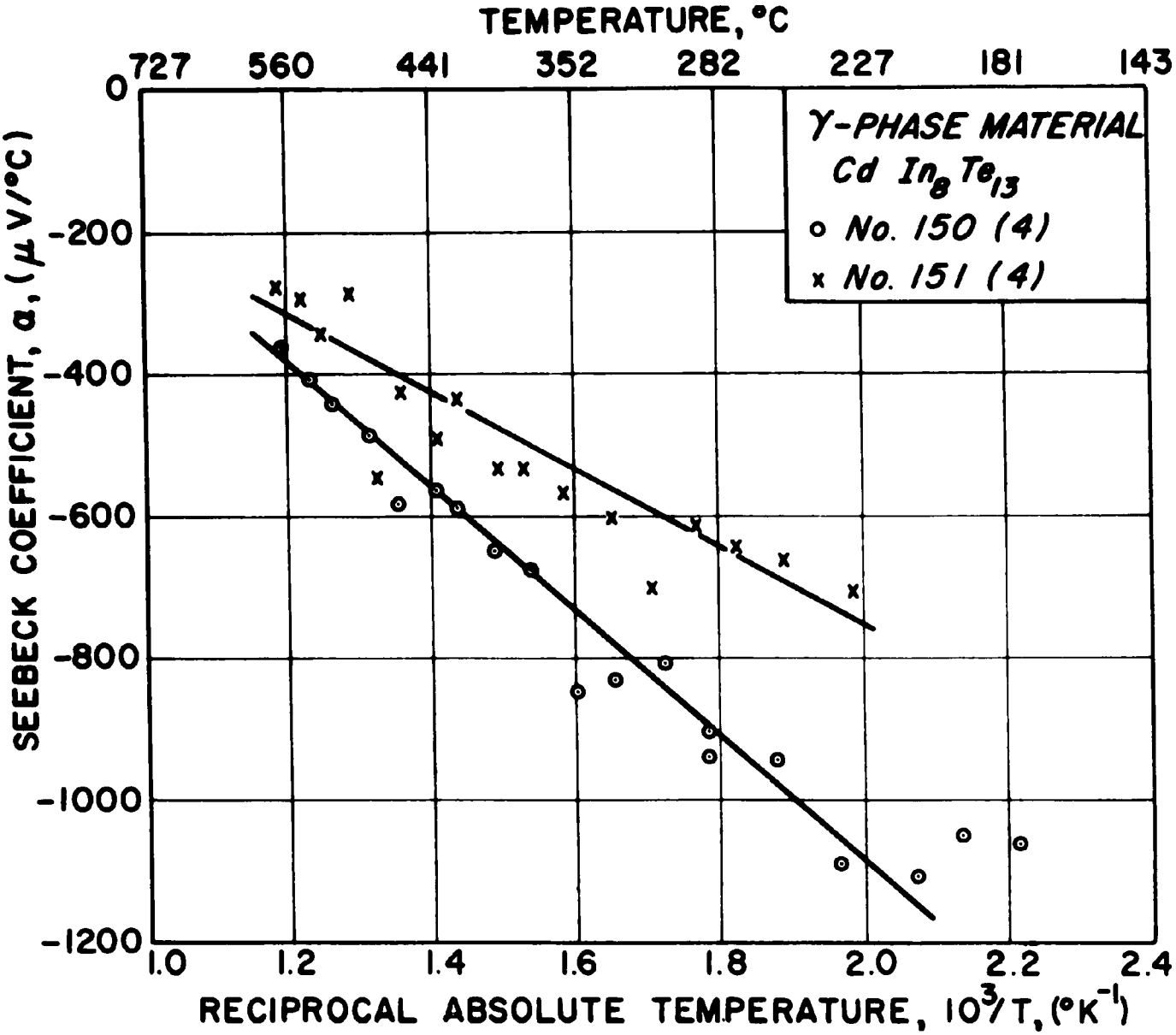


Figure 12. Seebeck Coefficient vs. Reciprocal Absolute Temperature for the γ-phase Material, Sample Numbers 150 (4) and 151 (4), from the CdTe-In_2Te_3 System.

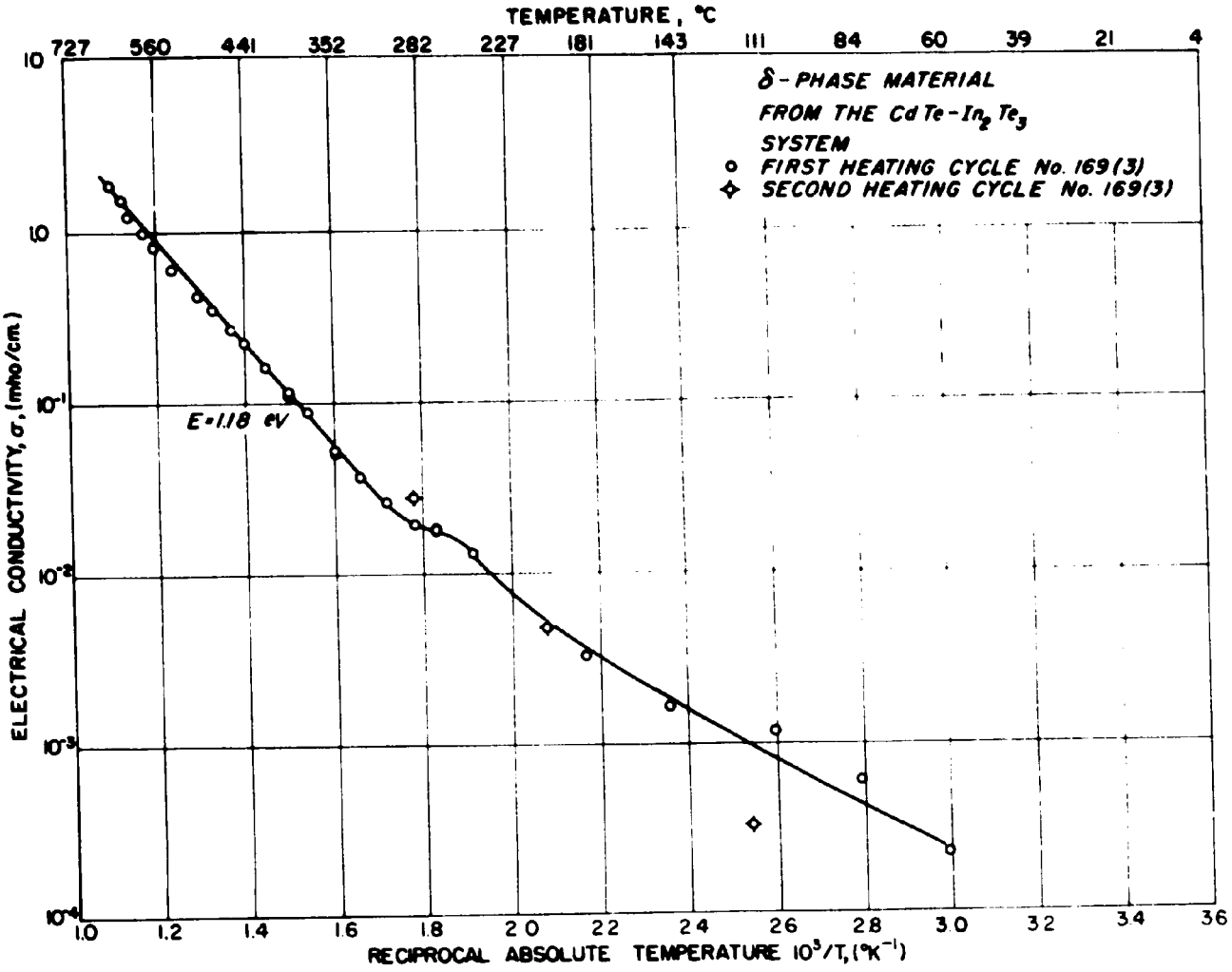


Figure 13. Logarithm of Electrical Conductivity vs. Reciprocal Absolute Temperature for the δ-phase Material, Sample Number 169 (3), from the CdTe-In_2Te_3 System.

coefficient values for the δ-phase material between 250°C and 479°C are shown in Table V. The energy gap calculated from the slope of the log $R_H T^{3/2}$ vs. $10^3/T$ data in Figure 14 was 1.15 eV. The intrinsic carrier concentration, n_i, calculated from Equation (13) is $7 \times 10^{15}/cm^3$ at 331°C.

The Hall mobility for this material is plotted in Figure 15 as a function of the logarithm of the absolute temperature. The temperature dependence of $\mu_{H,n}$ is $T^{-1.1}$, and the standard deviation of the power term is 0.16 units. By extrapolation, the Hall mobility at 300°K is 80 cm^2/v sec. The results of electrical measurements on the δ-phase are summarized in Table III.

The Seebeck coefficient as a function of temperature is shown in Figure 16 for sample number 169(3). The material becomes intrinsic near 330°C. The slope of the Seebeck coefficient versus reciprocal absolute temperature was determined from Figure 17. Again, the large value of m in the expression $\alpha = m/T + c$ does not permit an estimation of the electron-to-hole mobility ratio. Although the model apparently does not apply, the sign of the Seebeck coefficient does say that the electron mobility is higher.

Discussion of the Semiconducting Properties of Materials from the CdTe - In_2Te_3 System

No basic change in crystal structure is observed in going from In_2Te_3 to the δ-phase sample in the CdTe - In_2Te_3 system which is shown in Figure 1. In_2Te_3 has a zinc blende or antifluorite structure[32] and contains a large number of vacancies in the indium sublattice. The δ-phase sample is about 9 mole % CdTe - 91 mole % In_2Te_3 and has a zinc blende cubic type structure. The defect structure of In_2Te_3 results in a low carrier mobility and low thermal conductivity. Zhuze[33] found the room temperature mobility of In_2Te_3 to be between 5 cm^2/volt-second and 70 cm^2/volt-second, and it was independent of temperature between about 300°K and 650°K. The δ-phase material

TABLE V.

HALL COEFFICIENT AS A FUNCTION OF TEMPERATURE

FOR THE δ-PHASE IN THE CdTe-In_2Te SYSTEM

Sample Number 169(3)

Temperature T, °K	Hall Coefficient R_H, cm^3/coulomb	Temperature T, °K	Hall Coefficient R_H, cm^3/coulomb
523	-3440	648	-454
523	-3530	648	-442
547	-2370	667	-331
547	-2480	666	-287
561	-2030	690	-230
561	-2030	690	-184
583	-1510	714	-164
583	-1540	714	-118
604	-1060	730	-138
604	-1010	729	-100
623	-697	752	-93.6
623	-667	752	-76.7

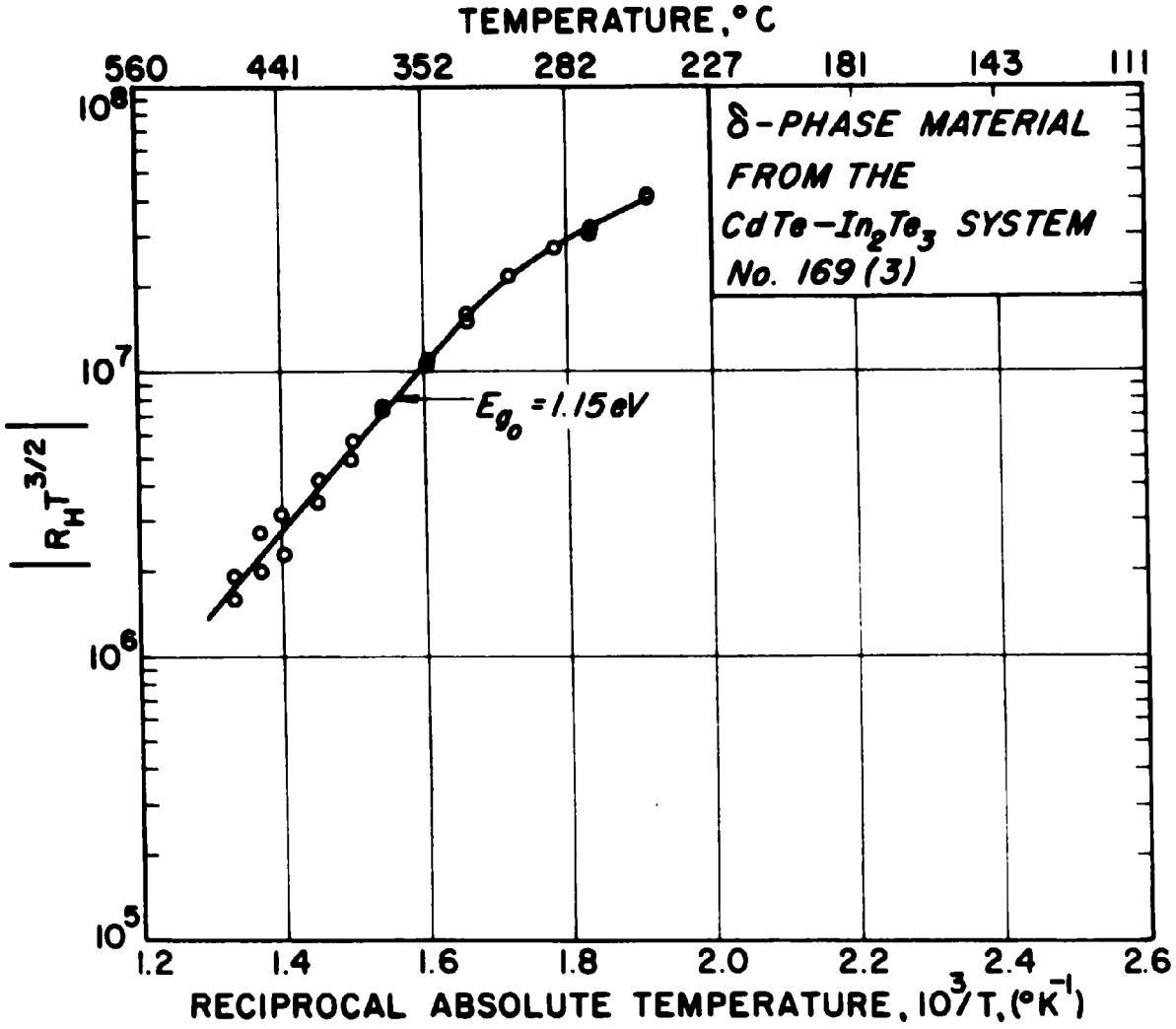


Figure 14. Logarithm of $|R_H T^{3/2}|$ vs. Reciprocal Absolute Temperature for the δ-phase Material, Sample Number 169 (3), from the CdTe-In_2Te_3 System.

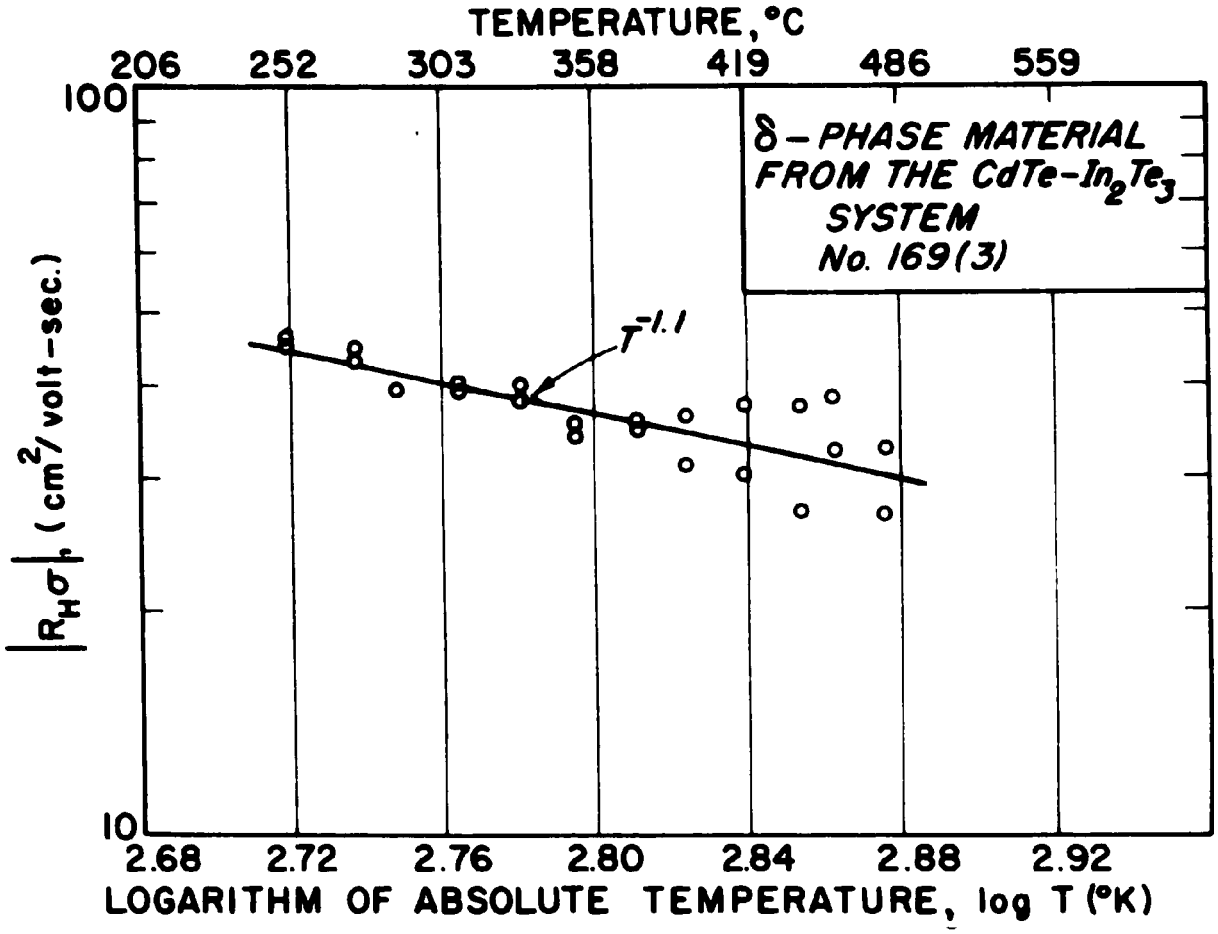


Figure 15. Logarithm of Hall Mobility vs. Logarithm of Absolute Temperature for the δ-phase Material, Sample Number 169 (3), from the $CdTe-In_2Te_3$ System.

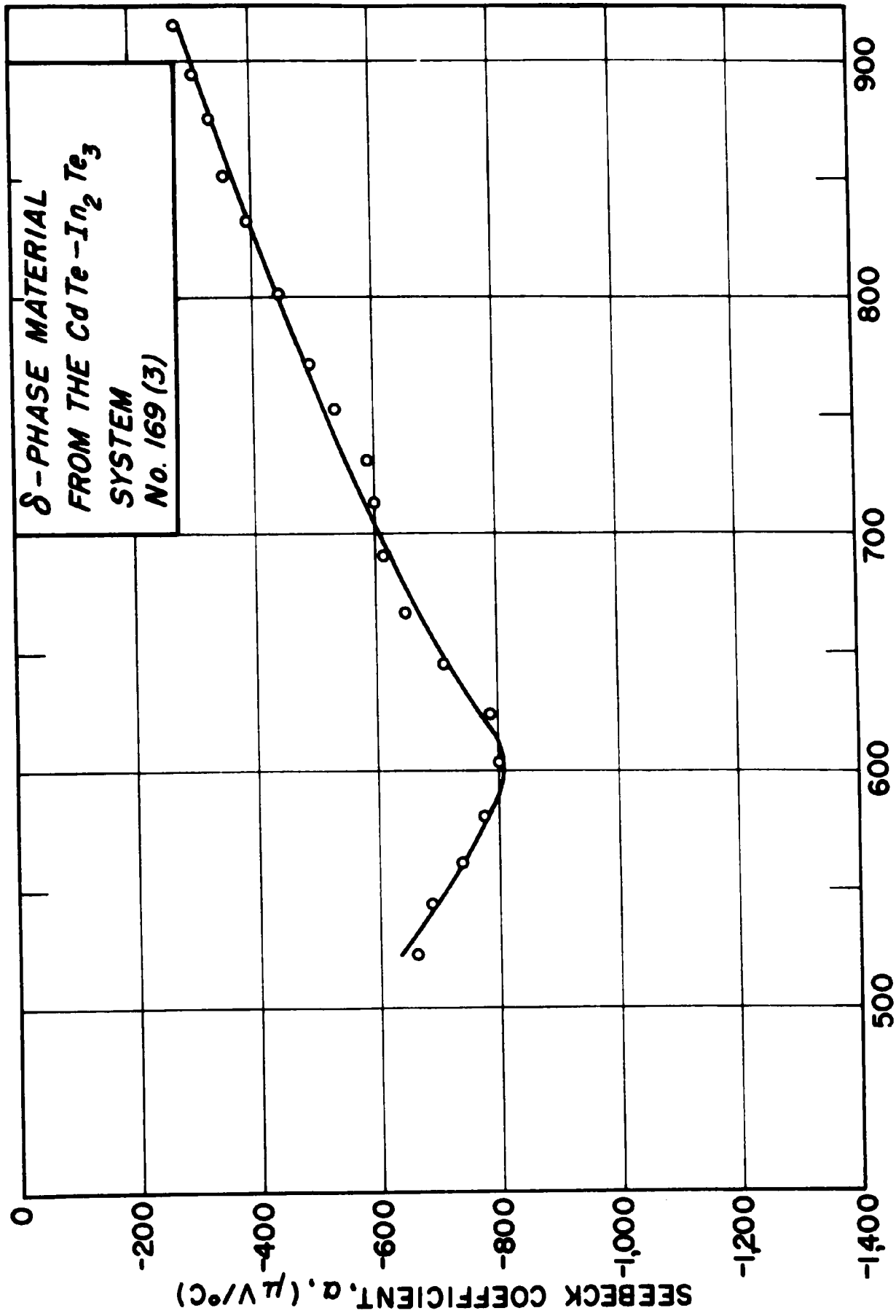


Figure 16. Seebeck Coefficient vs. Absolute Temperature for the δ-phase Material, Sample Number 169 (3), from the CdTe-In_2Te_3 System.

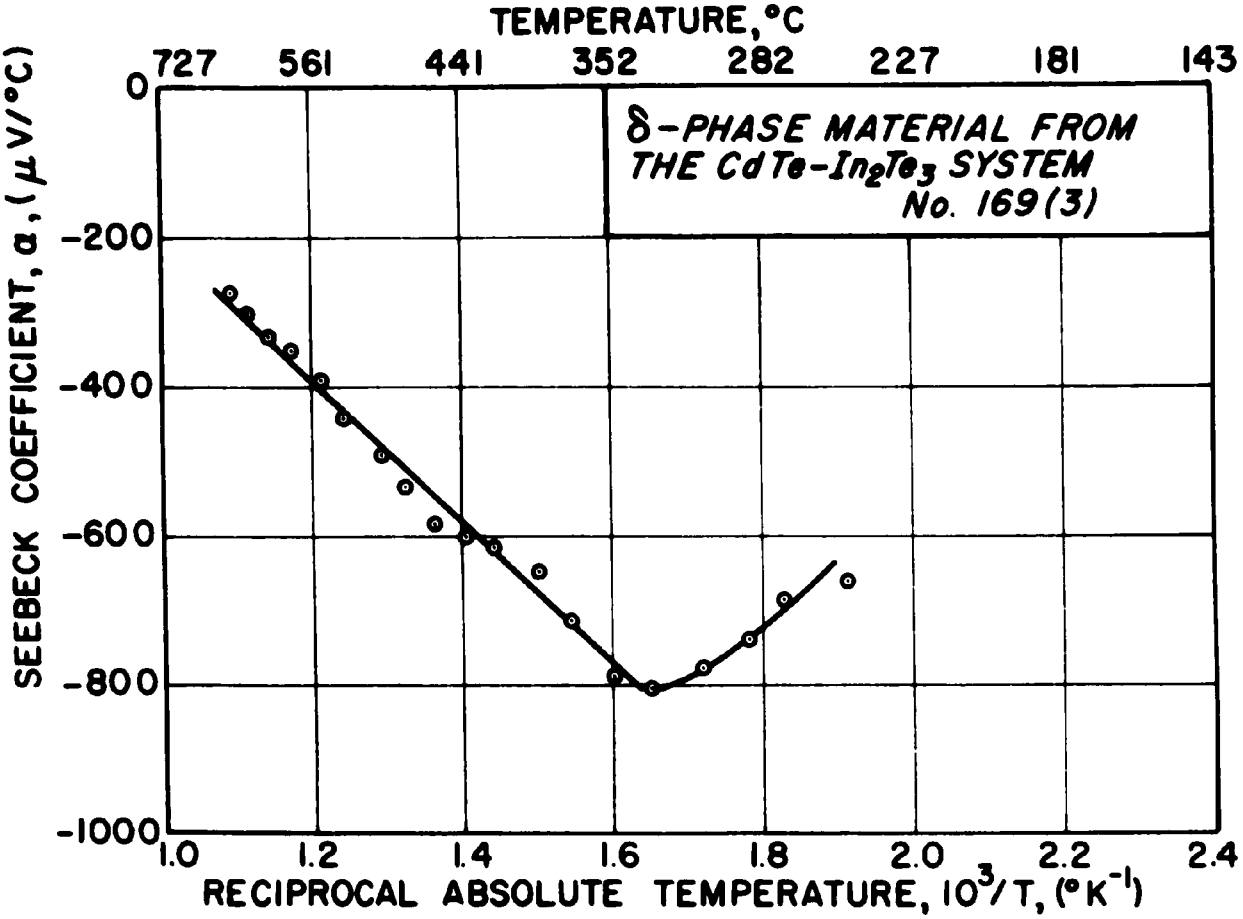


Figure 17. Seebeck Coefficient vs. Reciprocal Absolute Temperature for the δ-phase Material, Sample Number 169 (3), from the CdTe-In_2Te_3 System

has an electron mobility near 80 cm^2/volt-second at 300° K and a temperature dependence for the mobility of $T^{-1.1}$ between 500° K and 750° K. This temperature dependence may be a combination of scattering by neutral centers which is independent of temperature and lattice type scattering which has a=3/2 power dependence.

The energy gap for In_2Te_3 at 0° K is 1.12 eV[33]; this is very close to the value of 1.17 (± 0.05) eV obtained for the δ-phase material. The γ-phase, $CdIn_8Te_{13}$, has a lower energy gap, 1.02 (± 0.10) eV, a slightly higher electron mobility, and a greater dependence of mobility on temperature. The β-phase material, which is in the center region of the CdTe-In_2Te_3 system, has an energy gap of 1.38 eV.

The energy gap of the β-phase is almost midway between the reported values of 1.56 eV for CdTe[34] and 1.12 eV for In_2Te_3.[33] The temperature dependence of the energy gap for the β-phase can be estimated by a comparison of the energy gap obtained from electrical conductivity measurements in this investigation and the optical energy gap at room temperature reported by Edwards[14] for $CdIn_2Te_4$ which is also β-phase. Edwards found a value of 1.08 eV; this means the temperature dependence is about -1×10^{-3} eV/° K.

CdTe has the same zinc blende crystal structure as In_2Te_3, but there are no vacancies in the cadmium sublattice. Zaslavskii[35] reported the thermal conductivity for both binary compounds at 300° K: 0.011 watts/cm. °C for ordered In_2Te_3, and 0.063 watts/cm. °C for CdTe. The low value for In_2Te_3 is attributed to the defect structure. Measurements on the β-phase material showed a thermal conductivity of 0.011 watts/cm. °C at 330° K; this is identical to the ordered In_2Te_3.

THE PHASE DIAGRAM BEHAVIOR OF THE PSEUDO-BINARY SYSTEM OF Ag_2Te-In_2Te_3 AND THE SEMICONDUCTING PROPERTIES OF $AgIn_3Te_5$.

Introduction

A review will be given of the published literature on compositions in the Ag_2Te-In_2Te_3 pseudo-binary phase diagram. In addition, the results of differential thermal analysis (DTA) measurements on certain compositions in this system will be presented. These led to the location of the congruently melting compound $AgIn_3Te_5$. Electrical conductivity, Hall effect, Seebeck coefficient, thermal conductivity, and melting point were measured on zone refined, polycrystalline samples of this compound.

Literature Review

Previous work on the Ag_2Te - In_2Te_3 system consists of studies on Ag_2Te, In_2Te_3, and six compositions within the phase diagram. The properties of $AgInTe_2$, which is 50 mole % Ag_2Te-50 mole % In_2Te_3, have also been reported; these are crystal structure, energy gap, electrical conductivity, carrier type, and melting point.

Hansen[36] reported the melting point of Ag_2Te as 959°C and a solid-solid transition at 135°C. In_2Te_3 has a melting point of 667°C and an order-disorder reaction near 600°C, according to Grochowski and Mason.[37]

Hahn, et al.[1] reported the following lattice parameter values for compositions in the Ag_2Te-In_2Te_3 system: c = 12.38, a = 6.19 at 9 and 20 mole % Ag_2Te; c = 12.53, a = 6.36 at 33 mole % Ag_2Te_3; c = 12.54, a = 6.37 at 43 mole % Ag_2Te; c = 12.55, a = 6.41 at 50 mole % Ag_2Te; and c = 12.56, a = 6.41 at 57 mole % Ag_2Te. At the low Ag_2Te end of the phase diagram, the crystal structure is chalcopyrite with a c/a ratio of 2.00, and at higher Ag_2Te content, the same structure type was observed with a c/a ratio of 1.91. Hahn made no attempt to describe the phase diagram.

Austin, Goodman, and Pengelly[18] zone refined $AgInTe_2$ and

obtained an energy gap of 0.96 eV from infrared measurements on the material. They reported evidence of thermal disordering above 400°C. Zhuze, Sergeeva, and Shtrum[19] investigated the composition $AgInTe_2$ and found only one phase with X-ray analysis. The crystal structure was chalcopyrite, and the material melted at 680°C. Measurements on cast polycrystalline samples indicated an energy gap of 0.95 eV from electrical conductivity results and an optical energy gap of 0.93 eV. The room temperature electrical conductivity of an n-type sample was 0.78 mho/cm. An irreversible volume change was reported above 550°C.

Phase Diagram Study

Differential Thermal Analysis Results

This investigation began with differential thermal analysis (DTA) measurements at the following compositions in the phase diagram of Ag_2Te-In_2Te_3: 0, 17, 20, 25, 40, 50, 60, and 80 mole % Ag_2Te. The heating and cooling curves obtained by DTA are shown in Figure 18. The samples for DTA were cooled from the liquid state, after fusion of the elements, by quenching in either air or a water bath. The material was then rebottled in a DTA tube and annealed under the conditions shown in Table VI. The exception to this procedure is the In_2Te_3 which was obtained by zone refining.

The liquidus, solid-liquidus, and solid-solid transformation temperatures are listed in Table VI. The cooling curve for the 17 mole % Ag_2Te composition shown in Figure 18 indicates solidification beginning at 697°C. An incomplete heating curve was also obtained showing two peaks in the region of 686°C to 710°C. The 20 mole % Ag_2Te begins to melt near 664°C and the principal heat effect occurs at about 700°C. Solidification starts at 692°C. The heating and cooling curves for the 25 mole % Ag_2Te are characteristic of a congruently melting compound at 699 (± 3)°C.

The 40 mole % Ag_2Te shows a series of solid-solid type re-

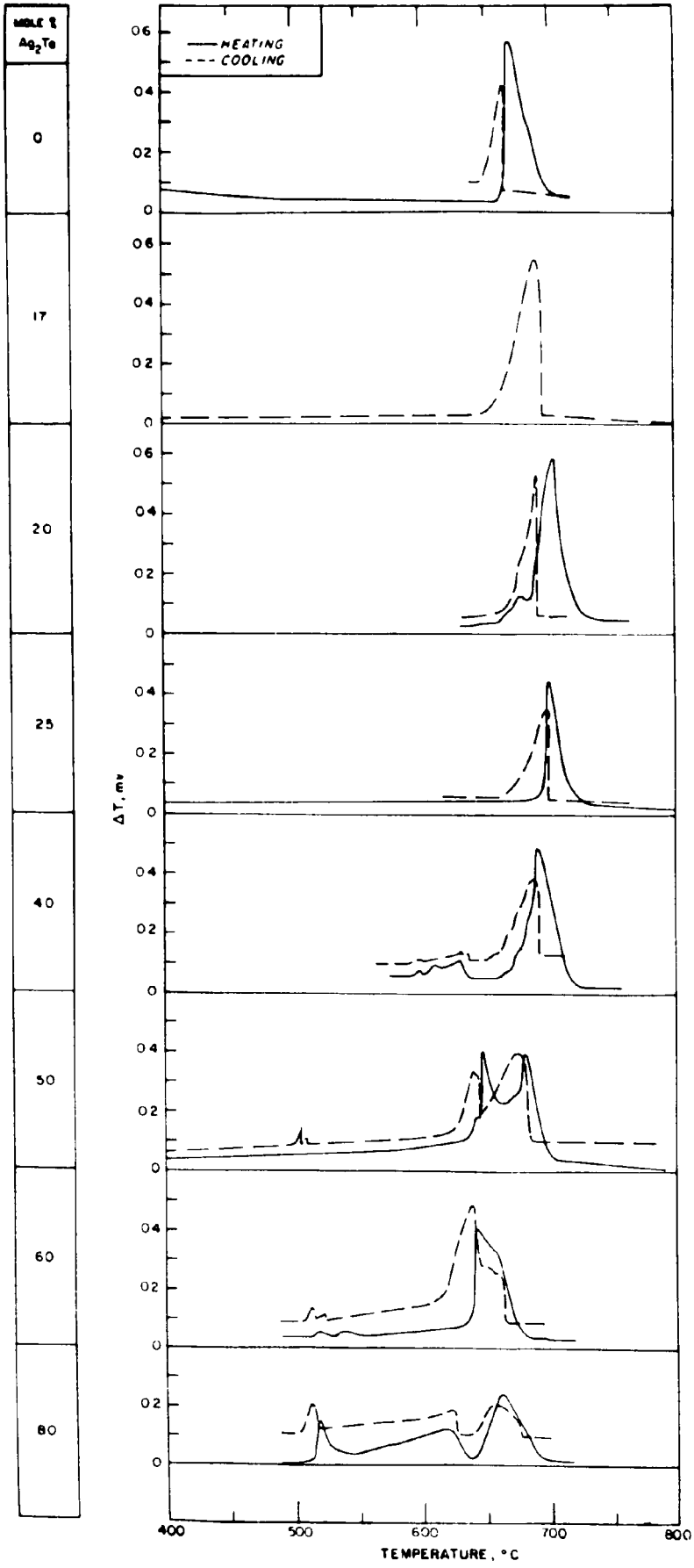


Figure 18. Differential Thermal Analysis Heating and Cooling Curves for the Ag_2Te-In_2Te_3 System.

TABLE VI.

SUMMARY OF DIFFERENTIAL THERMAL ANALYSIS MEASUREMENTS FOR THE PSEUDO-BINARY PHASE DIAGRAM OF Ag_2Te - In_2Te_3.

Sample Composition		Sample Number	Annealing Conditions	Differential Thermal Analysis Results			
				Heating		Cooling	
Mole % Ag_2Te	Mole % In_2Te_3			Liquidus Temp. °C	Transition Temp. °C	Liquidus Temp. °C	Transition Temp. °C
0	100	147	None	669		667	
17	83	672	5 days at 595° C		686	697	
20	80	633	None	722	680, 664	692	
25	75	735	None	698		700	
40	60	630	None	717	668, 631 612, 600	692	637, 602
50	50	732	4 days at 480° C	698	647	684	645, 511, 505
60	40	631	None	676	640, 538, 518	664	642, 523, 516
80	20	647	None	690	618, 516, 140	674	624, 516
100	0			957[36]	135[36]	957[36]	135[36]

actions in the region of 600°C to 630°C and apparent melting beginning about 668°C. Solidification starts at 692°C, and two small reactions occur at 637°C and 602°C. The 50 mole % Ag_2Te shows a gradual melting which may begin in the region of 580°C. A reaction occurs at 647°C and melting is complete at about 698°C. Solidification starts at 684°C, followed by a reaction at 645°C, and two small transformations at 511°C and 505°C.

The 60 mole % Ag_2Te shows two small transitions between 515°C and 540°C during heating and cooling. Very gradual melting of the material may begin above 540°C. A large heat absorption occurs at 640°C and melting is complete at 676°C. Solidification starts at 664°C and is followed by a reaction at 642°C. The 80 mole % Ag_2Te composition has a solid-solid transition at 140°C which is not shown in Figure 18, because it was the only transition observed below 500°C within the Ag_2Te-In_2Te_3 system. At 516°C, melting appears to start and is followed by a gradual absorption of heat up to 618°C. A large reaction occurs between 640°C and 690°C. Solidification begins at 674°C and is followed by reactions at 624°C and 516°C.

Discussion of the Differential Thermal Analysis Results

A tentative outline of a portion of the phase diagram for the Ag_2Te-In_2Te_3 system is given in Figure 19 on the basis of the observed heating and cooling transitions. At the low Ag_2Te end of the diagram, a congruently melting compound (699°C) exists at 25 mole % Ag_2Te. The 17 and 20 mole % Ag_2Te melt over a relatively short range, about 660°C to 700°C, and it is not possible to describe the diagram in this area.

The 40 mole % Ag_2Te composition, with its solid-solid type reactions between 600°C and 640°C, is distinctly different from the 25 and 50 mole % Ag_2Te samples.

By considering the 50, 60, and 80 mole % Ag_2Te samples together, it appears that a peritectic compound, with a decomposition temperature of about 647°C, exists near the 50 mole % Ag_2Te. In addition, a peritectic compound may occur between the 60 and 50 mole %

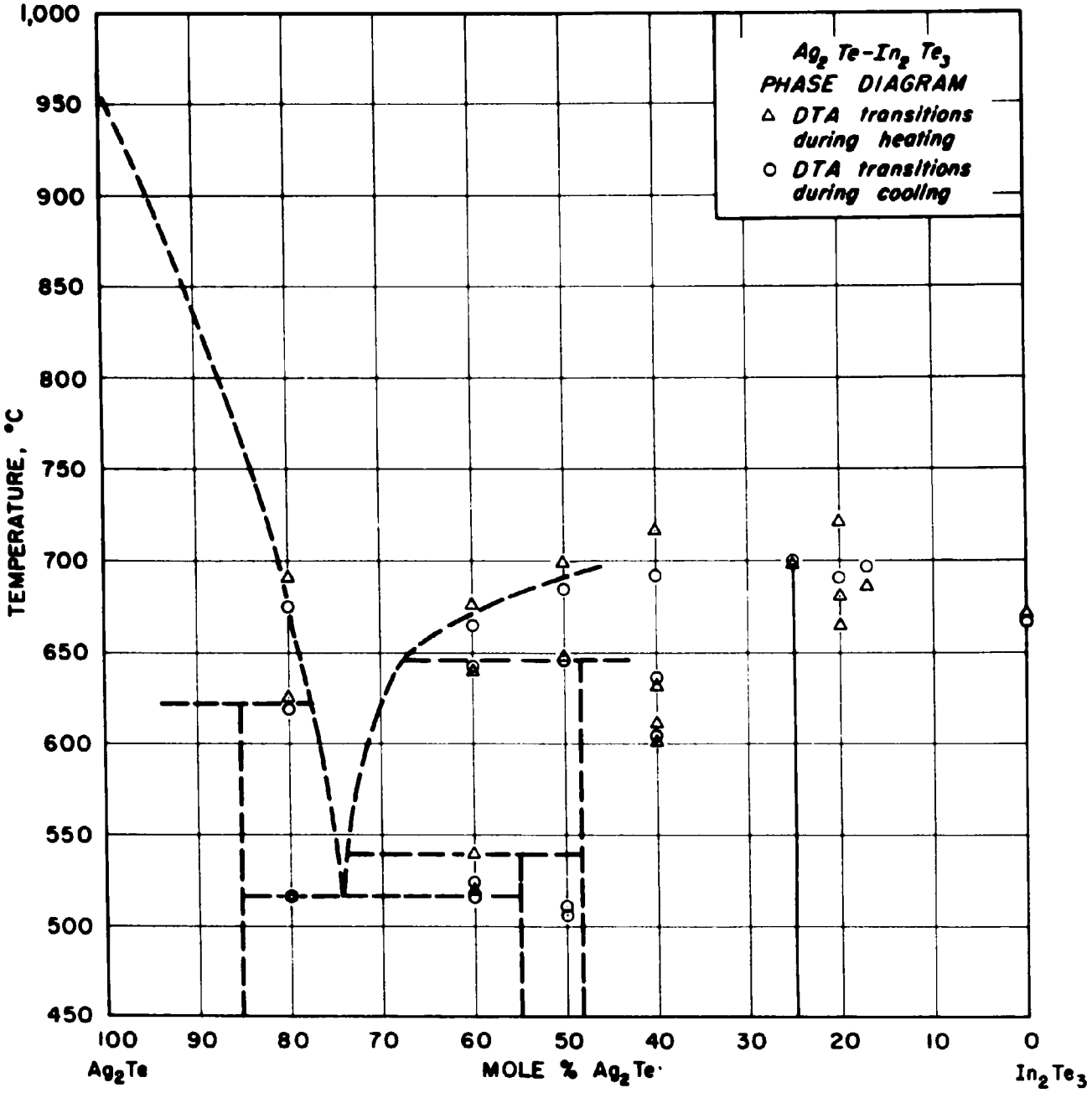


Figure 19. Partial Phase Diagram for the Ag_2Te-In_2Te_3 System.

temperature of about 647°C, exists near the 50 mole % Ag_2Te. In addition, a peritectic compound may occur between the 60 and 50 mole % Ag_2Te. This would account for the transition at 538°C in the 60 mole % Ag_2Te and the double peaks, a peritectic and a eutectic, near 510°C in the 50 mole % Ag_2Te when it is cooled slowly and segregation can easily occur. The 80 mole % Ag_2Te provides support for the existence of a eutectic at 516°C which may be at about 74 mole % Ag_2Te. The liquidus line extends up from the eutectic to about 624°C which is probably another peritectic temperature. This peritectic would be between 80 and 100 mole % Ag_2Te.

The sharp fall of the liquidus line from 957°C at 100 mole % Ag_2Te to the eutectic at 518°C and 74 mole % Ag_2Te is similar to the behavior of the Ag-Te binary phase diagram in the vicinity of Ag_2Te, as described by Hansen.[36]

Semiconducting Properties of $AgIn_3Te_5$.

Results of Electrical and Thermal Measurements

Electrical conductivity measurements were made on six samples of $AgIn_3Te_5$ between room temperature and the melting point of the compound. Five of the samples were obtained by zone refining and the sixth was prepared by casting the compound after reacting the high purity elements. Sufficient Hall effect data to estimate the energy gap was obtained on one sample. The Seebeck coefficient data in the intrinsic region was used to calculate the ratio of electron to hole mobility. Thermal conductivity measurements were made on one sample in order to establish the thermoelectric figure of merit.

Electrical conductivity measurements are shown in Figure 20 for the single phase material separated by zone refining a sample, number 181, of 30 mole % Ag_2Te - 70 mole % In_2Te_3. Chemical analysis using the procedures described in Appendix III indicated a composition of 25 (± 1) mole % Ag_2Te - 75 (± 1) mole % In_2Te_3

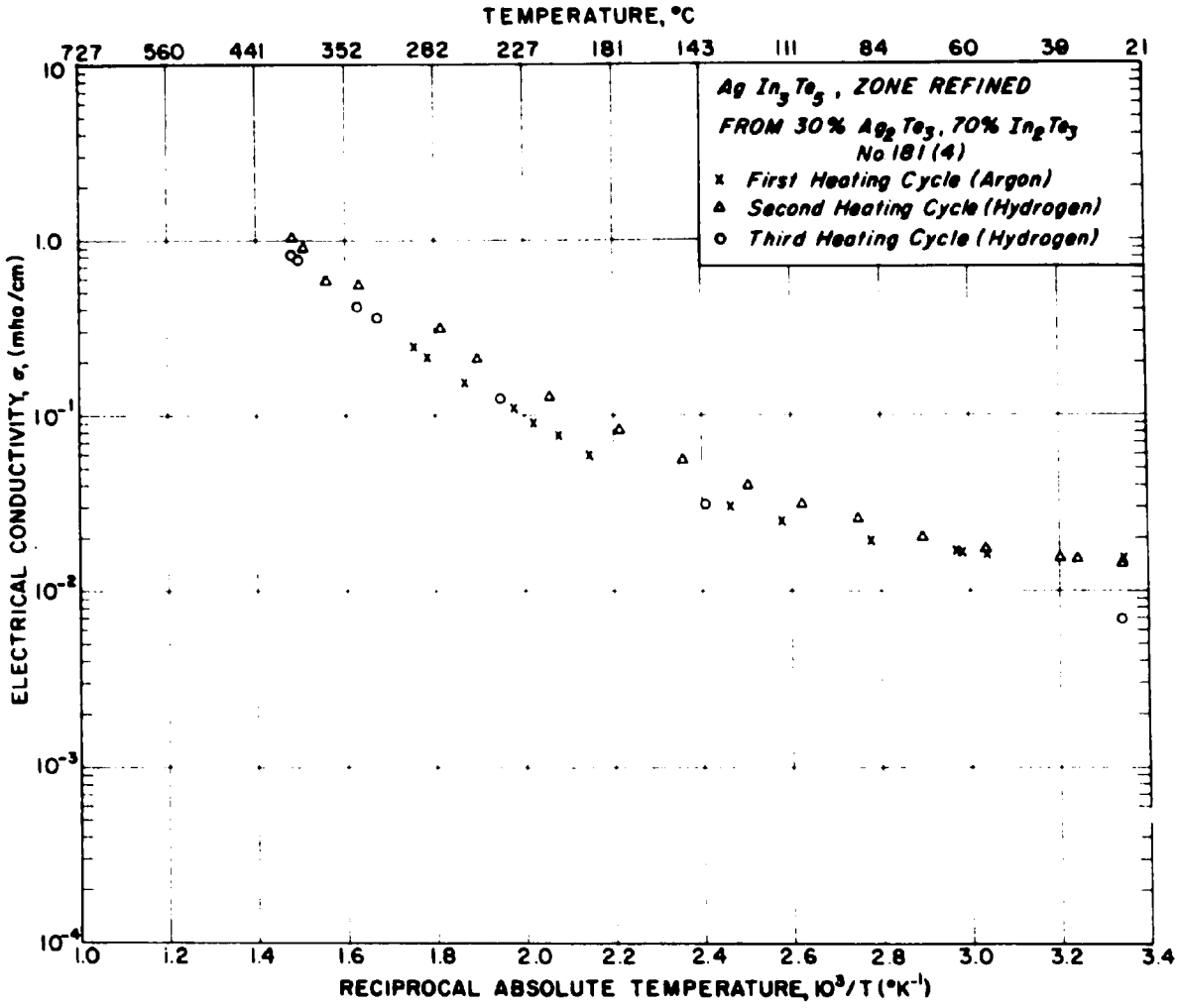


Figure 20. Logarithm of Electrical Conductivity vs. Reciprocal Absolute Temperature for Sample Number 181, Zone Refined from 30 mole % Ag_2Te-70 mole % In_2Te_3.

($AgIn_3Te_5$) for the single phase material. In addition, the differential thermal analysis heating and cooling curves are identical to those for a cast sample of $AgIn_3Te_5$ as well as zone refined samples. The electrical sample of number 181 was n-type at room temperature. The three heating cycles in argon (99.995%) and hydrogen indicate that the electrical conductivity does not undergo any irreversible change when heated as high as 400°C. This is shown in Figure 20. Since Hall effect and Seebeck coefficient data are lacking for this sample, it is not known if the material is intrinsic at the higher temperatures.

A sample of $AgIn_3Te_5$, number 735, was prepared from the high purity elements and measured in the differential thermal analysis equipment. The heating and cooling curves were identical to those obtained on the zone refined samples 181 and 194. After microscopic examination showed number 735 to be single phase, electrical measurements were made to provide a basis for comparison with the zone refined samples.

Electrical conductivity results for sample number 735 are given in Figure 21. The slope of the logarithm of electrical conductivity versus the reciprocal absolute temperature is linear in the region 256°C to 551°C. If the material is intrinsic, then the energy gap, E_{g_o}, is equal to 0.94 eV.

Electrical conductivity results are plotted in Figure 21 for two sections, 3B and 5, of sample number 194 which received 13 zone refining passes. When these samples were heated above 440°C, the slope of log σ vs. $10^3/T$ was not linear. However, if a straight line, determined by a least squares analysis, is drawn through the data for section 5, the energy gap obtained is 1.10 eV.

Sample number 206 was the only $AgIn_3Te_5$ sample prepared in a large diameter, 18 mm., fused silica, zone refining tube; six zone refining passes were made on the 220 gram sample. A section from the pure end of the refined ingot was sealed in another 18 mm. tube and slowly cooled through the melting point to promote crystal growth and

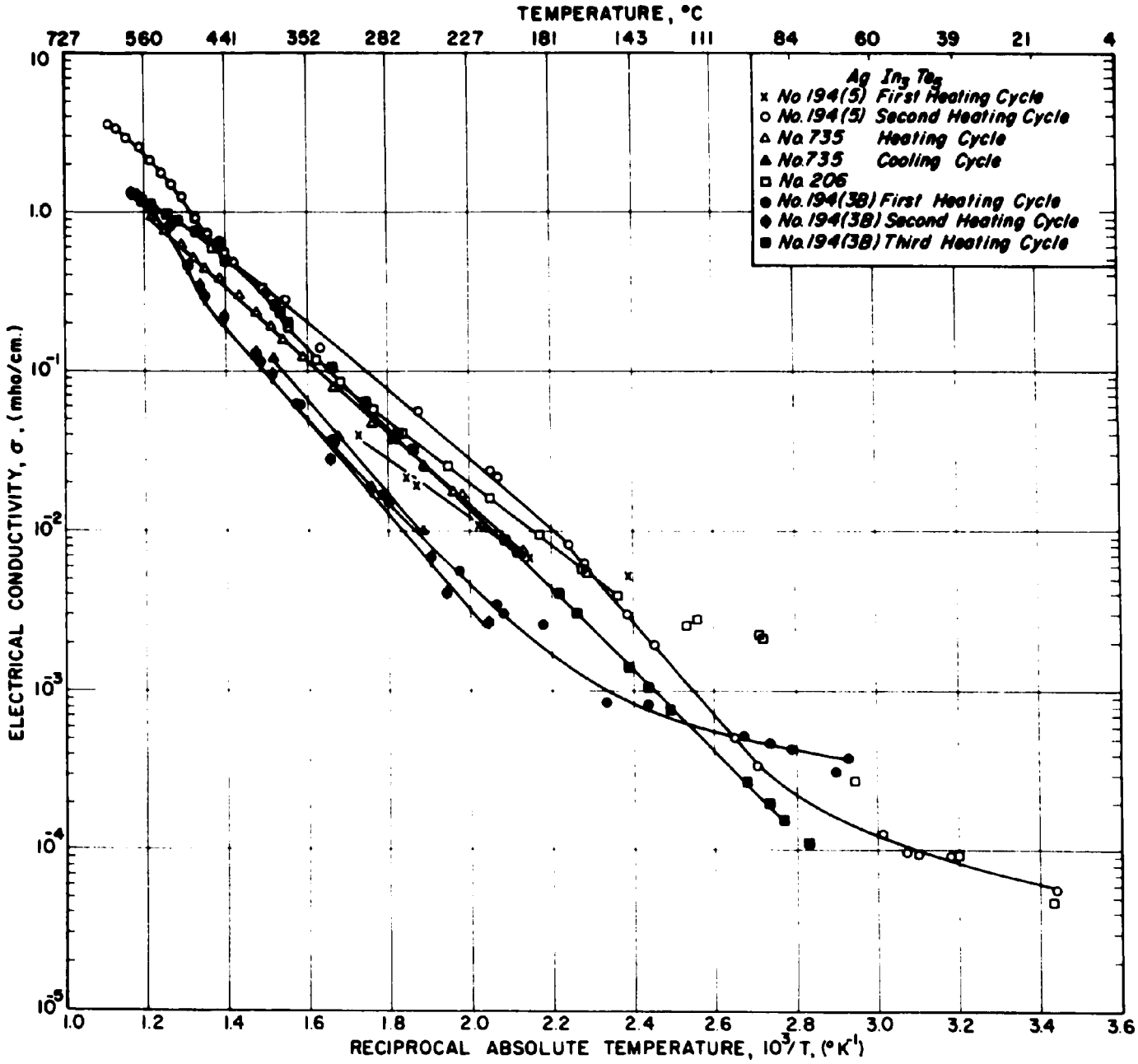


Figure 21. Logarithm of Electrical Conductivity vs. Reciprocal Absolute Temperature for $AgIn_3Te_5$, Sample Numbers 735, 194, and 206.

obtain a cylindrical specimen for thermal conductivity measurements. Following the thermal conductivity measurements, the material was tested in the electrical measuring system. The electrical conductivity data shown in Figure 21 indicate a donor level, E_d, of 0.77 eV for the temperature region 150°C to 324°C. For the linear region between 324°C and 462°C, the energy gap, E_{g_o}, is equal to 1.13 eV.

The electrical conductivity results on two sections, 1 and 2, of sample number 217 are shown in Figure 22. This sample, which received one zone refining pass, was prepared from zone refined tellurium. The slope of the electrical conductivity data below 440°C indicates an energy gap, E_{g_o}, of 1.12 eV for 217(1);and between 531°C and 687°C, the energy gap is 1.00 eV. It is questionable if this actually represents a change in energy gap. On the first heating cycle for 217(2) intrinsic conductivity does not appear to occur before 350°C. A value of E_d equal to 0.95 eV was obtained on the second heating cycle for 217(2)in the range 140°C to 379°C.

The electrical conductivity results on sections 1C and 4A of sample 238 are given in Figure 22. This sample, which was made with zone refined tellurium, received three zone refining passes. On the basis of the conductivity data for section 1C in the range of 325°C to 439°C, the energy gap is 1.19 eV. For section 4A, the energy gap is 1.08 eV using the data between 307°C and 390°C; and in the range 473°C to 668°C, the value is 1.06 eV. This is not a significant difference between the low and high temperature values. These results are all summarized in Table VII.

Hall coefficient data for samples 206, 217(2),238 (1C), and 238 (4A) are contained in Table VIII. The energy gap of $AgIn_3Te_5$ was determined from the slope of the log $R_H T^{3/2}$ vs. $10^3/T$ data in Figure 23 using Equation (15). In the range 286°C to 390°C for sample 238, section 4A, the energy gap is 1.09 eV; and for section 1C, the energy gap is 1.20 eV by considering the range 325°C to 440°C. A summary of energy gap values obtained from Hall coefficient data is also given

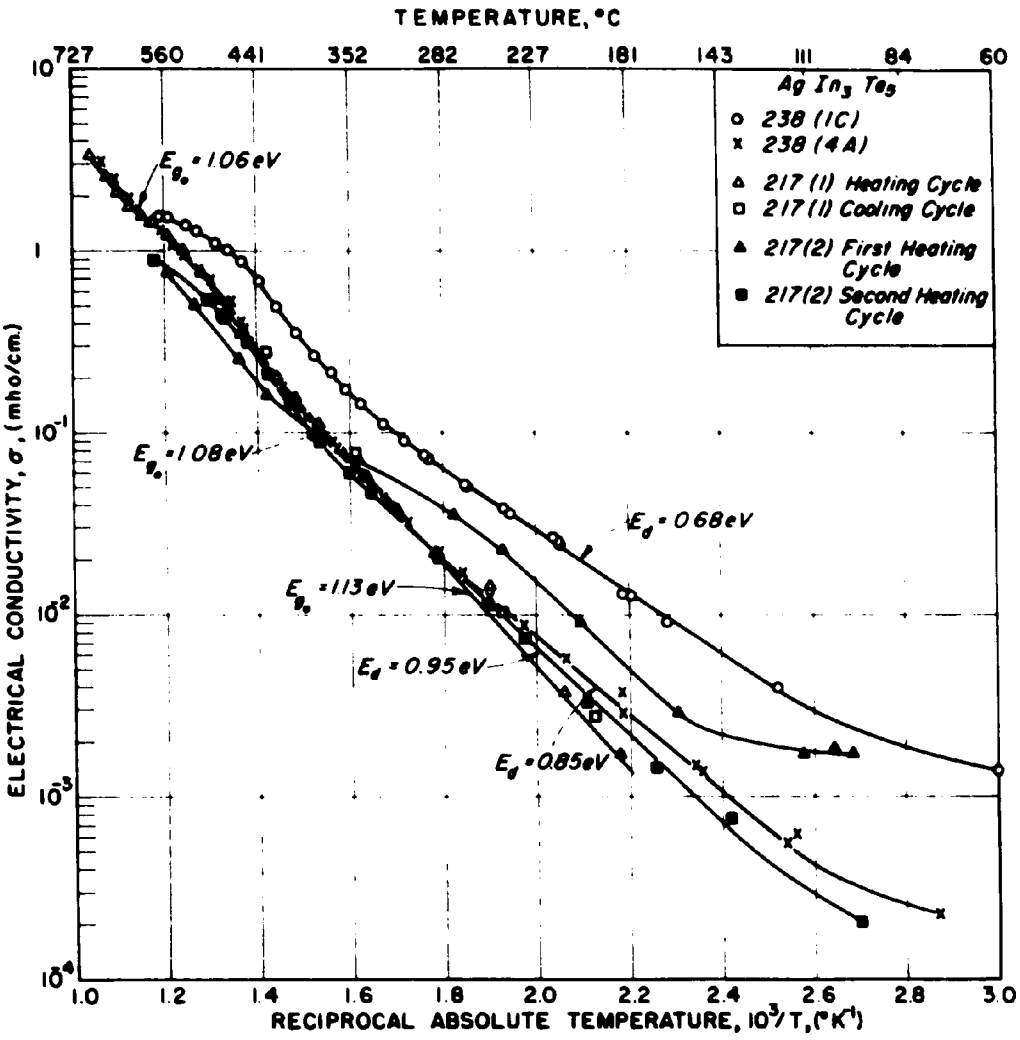


Figure 22. Logarithm of Electrical Conductivity vs. Reciprocal Absolute Temperature for $AgIn_3Te_5$, Sample Numbers 217 and 238.

TABLE VII

SUMMARY OF ELECTRICAL PROPERTIES OF $Ag\ In_3\ Te_5$

Sample Number	Energy Gap ($\log \sigma$ vs. $1/T$)		Energy Gap ($\log RT^{3/2}$ vs. $1/T$)		Temp. Dependence of Hall Mobility $\mu_{H,n} = \mu_{300}(T/300)^{\gamma}$			Seebeck Coefficient $\alpha = m/T + c$			Mobility Ratio from Seebeck Coefficient $\frac{\mu_n}{\mu_p}$
	E_{g_o}, eV	Temp. Range	E_{g_o}, eV	Temp. Range	μ_{300}	γ	Temp. Range	m, mv	c mv/°K	Temp. Range	
206 (6 ZR passes)	1.13	324°C-462°C									
217(1) (1 ZR pass)	1.12 1.00	253°C-437°C 531°C-687°C						-396	+0.13	254°C-436°C	6.1
238(1C) (3 ZR passes)	1.19	325°C-439°C	1.20	325°C-440°C	250	-2.0	244°C-440°C				
238(4A) 3 ZR passes)	1.08 1.06	307°C-390°C 473°C-668°C	1.09	286°C-390°C	240	-2.0	189°C-389°C	-417	+0.40	307°C-390°C	7.2
735 (cast)	0.94	256°C-551°C									

TABLE VIII.

HALL COEFFICIENT OF $AgIn_3Te_5$ AS A FUNCTION OF TEMPERATURE

Sample Number 206

Temperature T, °K	Hall Coefficient R_H, cm^3/coulomb
336	-89000
369	-5820
441	-5410
461	-1510
491	-1400
517	-1870
546	-491
591	-850
597	-424
619	-376
645	-259
672	-131
695	-65.7
717	-26.8

Sample Number 217 (2)

First Heating Cycle

Temperature T, °K	Hall Coefficient R_H, cm^3/coulomb
619	-844
708	-254

Sample Number 217 (2)

Second Heating Cycle

Temperature T, °K	Hall Coefficient R_H, cm^3/coulomb
475	-16200
530	-4850
653	-527

TABLE VIII (Cont'd)

HALL COEFFICIENT OF $AgIn_3Te_5$ AS A FUNCTION OF TEMPERATURE

Sample Number 238 (1C)		Sample Number 238 (4A)	
Temperature T, °K	Hall Coefficient R_H, cm^3/coulomb	Temperature T, °K	Hall Coefficient R_H, cm^3/coulomb
490	- 4030	427	- 102000
491	- 2300	428	- 59800
491	- 2370	462	- 26800
518	- 1780	462	- 31700
540	- 1580	486	- 15600
567	- 986	486	- 18400
567	- 797	508	- 8290
583	- 577	508	- 10040
598	- 565	528	- 5850
616	- 440	528	- 6300
616	- 457	544	- 4170
628	- 274	544	- 4270
628	- 404	560	- 3080
642	- 221	560	- 3040
642	- 314	582	- 2080
657	- 218	582	- 1890
657	- 204	600	- 1270
674	- 168	600	- 1270
674	- 138	623	- 889
691	- 130	623	- 898
691	- 85.7	642	- 594
712	- 83.2	642	- 625
713	- 61.6	662	- 395
731	- 51.3	663	- 429
731	- 57.7	688	- 236
747	- 41.1	688	- 267
747	- 51.2	710	- 164
762	- 36.1	710	- 183
762	- 41.1	735	- 102
		735	- 121
		747	- 81.0
		747	- 84.4
		770	- 55.6
		771	- 63.5
		512 (cooling)	- 89.7
		512	- 89.4

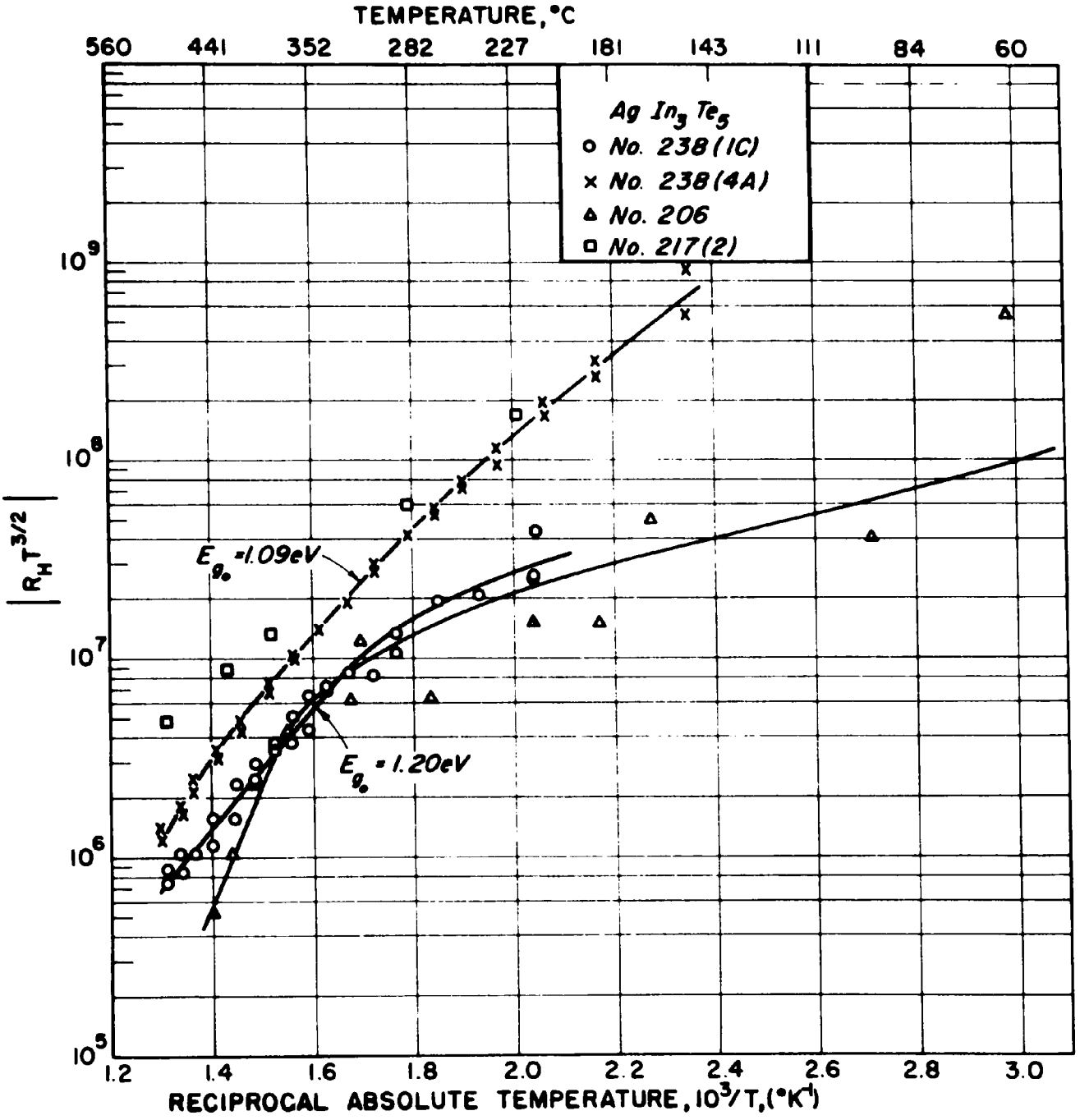


Figure 23. Logarithm of $|R_H T^{3/2}|$ vs. Reciprocal Absolute Temperature for $AgIn_3Te_5$, Sample Numbers 206, 217 (2), 238 (1C), and 238 (4A).

in Table VII. All reported values were calculated by the method of least squares.

The following carrier concentrations are obtained if the Hall coefficient data is interpreted on the basis of a single carrier: $10^{15}/cm^3$ for sample number 206 at 167°C; $3 \times 10^{15}/cm^3$ for sample number 238 (1C) at 218°C; and $10^{13}/cm^3$ for sample number 238 (4A) at 154°C.

The Hall mobility data for two sections, 1C and 4A, of sample number 238, $AgIn_3Te_5$, are plotted in Figure 24. The mobility is proportional to $T^{-2.0}$ for both samples and the standard deviations of the two slopes are 0.3 and 0.1 for 238 (1C) and 238 (4A), respectively. The temperature ranges used were 244°C to 440°C for 238 (1C) and 189°C to 389°C for 238 (4A).

The Seebeck data provide an indication of the temperature at which the intrinsic region begins and the relative purity of the samples. Also, the existence of an unidentified transformation phenomenon in $AgIn_3Te_5$ near 440°C is suggested by the Seebeck coefficient data.

Seebeck coefficient measurements between 125°C and 680°C are shown in Figure 25 for three samples of $AgIn_3Te_5$, numbers 735, 217 and 238. Sample number 735, the only sample not zone refined, changed from p-type to n-type near 150°C. The decrease in Seebeck coefficient in the intrinsic range followed by a gradual rise near 425°C is similar to that observed on the two zone refined samples.

The Seebeck data for samples 217 (1), 217 (2), 238 (1C), and 238 (4A) are plotted against reciprocal absolute temperature in Figure 26. The slopes of the data for 217 (1), 238 (1C), and 238 (4A) are linear in the approximate ranges of 250°C to 440°C and 500°C to 640°C. The slope in the high temperature range is about four times higher. This data was fitted to Equation (27), $\alpha = m/T + c$, which permits the calculation of the electron-to-hole mobility ratio, b, from Equation (28). This assumes that the spherical energy band approximation is valid and that lattice scattering predominates. Since the

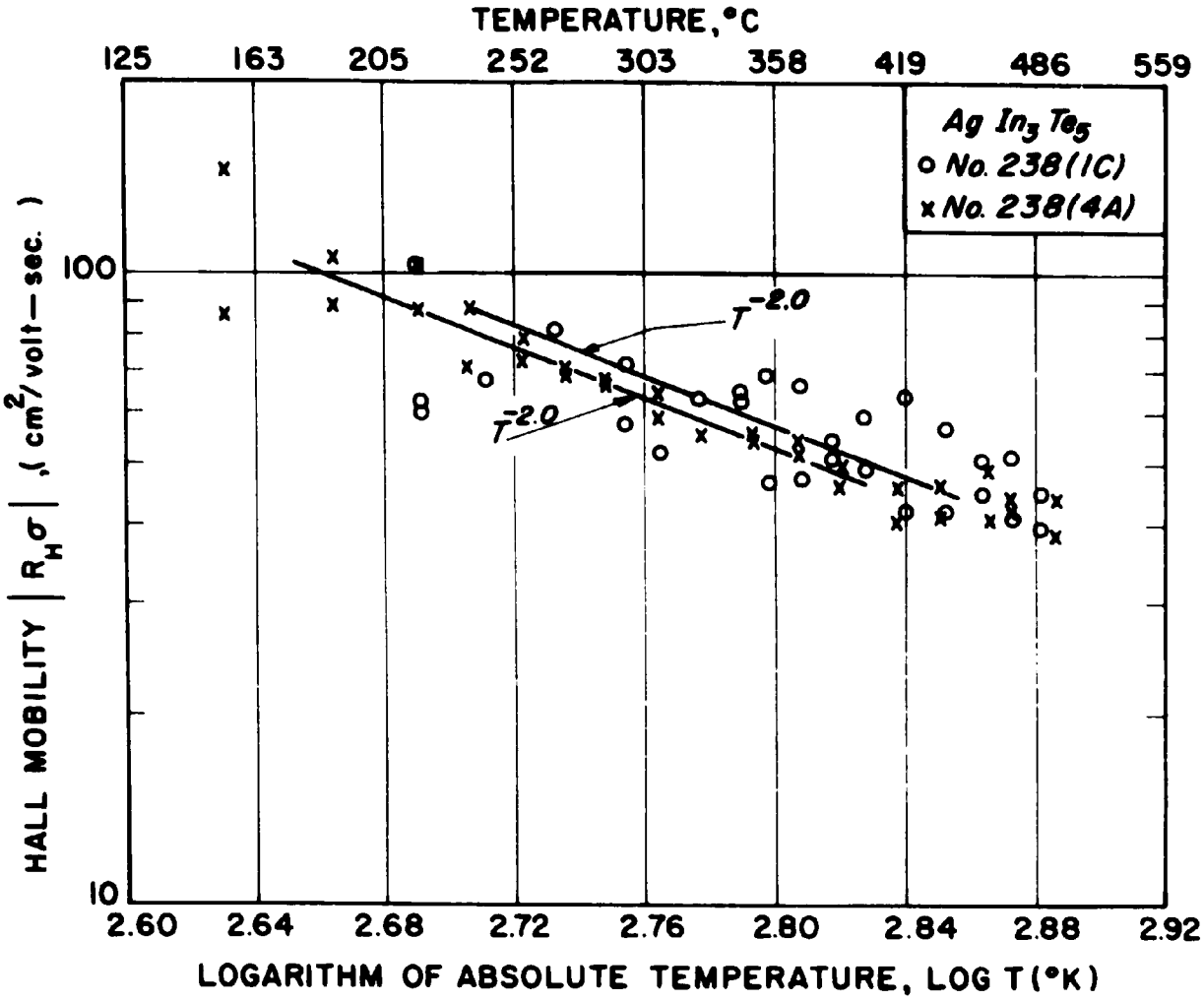


Figure 24. Logarithm of Hall Mobility vs. Logarithm of Absolute Temperature for $AgIn_3Te_5$, Sample Numbers 238 (1C) and 238 (4A).

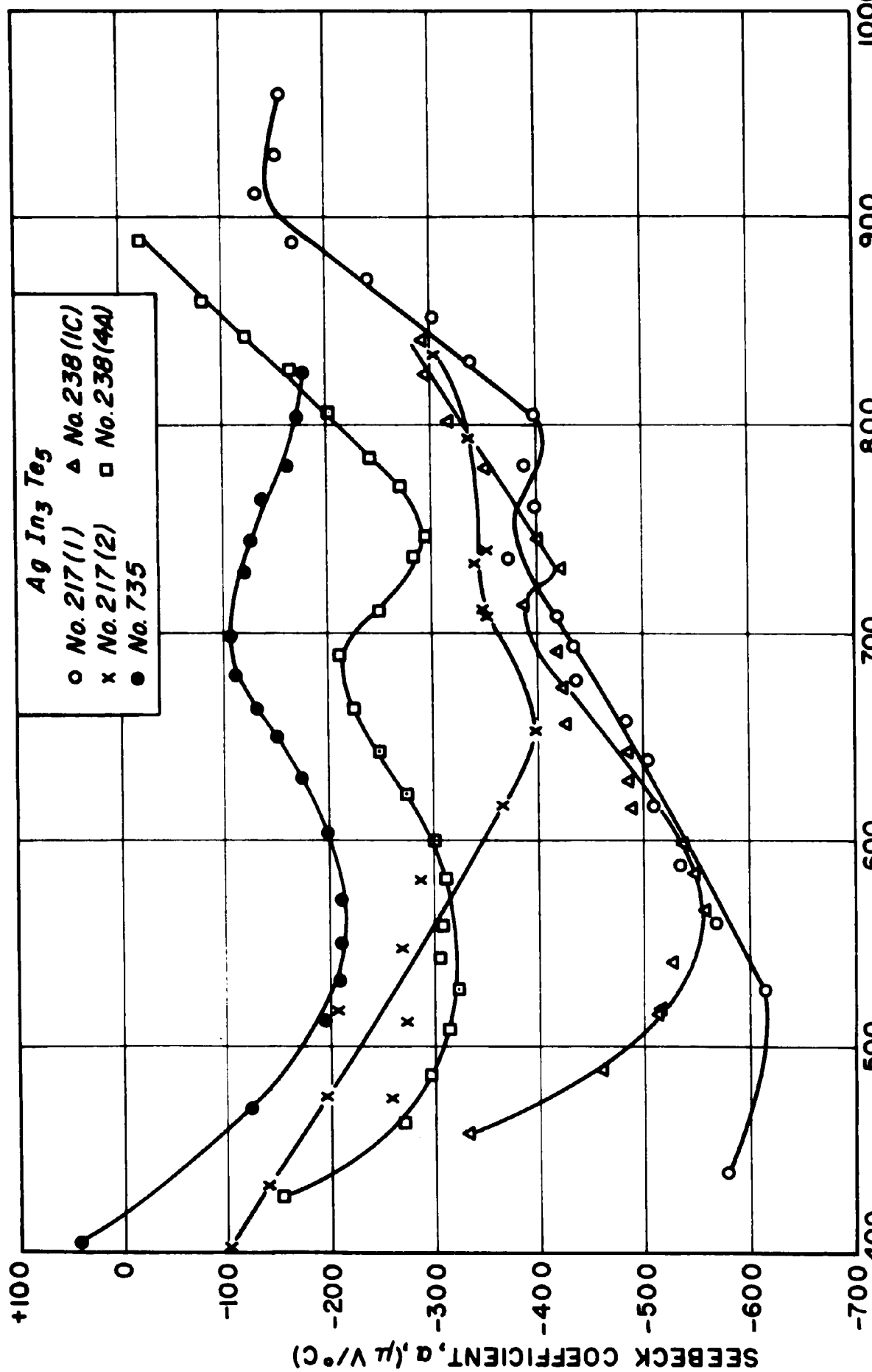


Figure 25. Seebeck Coefficient vs. Absolute Temperature for $AgIn_3Te_5$, Sample Numbers 735, 217(1), 217 (2), 238 (1C), and 238 (4A).

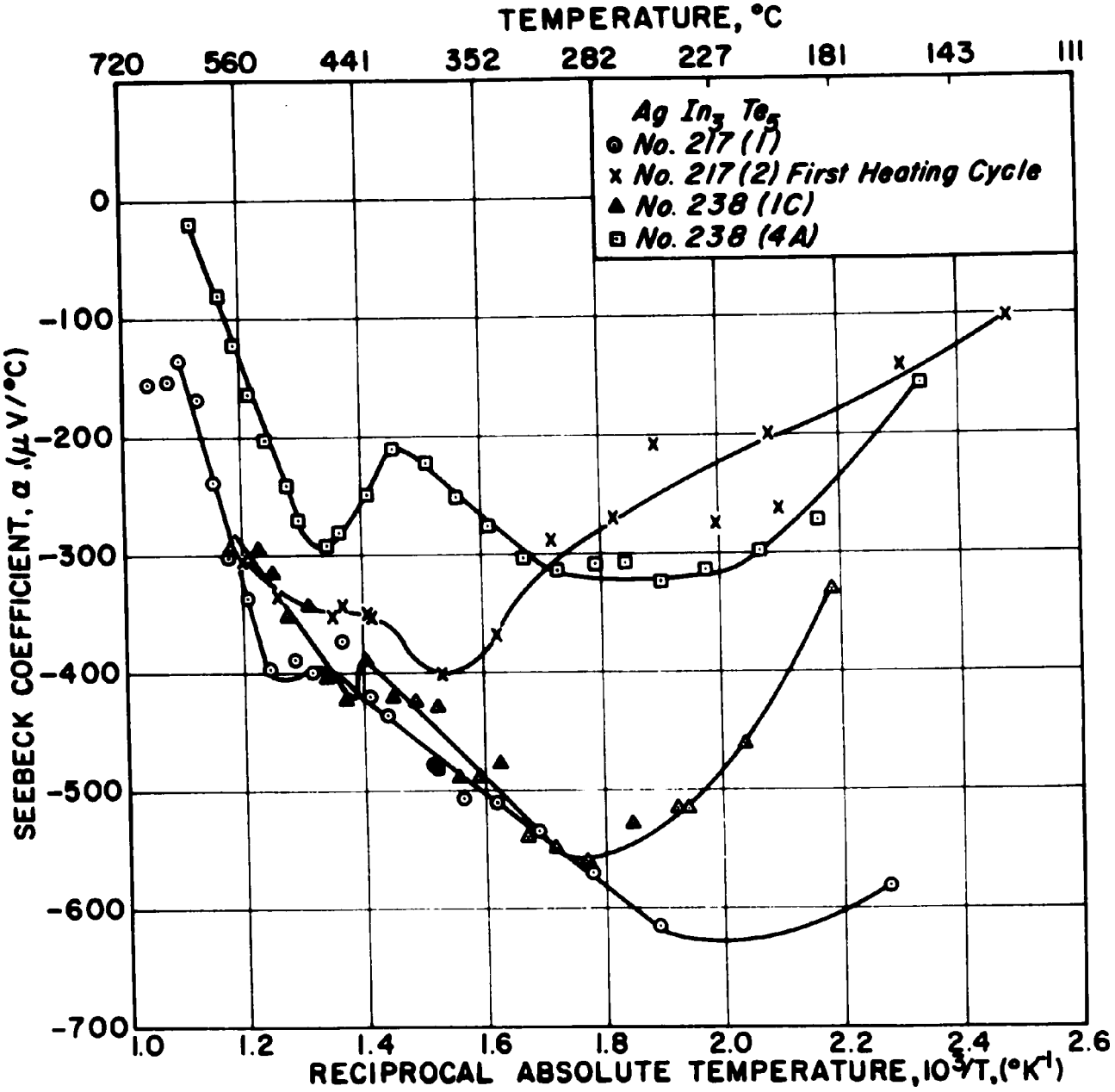


Figure 26. Seebeck Coefficient vs. Reciprocal Absolute Temperature for $AgIn_3Te_5$, Sample Numbers 217 (1), 217 (2), 238 (1C), and 238 (4A).

fit of the Seebeck data to Equation (27) appears to be good, this model may apply in the low temperature range for $AgIn_3Te_5$.

Using the energy gap of 1.1 eV obtained from electrical measurements, the mobility ratios are 6.1 and 7.2 for samples 217 (1) and 238 (4A), respectively, in the temperature range below 440°C. These results are shown in Table VII. The temperature dependence of the energy gap was calculated from Equation (29) using the α vs. $10^3/T$ data on 217 (1) and 238 (4A) below 440°C. Values of -6×10^{-4} eV/°K and -1×10^{-3} eV/°K were obtained for 217 (1) and 238 (4A), respectively. This assumes the mobility ratio is proportional to $(m_p^*/m_n^*)^{5/2}$. The slope of α vs. $10^3/T$ in the high temperature region above 500°C results in a negative mobility ratio which implies that the theory does not hold. The results of the Seebeck coefficient measurements are summarized in Table VII.

The thermal conductivity of $AgIn_3Te_5$, sample number 206, between 0°C and 300°C is shown in Figure 27. Between 0°C and 70°C, the thermal conductivity decreases from 0.010 watts/cm, °C, to 0.009 watts/cm, °C, and then remains constant up to 300°C. The electrical conductivity and Hall coefficient data in Figures 21 and 23 suggest that the intrinsic conduction region begins above 300°C. The maximum contribution from the electronic component of thermal conductivity will occur at 300°C where the electrical conductivity is a maximum over the temperature range in which thermal conductivity measurements were made. Using the electrical conductivity contained in Figure 21 and Equation (34), $\lambda_e = 2 (k/q)^2 (\sigma T)$, the electronic component is 5×10^{-7} watts/cm, °C at 300°C, which is negligible.

The thermoelectric figure of merit for $AgIn_3Te_5$ can be calculated from the thermal conductivity of sample number 206 and the Seebeck coefficient and electrical conductivity data on sample number 735. The latter sample appears to have the highest impurity concentration. Any difference in thermal conductivity between numbers

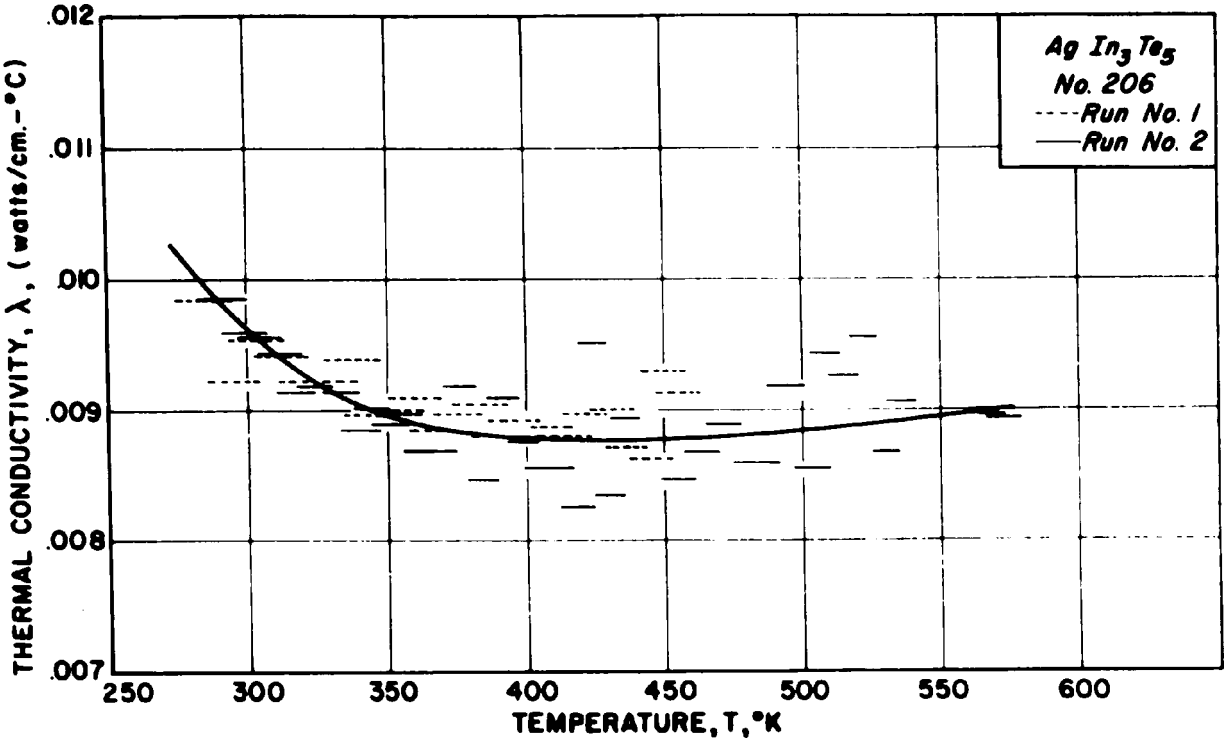


Figure 27. Thermal Conductivity vs. Absolute Temperature for $AgIn_3Te_5$, Sample Number 206.

206 and 735 would be expected to result from the electronic contribution to the thermal conductivity $| \lambda_e = 2 (k/e)^2 \sigma T |$. This is equal to 4×10^{-7} watts/cm $^{\circ}$C for number 735 at 300°C and 5×10^{-7} watts/cm $^{\circ}$C for number 206 at 300°C. The electronic contribution is a maximum at 300°C, but it is still negligible compared to the total thermal conductivity (0.009 watts/cm $^{\circ}$C at 300°C).

Using σ equal to 0.05 mho/cm, α equal to 210 μ v/ $^{\circ}$C, and λ_{th} equal to 0.009 watts/cm $^{\circ}$C, the figure of merit, $Z = \alpha^2 \sigma / \lambda_{th}$, of $Ag In_3Te_5$ is 2.4×10^{-7}/ $^{\circ}$K and Z T is equal to 1.4×10^{-4} at 300°C. It is not possible to calculate an optimum figure of merit, Z_{max}, from Simon's paper[7] because the dimensionless parameters obtained from the data on $Ag In_3Te_5$ result in a value of Z_{max} which is beyond the limits of the graphs provided. There is little doubt that the figure of merit for $Ag In_3Te_5$ is low, especially since the mobility is low.

Discussion of the Semiconducting Properties of $Ag In_3Te_5$.

A significant difference in electrical conductivity was observed between the compounds prepared by zone refining the 30 mole % Ag_2Te - 70 mole % In_2Te_3 composition and the 25 mole % Ag_2Te - 75 mole % In_2Te_3 composition. Also, there is some variation in the energy gap values obtained on zone refined and cast samples of $Ag In_3Te_5$. Since the characteristics of the pseudo-binary phase diagram of Ag_2Te - In_2Te_3 are not known in the vicinity of the congruently melting composition, 25 mole % Ag_2Te - 75 mole % In_2Te_3, some variation in properties between samples may be accounted for by the extent of the solubility region for the compound $Ag In_3Te_5$.

Differential thermal analysis measurements on $Ag In_3Te_5$ did not show any transition between room temperature and the melting point, 699 (± 3) $^{\circ}$C. However, the Seebeck coefficient results on $Ag In_3Te_5$ indicate a transition in the region of 440°C to 500°C. The log σ vs. 1/T curves show a slight departure from linearity in

this temperature range, but the energy gaps calculated from the electrical conductivity data above 500°C and below 440°C are not significantly different from the value of 1.1 eV. Hall effect measurements are available only below 440°C, and the energy gap obtained from the log $R_H T^{3/2}$ vs. 1/T data agrees with the value calculated from electrical conductivity results.

$AgIn_3Te_5$ can be considered as In_2Te_3 with 1/10 of the indium atoms replaced by silver atoms; three silver atoms replace each indium atom. Denning[38] reported the crystal structure of $AgIn_3Te_5$ to be either diamond (F d 3 m) or sphalerite (F $\bar{4}$ 3 m) with a lattice parameter of a_o = 6.2476 (± 0.001) Å. This means there is only a slight change from the zinc blende or antifluorite structure reported for In_2Te_3.[32] The effect of introducing silver into the lattice can be seen by comparing the electrical properties shown in Table VII with the properties of In_2Te_3 given by Zhuze.[33] If the energy gap of $AgIn_3Te_5$ is 1.1 eV, then there is no significant change from the 1.12 eV value for In_2Te_3. The mobility of $AgIn_3Te_5$, which was measured as 120 cm^2/volt-second at 155°C and extrapolated to a value of 250 cm^2/volt-second at 300°K, does appear to be higher than the 5 cm^2/volt-second to 70 cm^2/volt-second for In_2Te_3[33] at room temperature. Also, the mobility of $AgIn_3Te_5$ has a temperature dependence of $T^{-2.0}$, whereas Zhuze[33] reports that the mobility of In_2Te_3 is independent of temperature between about 50°C and 350°C.

The thermal conductivity of $AgIn_3Te_5$, which is 0.009 watts/cm °C between 70°C and 300°C, is essentially the same as that of ordered In_2Te_3, 0.011 watts/cm °C, reported by Zaslavskii.[35]

THE PHASE DIAGRAM BEHAVIOR OF THE PSEUDO-BINARY SYSTEM OF Ag_2Se - In_2Se_3 AND THE SEMICONDUCTING PROPERTIES OF $Ag_2In_8Se_{13}$

Introduction

A review will be given of the published literature on compositions in the Ag_2Se - In_2Se_3 pseudo-binary phase diagram. Also, the results of differential thermal analysis measurements on certain compositions in this system will be presented. These led to the location of the congruently melting compound $Ag_2In_8Se_{13}$. Electrical conductivity, Hall effect, Seebeck coefficient, thermal conductivity, and melting point measurements were made on zone refined, polycrystalline samples of this compound.

Literature Review

Previous investigations of the Ag_2Se - In_2Se_3 system consist of studies on Ag_2Se, In_2Se_3, and six compositions within the pseudo-binary phase diagram. The only ternary composition studied in any detail has been 50 mole % Ag_2Se - 50 mole % In_2Se_3 which is $AgInSe_2$. The crystal structure, energy gap, electrical conductivity, carrier type, and melting point have been reported for this material.

Hansen[36] reported the melting point of Ag_2Se as 897°C and an allotropic transformation at 128°C. In_2Se_3 has a melting point of 888°C and a solid-solid transition at 740 (± 20) °C according to Mason and O'Kane.[20] Miyazawa and Sugaike[29] report a transformation in In_2Se_3 near 200°C. Semiletov[31] reported that In_2Se_3 has four crystal modifications: two hexagonal; a cubic; and a monoclinic. The crystal structure of In_2Se_3 is very close to zinc blende type structure.[31] Brice, Newman, and Wright[39] obtained an optical energy gap of 1.2 eV for In_2Se_3 at room temperature.

Hahn[1] reported X-ray lattice parameter values at the following compositions in the pseudo-binary phase diagram of Ag_2Se-In_2Se_3: 10, 20, 33, 43, 50, and 57 mole % Ag_2Se. The 10 mole % Ag_2Se had lower lattice parameter values than the 20 and 30 mole % Ag_2Se com-

positions. At 30 mole % Ag_2Se, two phases are present, while at 43, 50, and 57 mole % Ag_2Se only one set of lattice parameters is given and its value is constant over this range. The 20 mole % Ag_2Se sample had a chalcopyrite-like structure with a c/a ratio of 2.00. Hahn made no attempt to describe the phase diagram on the basis of his X-ray results.

The 50 mole % Ag_2Se composition, which is $AgInSe_2$, was investigated by Zhuze.[19] The material was single phase according to X-ray analysis and had a chalcopyrite structure. The melting point was 773°C, and the optical energy gap was 1.18 eV. Cast, polycrystalline samples were used for the measurement of electrical conductivity, 0.48 mho/cm., and Seebeck coefficient, -140 μV/°C, at room temperature.

Austin, Goodman, and Pengelly[18] reported an optical energy gap of 1.18 eV for $AgInSe_2$.

Phase Diagram Study

Differential Thermal Analysis Results

Differential thermal analysis (DTA) measurements are reported for the following eight compositions in the Ag_2Se-In_2Se_3 pseudo-binary phase diagram: 0, 10, 20, 40, 50, 60, 80, and 100 mole % Ag_2Se. The heating and cooling curves obtained by DTA are shown in Figure 28. The DTA samples were cooled from the liquid state in fused silica tubes, after fusion of the elements, by quenching either in air or in a water bath. The materials were then rebottled in DTA tubes and annealed under the conditions shown in Table IX.

The liquidus, solidus, and solid-solid transformation temperatures are given for each composition in Table IX. The heating and cooling curves which are shown in Figure 28 for In_2Se_3 indicate that a large endothermic reaction occurs for the phase transformation near 210°C. A second transition occurs near 740°C before the binary compound melts at 888°C.

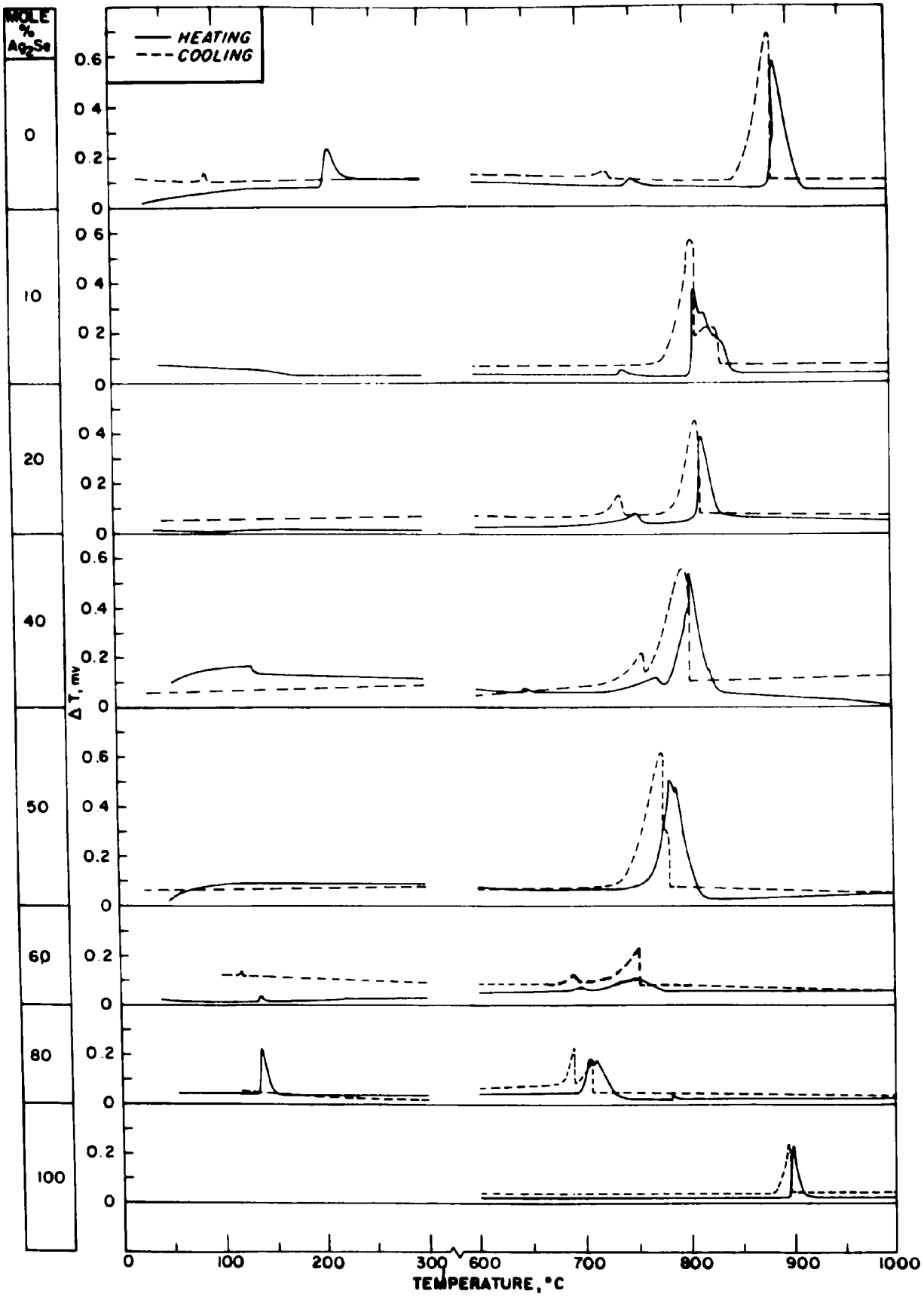


Figure 28. Differential Thermal Analysis Heating and Cooling Curves for the Ag_2Se-In_2Se_3 System.

TABLE IX.

SUMMARY OF DIFFERENTIAL THERMAL ANALYSIS MEASUREMENTS FOR THE PSEUDO-BINARY PHASE DIAGRAM OF $Ag_2Se - In_2Se_3$.

Sample Composition		Sample Number	Annealing Conditions	Differential Thermal Analysis Results			
				Heating		Cooling	
Mole % Ag_2Se	Mole % In_2Se_3			Liquidus Temp. °C	Transition Temp. °C	Liquidus Temp. °C	Transition Temp. °C
100	0	629	None	897		896	
80	20	642	4 days at 590° C	731	695, 134	708	690
60	40	654	5 days at 590° C	775	697, 135	754	698, 122
50	50	671	4 days at 600° C	814	780	781	775
40	60	675	5 days at 595° C	829	803, 770, 727, 644	804	761
20	80	646	6 days at 600° C, 4 days at 480° C	813	753	815	745
10	90	692	5 days at 590° C	847	809, 742	836	812
0	100	676	5 days at 595° C	888	751, 210	885	731, 98

The 10 mole % Ag_2Se - 90 mole % In_2Se_3 shows no evidence of a low temperature transition near 200°C; however, there is a phase transition at 742°C during the heating cycle. Melting appears to start near 809°C and is complete by 847°C. The cooling curve shows a liquidus region from 836°C to 812°C. The transition at 812°C may result from a eutectic reaction. The 20 mole % Ag_2Se composition, which melts congruently at 815 (± 3) °C, shows a solid-solid transition at 750 (± 10) °C with a large absorption of heat.

The 40 mole % Ag_2Se composition has a small transition at 644°C during heating and may begin to melt near 727°C. Two other transformations occur at about 770°C and 803°C. Solidification starts at 804°C and is followed by a transition at 761°C.

The 50 mole % Ag_2Se composition begins to melt just above 740°C and the principal heat absorption occurs at 780°C. Solidification begins at 781°C and is followed by a large transition at 775°C. The cooling curve appears to consist of a short liquidus region terminated by a peritectic type reaction at 775°C.

The 60 mole % Ag_2Se sample has a low temperature transition at 135°C on heating and at 122°C on cooling. The difference in temperatures can probably be attributed to supercooling. This composition begins to melt near 697°C and is entirely liquid at 775°C. Solidification starts at 754°C and continues until 698°C where a small transition occurs.

The 80 mole % Ag_2Se also contains a low temperature transition which occurs at 134°C on heating. On cooling, data was only taken as low as 122°C so that this transition was missed. Melting starts at 695°C and is complete before 731°C. Solidification begins at 708°C and is followed by a transition at 690°C.

The melting point of the binary compound Ag_2Se was determined to be 897 (± 3) °C. No differential thermal analysis measurements were made below 650°C.

Discussion of Differential Thermal Analysis Results

The differential thermal analysis results can best be considered by grouping the closely related compositions. The 100, 80, and 60 mole % Ag_2Se compositions make up one such group and the 20, 10, and 0 mole % Ag_2Se compositions are another group. The greatest uncertainty in the interpretation of the DTA results occurs in the region of the 40 and 50 mole % Ag Se compositions. A tentative outline of some sections of the pseudo-binary phase diagram for the Ag_2Se-In_2Se_3 system is given in Figure 29.

Beginning at the 100% Ag_2Se end of the phase diagram, a liquidus line extends downward from the 897°C melting point for the binary compound to a eutectic which may be near 78 mole % Ag_2Se. The eutectic temperature is about 695°C. The 60 mole % Ag_2Se also has this eutectic. The low temperature transition near 128°C in Ag_2Se[36] extends to the 80 and 60 mole % Ag_2Se samples, but it is not present in the 50 mole % Ag_2Se composition. The results on the 50 mole % Ag_2Se sample indicate that a peritectic compound may be present in this region of the phase diagram. If so, its decomposition temperature is about 775°C. The 40 mole % Ag_2Se has a similar transition between 760°C and 770°C and a liquidus region which extends as high as 804°C. However, between the 60 and 20 mole % Ag_2Se compositions the data are insufficient to establish a tentative outline of the phase diagram.

At the high In_2Se_3 side of the phase diagram, a congruently melting compound, 815 (± 3) °C. is present at the 20 mole % Ag_2Se composition. This compound is $Ag_2In_8Se_{13}$. A eutectic may exist between the 20 and 10 mole % Ag_2Se compositions; the eutectic temperature would be 812°C. The solid-solid transition in In_2Se_3 near 740°C is present in these compositions, but the low temperature transformation in In_2Se_3 near 210°C does not occur. In_2Se_3 melts congruently at 888 (± 3) °C.

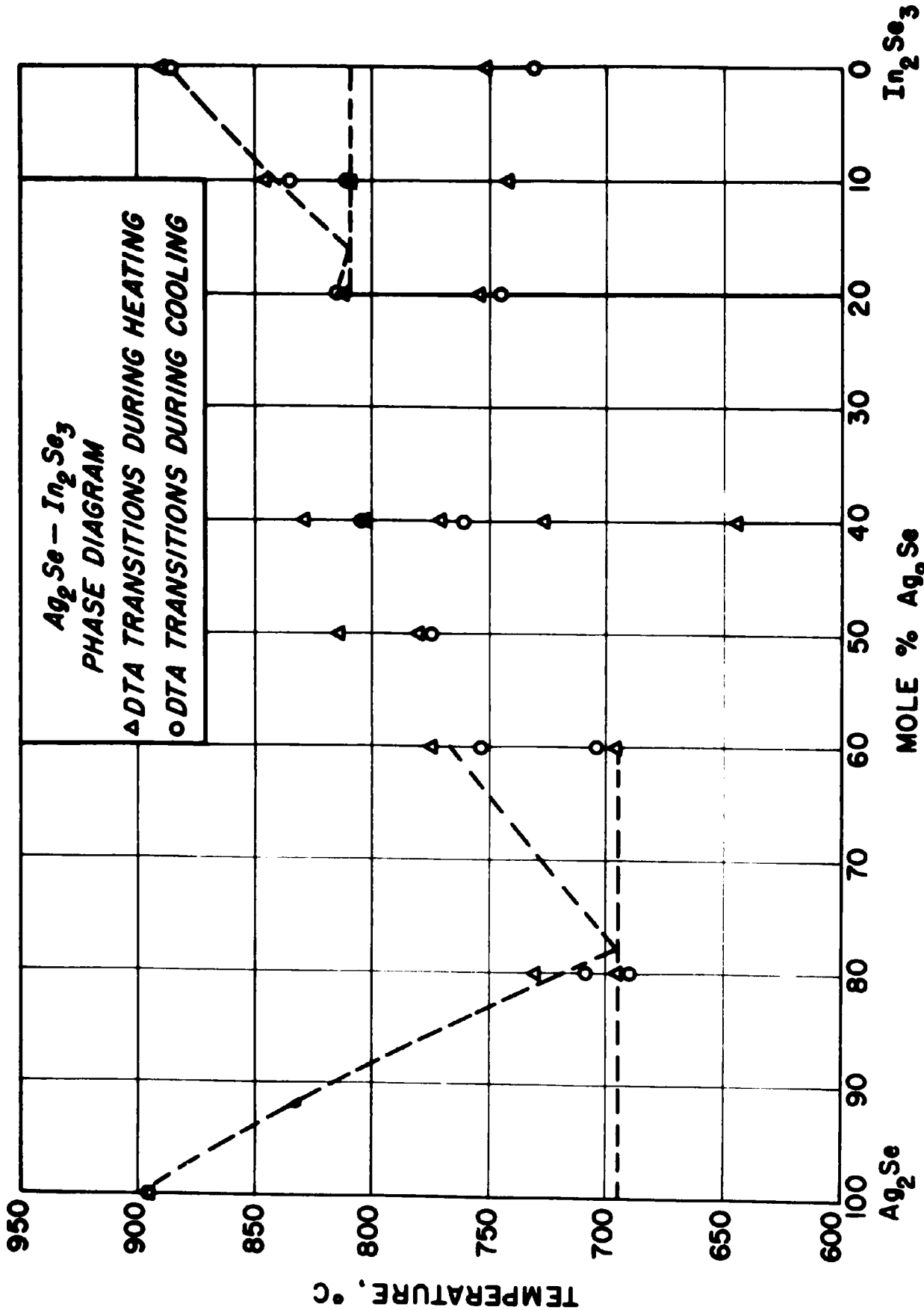


Figure 29. Partial Phase Diagram for the Ag_2Se-In_2Se_3 System.

Semiconducting Properties of $Ag_2In_8Se_{13}$.

Results of Electrical and Thermal Measurements

Electrical conductivity, Hall effect, Seebeck coefficient, and thermal conductivity measurements were made on zone refined, polycrystalline samples of $Ag_2In_8Se_{13}$. An apparent irreversible change in the electrical properties of $Ag_2In_8Se_{13}$ at high temperatures was investigated. In order to interpret the electrical measurements on this compound some understanding is needed of the change in electrical properties at high temperatures. This will be discussed after presenting the electrical and thermal measurements.

Electrical conductivity measurements were made on four zone refined samples of $Ag_2In_8Se_{13}$ and one doped sample containing 0.1 mole % Cu_2Br_2. Sample number 199 received ten zone refining passes and was removed from the zone refiner at 730°C into room air. Therefore, the cooling rate was high. The electrical conductivity results on two sections of this sample are shown in Figure 30. Measurements were made on section 5B of sample number 199 between 22°C and 803°C. In the region of 22°C to 180°C the constant value of electrical conductivity indicates that there is complete ionization of some impurities. The high concentration of impurities and the onset of an irreversible change above 350°C make it impossible to determine the energy gap from the data on this sample. The drop in electrical conductivity from 7.2 mho/cm. at 700°C to 2.0 mho/cm. at 750°C is believed to be related to the transformation observed near 750°C in the differential thermal analysis measurements. This is likely to be an order-disorder reaction.

The electrical conductivity results given in Figure 30 for section 4 of sample number 199 show a change in room temperature electrical conductivity from 6 mho/cm. to 39 mho/cm. as a result of heating above 460°C. The measurements on sample number 199 were made in a hydrogen atmosphere up to temperatures of 247°C, 462°C, and 640°C on the successive heating cycles.

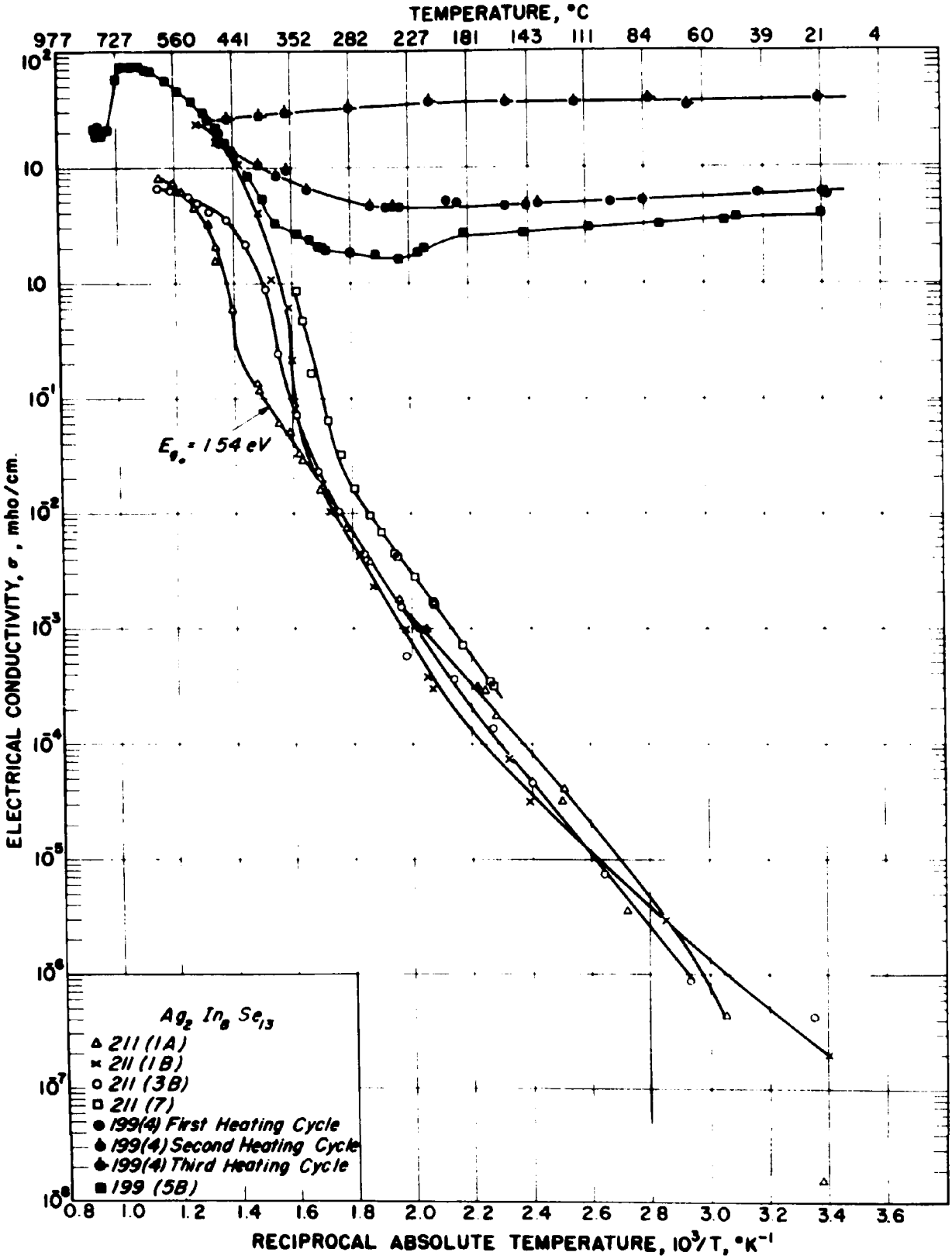


Figure 30. Logarithm of Electrical Conductivity vs. Reciprocal Absolute Temperature for $Ag_2In_8Se_{13}$, Sample Numbers 199(4), 199(5B), 211(1A), 211(1B), 211(3B), and 211(7).

Sample number 211 received thirteen zone refining passes and was annealed four days at 400°C. Electrical conductivity results on four different sections, 1A, 1B, 3B, and 7, were obtained in a hydrogen atmosphere and are shown in Figure 30. All showed a low electrical conductivity of about 10^{-7} mho/cm. at room temperature before heating, but after completion of the measurements samples 1A, 1B, and 3B had room temperature electrical conductivities between 3 mho/cm. and 19 mho/cm. Section 7 was not checked after heating. The slope of the log σ vs. 1/T data for sample number 211 (1A) was measured in the range of 235°C to 402°C, and the energy gap was calculated to be 1.54 eV.

Sample number 215 received thirteen zone refining passes and was removed from the zone refiner at 730°C into room air. Electrical conductivity results on three sections, 2A, 2B, and 5, are shown in Figure 31. The results on section 1C are given in Figure 32. This sample was used to determine the effect of repeated heating cycles to progressively higher temperatures on the electrical conductivity. The more pure end of the zone refined ingot (sections 1C, 2A, and 2B) exhibits the same level of low electrical conductivity which was found in sample number 211. However, section 5 shows a considerably higher conductivity in the low temperature region. Some of the impurities are completely ionized in the region of 70°C to 180°C.

Sample number 225 was prepared using zone refined selenium. After fusion of the elements to form the compound, and after zone refining of the compound in an 18 mm. quartz tube, a section of the pure compound was cast in a vertical 18 mm. quartz tube. This ingot was prepared in order to provide a pure thermal conductivity specimen with a large diameter. Electrical measurements shown in Figure 31 were made on two sections, A and B, directly adjacent to the thermal conductivity specimen to ascertain the purity of the ingot.

The electrical measurements on sample number 225 (A) were

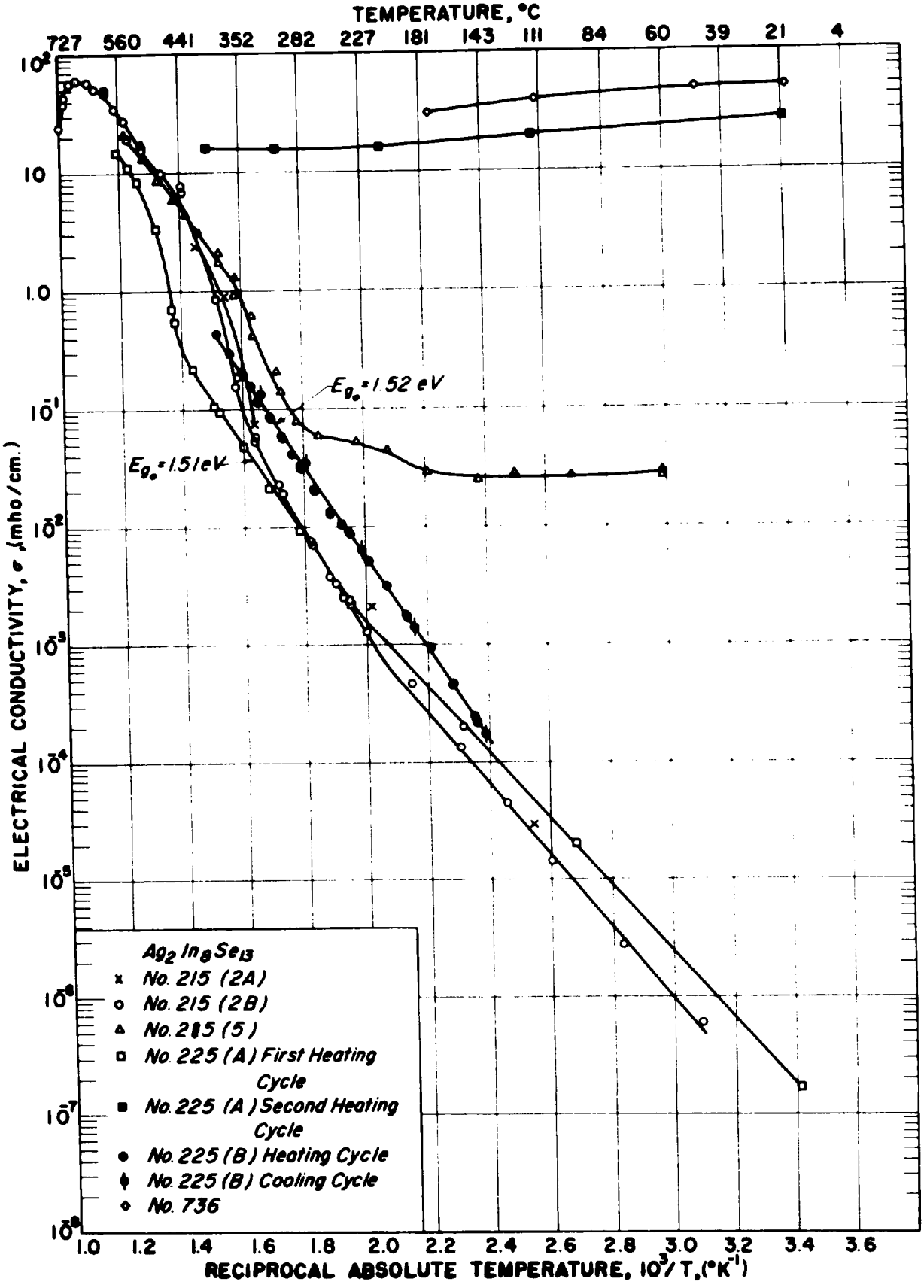


Figure 31. Logarithm of Electrical Conductivity vs. Reciprocal Absolute Temperature for $Ag_2In_8Se_{13}$, Sample Numbers 215(2A), 215(2B), 215(5), 225(A), 225(B), and 736.

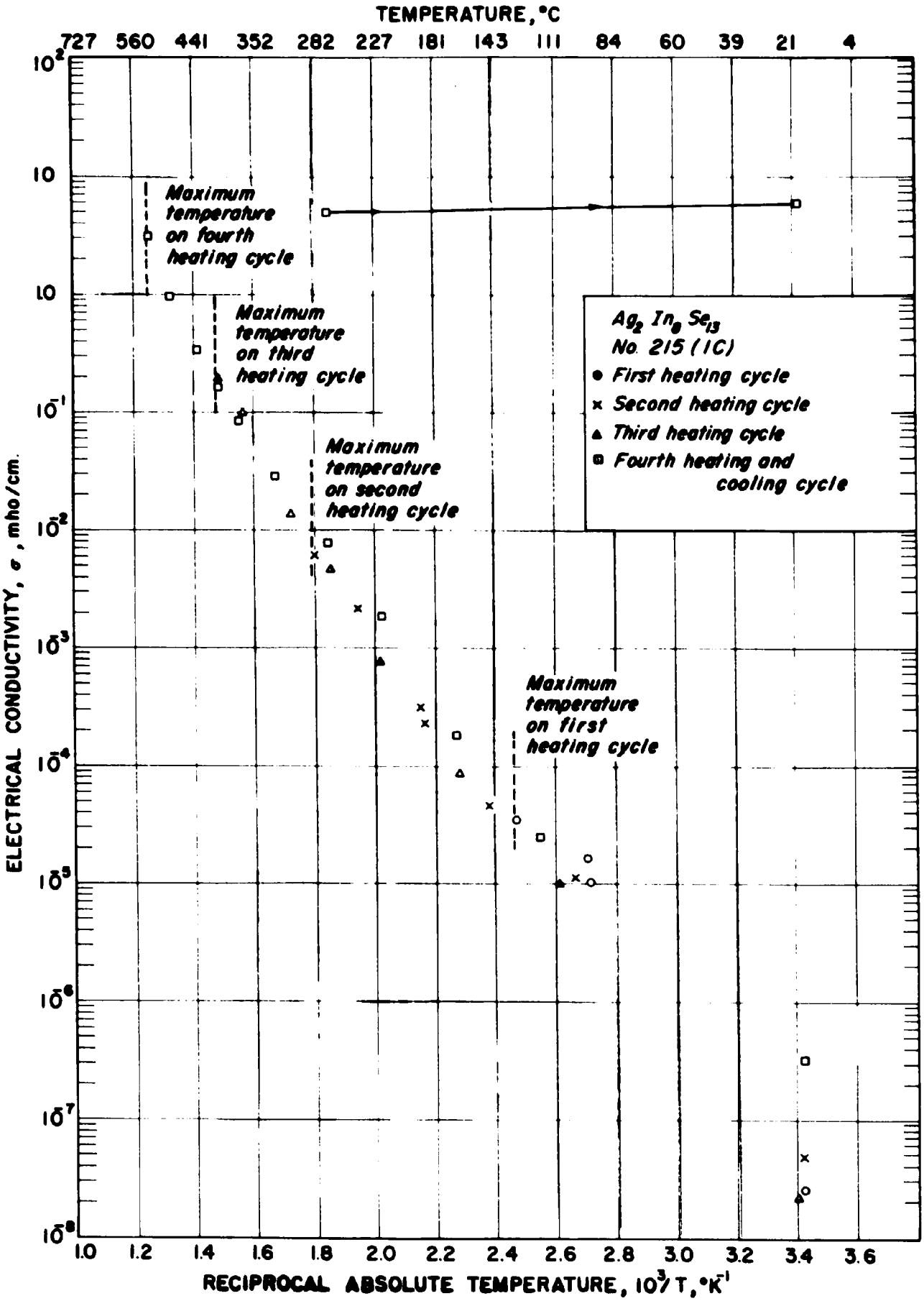


Figure 32. Apparent Irreversible Change in the Electrical Conductivity of $Ag_2In_8Se_{13}$, Sample Number 215(1C), After Heating to a High Temperature.

made in argon (99.995%), and sample number 225 (B) was measured in a hydrogen atmosphere. The electrical conductivity results are identical. The energy gap calculated from the electrical conductivity data on 225 (A) between 238°C and 421°C is 1.51 eV, and the energy gap from the data on 225 (B) between 189°C and 485°C is 1.52 eV. These results are summarized in Table X. The second heating cycle on number 225 (A) demonstrates the change which occurs as a result of heating to high temperatures.

A doped sample, number 736, was prepared by adding 0.1 mole % Cu_2Br_2 to $Ag_2In_8Se_{13}$. The material was slowly cooled through the melting point (815°C) and then annealed 14 hours at 650°C. The electrical conductivity results are shown in Figure 31.

The Hall coefficient data on sample numbers 211 (1A), 211 (1B), 211 (7), 215 (2B), 215 (5), 225 (A), and 225 (B) are given in Table XI. The slope of the log $|R_H T^{3/2}|$ vs. 1/T data in Figure 33 was used to determine the energy gap of $Ag_2In_8Se_{13}$ using Equation (15). The following energy gap values were obtained: 1.48 eV from the data on 211 (1A) between 217°C and 364°C; 1.47 eV for 211 (7) between 187°C and 280°C; 1.51 eV for 225 (A) between 238°C and 421°C; and 150 eV for 225 (B) between 189°C and 440°C. Insufficient data were available on the remaining samples to provide a reliable estimate of the energy gap value. However, it is apparent that they do not differ significantly from sample numbers 211 (1A), 211 (7), 225 (A), and 225 (B). The only exception is section 5 of sample number 215 which is extrinsic below 280°C. After heating above 500°C, the Hall coefficient for number 225 (A) decreased to 9 $cm.^3$/coulomb.

The extrinsic carrier concentration for section 5 of sample number 215 is about $2 \times 10^{15}/cm.^3$ at 190°C. The intrinsic material represented by sample number 225 (B) has a carrier concentration of about $2 \times 10^{13}/cm.^3$ at 190°C and $3 \times 10^{16}/cm.^3$ at 439°C. This assumes the mobility ratio is high. In the region of 115°C to 405°C,

TABLE X

SUMMARY OF ELECTRICAL PROPERTIES OF $Ag_2In_8Se_{13}$.

Sample Number	Energy Gap ($\log \sigma$ vs. 1/T)		Energy Gap ($\log R_H T^{3/2}$ vs. 1/T)		Seebeck Coefficient $\alpha = m/T + c$		
	E_{g_o}, eV	Temp. Range	E_{g_o}, eV	Temp. Range	m, mv	mv/°K	Temp. Range
211(1A)	1.54	235°C - 402°C	1.48	217°C - 364°C	-706	+0.256	236°C - 400°C
211(7)	1.43	167°C - 280°C	1.47	187°C - 280°C			
225(A)	1.51	238°C - 421°C	1.51	238°C - 421°C	-742	+0.191	245°C - 393°C
225(B)	1.52	189°C - 485°C	1.50	189°C - 440°C			

TABLE XI

HALL COEFFICIENT OF $Ag_2In_8Se_{13}$ AS A FUNCTION OF TEMPERATURE

Sample Number 211 (1A)

Temperature T, °K	Hall Coefficient R_H, cm^3/coulomb
491	- 51000
509	- 35300
536	- 15800
560	- 6610
590	- 3180
615	- 914
637	- 817
675	- 284
695	- 117
720	- 133
743	- 12

Sample Number 211 (1B)

Temperature T, °K	Hall Coefficient R_H, cm^3/coulomb
503	- 24700
549	- 13700
586	- 4600
625	- 1050
704	- 46
740	- 27

Sample Number 211 (7)

Temperature T, °K	Hall Coefficient R_H, cm^3/coulomb
460	- 96200
460	- 69300
483	- 47300
483	- 28000
483	- 37400
483	- 30500
499	- 20300
498	- 19200
514	- 11000
514	- 13300
514	- 9770
513	- 14400
512	- 11100
512	- 13500
527	- 7910
527	- 6520
539	- 4720
539	- 4720
553	- 2970
552	- 2490
567	- 1690
567	- 928
567	- 808
583	- 711
583	- 554
602	- 126
602	- 92
615	- 102
615	- 75
615	- 110
615	- 77

TABLE XI (Cont'd)

HALL COEFFICIENT OF $Ag_2In_8Se_{13}$ AS A FUNCTION OF TEMPERATURE

Sample Number 215 (2B)

Temperature T, °K	Hall Coefficient R_H, cm^3/coulomb
527	- 18200
531	- 12100
549	- 3810
583	- 2260
608	- 1950
631	- 279
659	- 9.9
684	- 18.1
706	- 3.0
708	- 1.8

Sample Number 225 (A)

First Heating Cycle

Temperature T, °K	Hall Coefficient R_H, cm^3/coulomb
513	- 32500
511	- 38000
559	- 7420
593	- 2960
626	- 1450
661	- 436
695	- 253
725	- 63.1
757	- 45.6
812	- 7.7

Sample Number 215 (5)

Temperature T, °K	Hall Coefficient R_H, cm^3/coulomb
398	- 6770
505	- 2350
539	- 805
554	- 616
555	- 841
582	- 683
610	- 200
633	- 97

Sample Number 225 (A)

Second Heating Cycle

Temperature T, °K	Hall Coefficient R_H, cm^3/coulomb
294	- 9 3
294	- 7.5
388	- 8 6
580	- 5.8
677	- 4.5

TABLE XI. (Cont'd)

HALL COEFFICIENT OF $Ag_2In_8Se_{13}$ AS A FUNCTION OF TEMPERATURE

Sample Number 225 (B)

Temperature T, °K	Hall Coefficient R_H, cm^3/coulomb	Temperature T, °K	Hall Coefficient R_H, cm^3/coulomb
463	-497000	593	-5360
463	-433000	593	-5140
479	-180000	611	-2940
479	-225000	611	-3360
497	-99700	628	-2020
497	-87000	628	-1950
516	-51300		
516	-49000	640	-1590
536	-22300	654	-1020
536	-23600	654	-1070
552	-13600	670	-666
552	-14400	670	-723
572	-8170	687	-556
572	-7770	687	-538
581	-7030	700	-343
581	-6550	700	-355
		712	-250
		713	-299

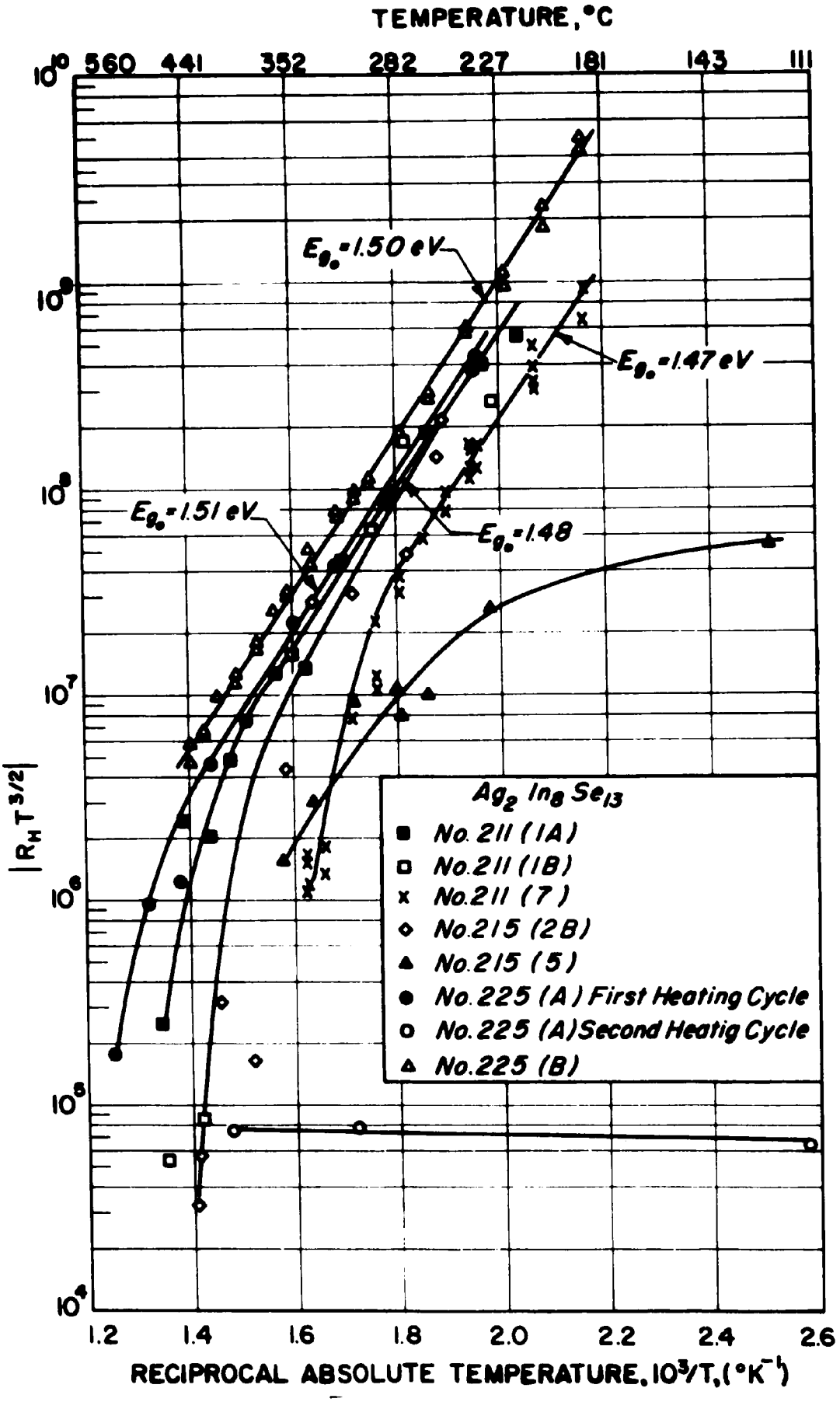


Figure 33. Logarithm of $|R_H T^{3/2}|$ vs. Reciprocal Absolute Temperature for $Ag_2In_8Se_{13}$, Sample Numbers 211(1A), 211(1B), 211(7), 215(2B), 215(5), 225(A), and 225(B).

the extrinsic carrier concentration is about $10^{18}/cm.^3$ after cooling $Ag_2In_8Se_{13}$ from above 500°C. |Sample number 225 (A)|.

The Hall mobility data for sample number 225 (B) are plotted in Figure 34. The mobility is proportional to $T^{-1.4}$ in the range 190°C to 440°C, and the standard deviation of the power term is 0.25 units. The temperature dependence of the Hall mobility can also be expressed as $\mu_{H,n} = \mu_{300} (T/300)^{\gamma}$. If the Hall mobility data can be extrapolated to 300°K, then μ_{300} represents the mobility of $Ag_2In_8Se_{13}$ at 300°K. The value of μ_{300} is 180 cm^2/volt-second for sample number 225 (B)

The Hall mobility data for section 7 of sample number 211 are included in Figure 34. The mobility values are lower than those for sample number 225 (B). The Hall mobility results on sample numbers 211 (1A), 211 (1B), 215 (2B), and 215 (5) are very limited so that a temperature dependence could not be obtained. The mobility values fall within the range of 30 cm^2/volt-second to 130 cm^2/volt-second over the temperature range of 200°C to 450°C

The Seebeck coefficient data on sample numbers 211 (1A), 211 (3B), 225 (A), and 736 of $Ag_2In_8Se_{13}$ are given in Figure 35 This data provides an indication of the start of intrinsic behavior, which is near 220°C for some of the samples The low Seebeck coefficient during the second heating cycle for 225 (A) corresponds to the large increase in electrical conductivity from about 10^{-7} mho/cm to 27 mho/cm after heating above 500°C Sample number 736 is the doped sample of $Ag_2In_8Se_{13}$

A plot of Seebeck coefficient against reciprocal absolute temperature is given in Figure 36 for sample numbers 211 (1A), 211 (3B), and 225 (A) The slope of α vs 1/T was used to calculate the electron-to-hole mobility ratio, b, from Equation (28), and the intercept allows the estimation of the temperature dependence of the energy gap from Equation (29) The data on number 211 (1A) could be well

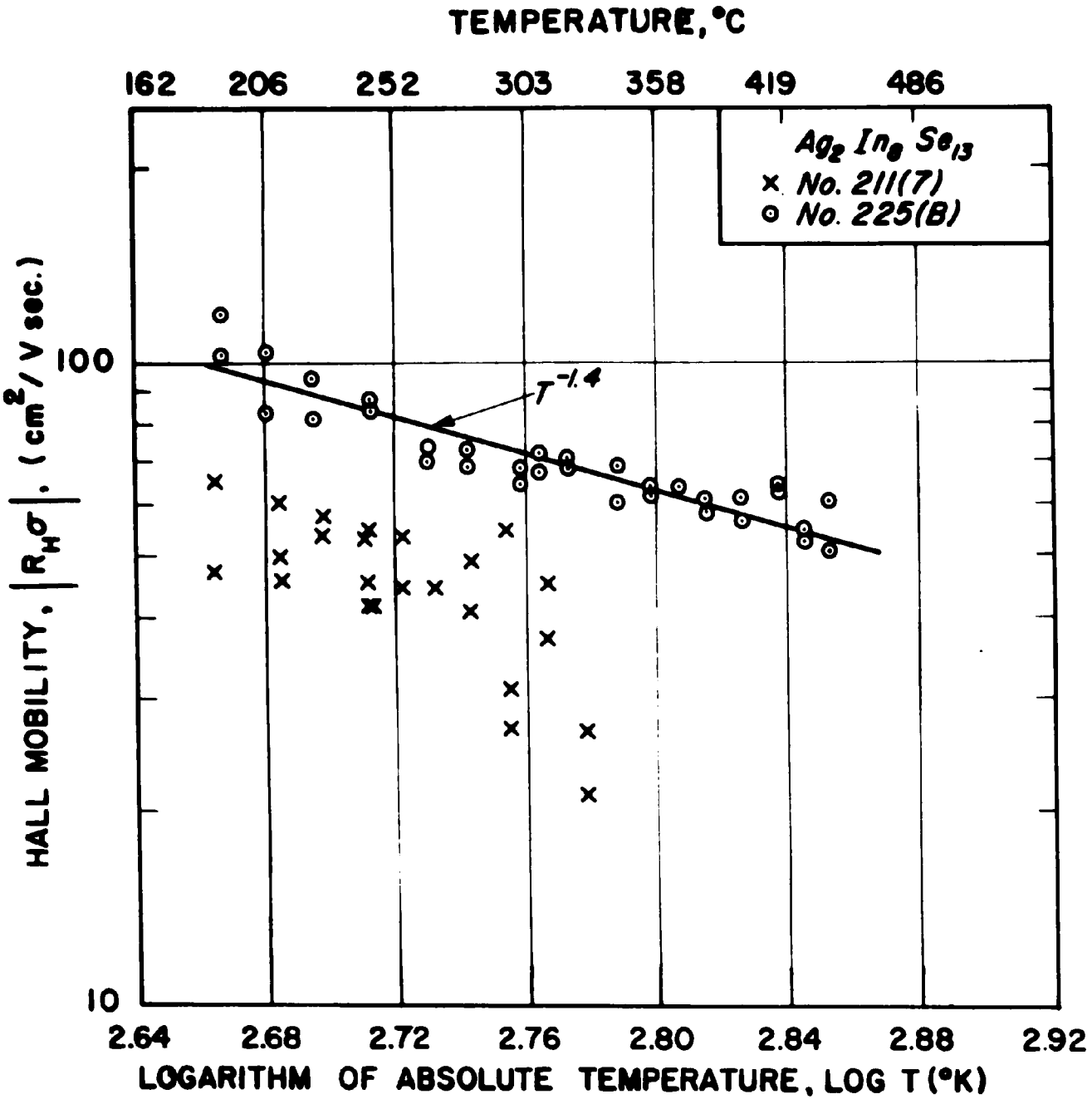


Figure 34. Logarithm of Hall Mobility vs. Logarithm of Absolute Temperature for $Ag_2In_8Se_{13}$, Sample Numbers 225(B) and 211(7).

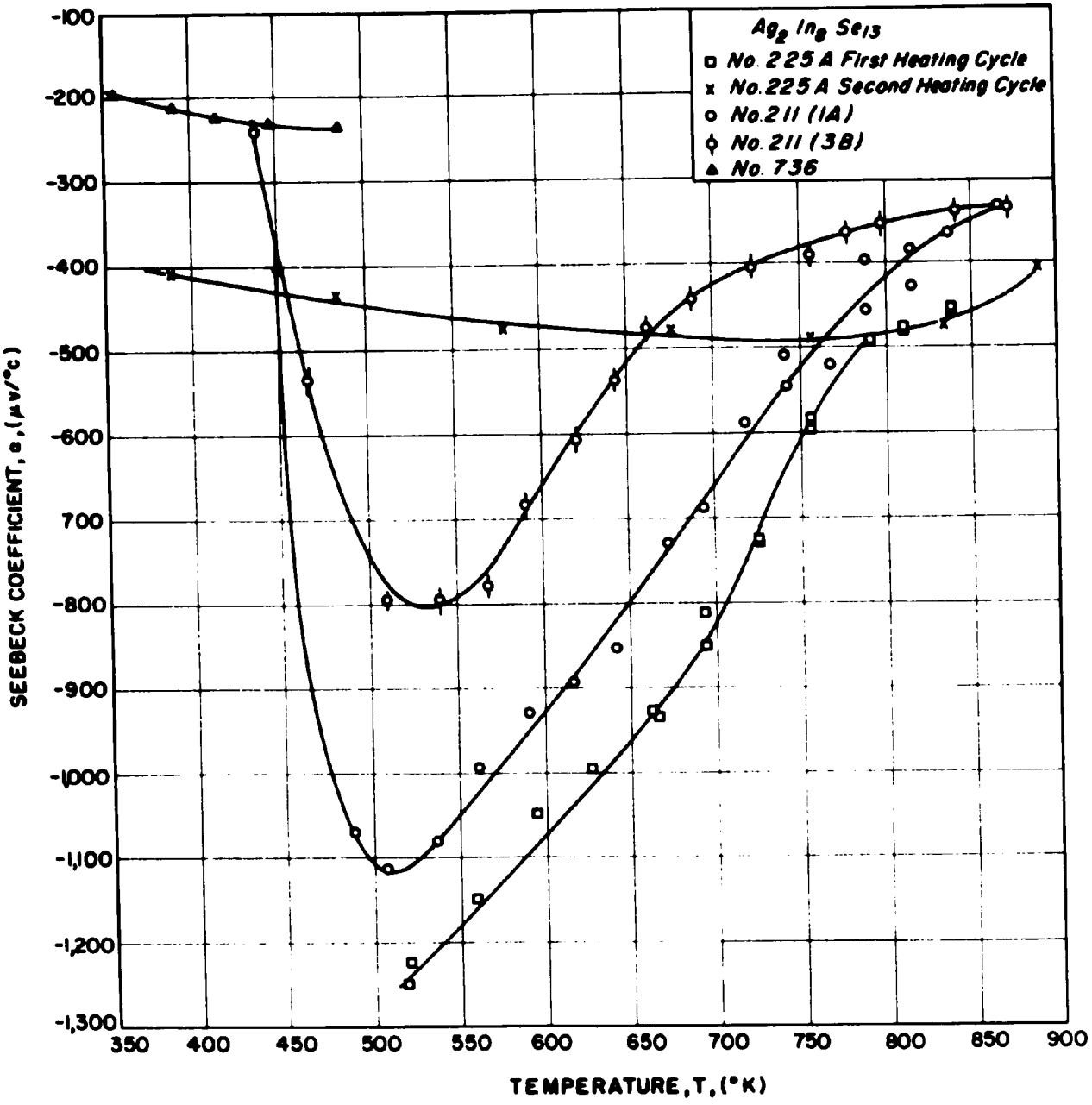


Figure 35. Seebeck Coefficient vs. Absolute Temperature for $Ag_2In_8Se_{13}$, Sample Numbers 211(1A), 211(3B), 225(A), and 736.

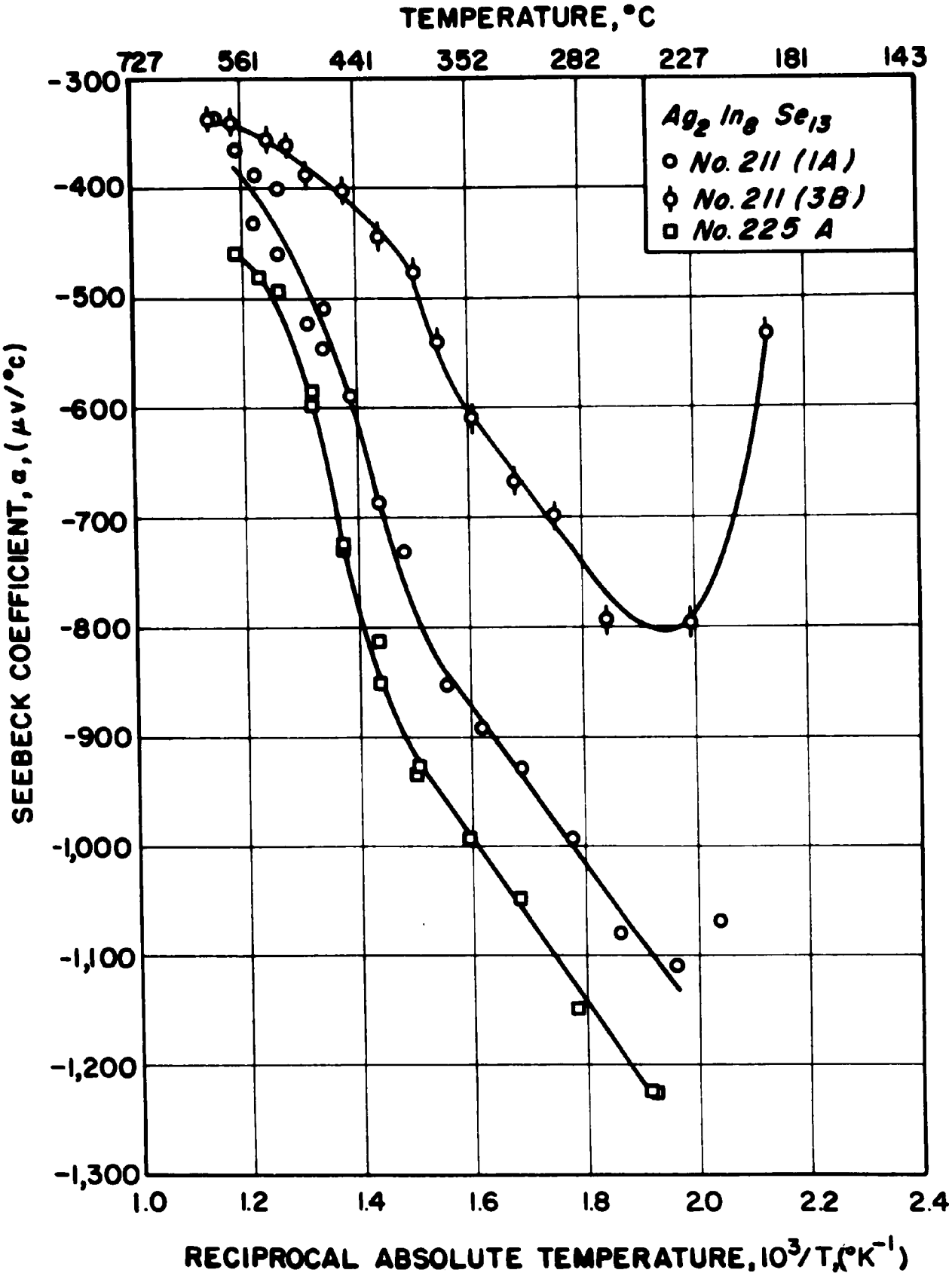


Figure 36. Seebeck Coefficient vs. Reciprocal Absolute Temperature for $Ag_2In_8Se_{13}$, Sample Numbers 211(1A), 211(3B), and 225(A).

approximated by the equation $\alpha = -(706/T) + 0.256$ mv/^{o}C between 236^{o}C and 400^{o}C. The data for sample number 225 (A) gave the equation $\alpha = -(742/T) + 0.191$ mv/^{o}C between 245^{o}C and 393^{o}C.

If an energy gap of 1.51 eV is assumed on the basis of electrical conductivity and Hall effect data, then the mobility ratio is equal to 29 for number 211 (1A) and 104 for number 225 (A). The large difference in values results from the sensitivity of Equation (28) to small changes in the slope of α vs. 1/T when the mobility ratio is high. The temperature dependence of the energy gap was calculated to be -7×10^{-4} eV/^{o}C from the data on sample number 211 (1A) and -5×10^{-4} eV/^{o}C from the data on sample number 225 (A). These calculations were made with the following assumptions: the spherical energy band approximation is valid; lattice scattering predominates; and the mobility ratio is proportional to $(m_p^* / m_n^*)^{5/2}$

The thermal conductivity of $Ag_2In_8Se_{13}$, sample number 225, is shown in Figure 37. The measurements were made between 0^{o}C and 310^{o}C. The thermal conductivity is slightly less than 0.011 watts/cm. ^{o}C below 250^{o}C, and above this temperature there is an increase This corresponds to the intrinsic behavior observed in the electrical conductivity and Hall effect measurements. The maximum recorded value of thermal conductivity was 0.0125 watts/cm. ^{o}C at 310^{o}C, the maximum temperature at which measurements were made, and the thermal conductivity was rising.

The maximum contribution from the electronic component of thermal conductivity will occur at 310^{o}C where the electrical conductivity is a maximum for the temperature range of the thermal conductivity measurements. Using the electrical conductivity of sample number 225 (A)shown in Figure 31 and Equation (37), the electronic component is about 10^{-6} watts/cm. ^{o}C at 310^{o}C, which is negligible. This assumes joint diffusion of electrons and holes. The value of the mobility ratio used in Equation (37) will not change the

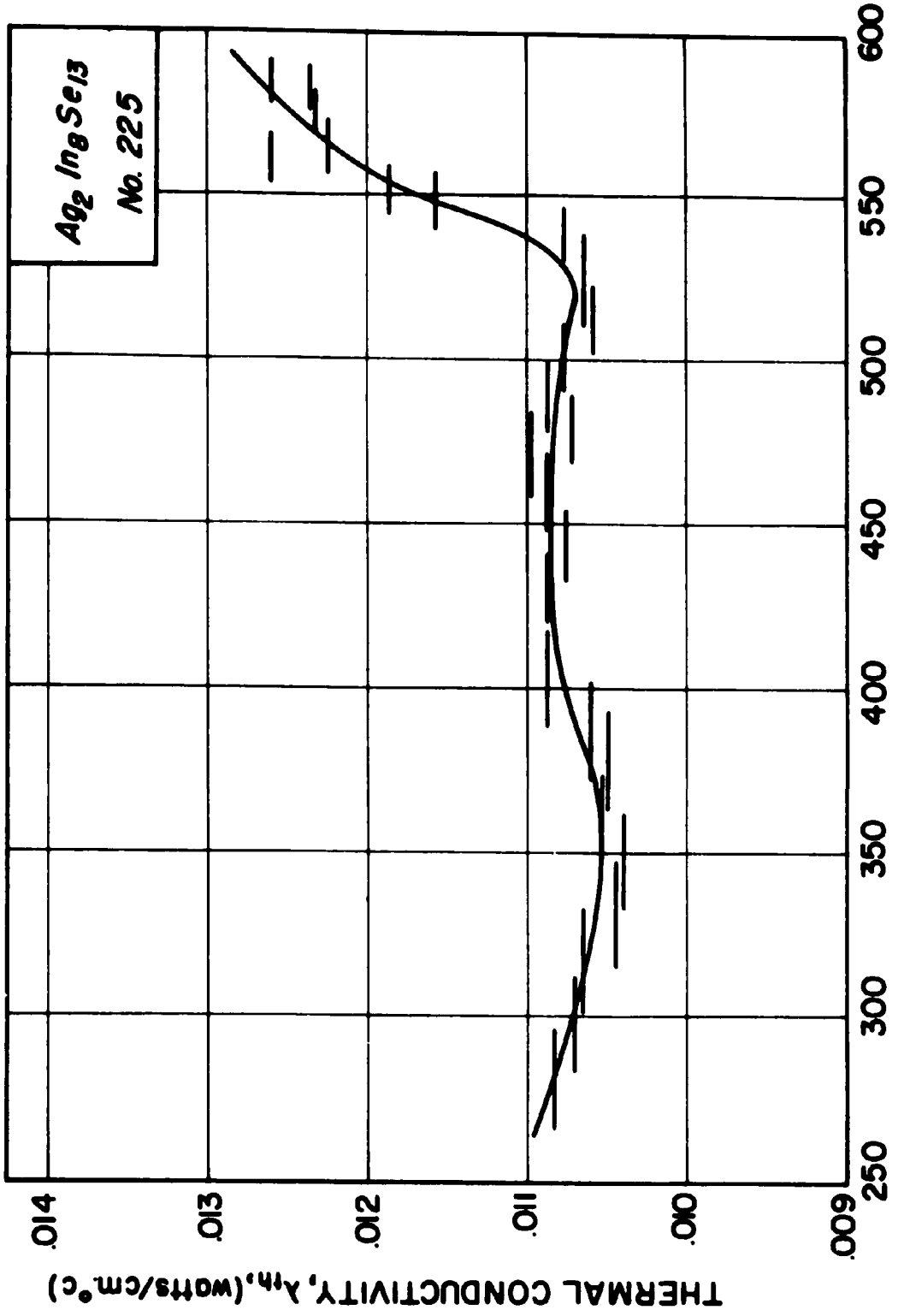


Figure 37. Thermal Conductivity vs. Absolute Temperature for $Ag_2In_8Se_{13}$, Sample Number 225.

conclusion that this mechanism does not account for the increase in thermal conductivity above 250°C. It may be that there is a diffusion of hole-electron pairs, excitons, or some other mechanism.

The thermoelectric figure of merit for $Ag_2In_8Se_{13}$ can be calculated from the thermal conductivity of sample number 225 and the extrinsic behavior observed on the second heating cycle of number 225 (A). Any difference in the thermal conductivity between the high purity of sample number 225 used for the measurements and the extrinsic properties of number 225 (A) on the second heating cycle should result from the electronic contribution to the thermal conductivity. This is equal to 1.4×10^{-4} watts/cm. °C in the extrinsic material and it is about 1% of the total thermal conductivity.

Using σ equal to 16 mho/cm., α equal to 480 uV/°C, and λ_{th} equal to 0.0125 watts/cm. °C, the figure of merit for $Ag_2In_8Se_{13}$ at 310°C is 3×10^{-4}/°K and ZT is equal to 0.2. The optimum value of ZT was calculated to be 0.6 with the curves supplied by Simon.[7]

Apparent Irreversible Effect in $Ag_2In_8Se_{13}$.

The apparent irreversible change in the electrical properties of $Ag_2In_8Se_{13}$ is shown by the electrical conductivity measurements on zone refined sample number 215, section 1C, in Figure 32. Repeated heating to progressively higher temperatures of 133°C, 284°C, and 408°C causes no appreciable change in the electrical conductivity after cooling the sample back to room temperature. However, heating to 525°C produced an irreversible change which was noted on every sample which had been heated above 500°C.

Any number of factors could produce this change in room temperature electrical conductivity from about 5×10^{-8} mho/cm. to 6 mho/cm. Several possibilities were examined and the results obtained are described. Briefly, the possibilities considered were: (1) impurities in the ambient gas; (2) formation of a surface film of high electrical conductivity at high temperatures; (3) contamination of the surface during the

preparation of the electrical specimens; (4) annealing effects; (5) crystalline transformation; (6) vaporization of selenium and impurity pick-up from the copper shield and heater supports around the sample in the measuring system. Each possibility is discussed in detail.

(1) No significant difference in electrical conductivity measurements was observed when argon was substituted for hydrogen as the ambient gas during the heating cycles. The results on sample number 215 (1C) in Figure 32 were obtained using a hydrogen atmosphere in the measuring system, whereas the results on 215 (2B) in Figure 31 were obtained with an argon atmosphere. Both samples were from the more pure end of the zone refined ingot; this is indicated by the section numbers of 1C and 2B.

(2) The high value for the room temperature electrical conductivity ($\simeq$ 6 mho/cm.) after heating above 500°C was shown to be a bulk property by polishing away at least 0.1 mm from all surfaces of an electrical specimen and remeasuring the conductivity. No change in conductivity at room temperature was observed.

(3) The sample preparation was considered as a possible source of contamination. If any impurities were left on the surface, they would be expected to diffuse into the sample at high temperatures. The electrical samples were polished with Linde B powder (aluminum oxide) to provide a mirror-like finish and then cleaned in an ultrasonic washer. The use of an acid etch was avoided because of the possibility of preferentially removing one element from the compound or plating of impurities in the acid onto the surface of the compound.

(4) The effect of annealing $Ag_2In_8Se_{13}$ after zone refining was investigated. After the completion of the zone refining operation, the samples were either air cooled from 750°C to room temperature or annealed at 400°C for four days in the sealed zone refining tube. Sample number 211, which was annealed after 13 zone refining

passes, had a low room temperature electrical conductivity (10^{-7} mho/cm.). Sample number 215, which received 13 zone refining passes and was cooled rapidly from 750°C, had the same electrical conductivity. However, sample number 199 had a room temperature electrical conductivity of 4 mho/cm. after 10 zone refining passes and rapidly cooling the sample to room temperature. The difference in electrical properties can probably be attributed to the degree of purity of the samples.

(5) X-ray analysis on $Ag_2In_8Se_{13}$ up to 500°C did not show a crystalline transformation. In addition, no latent heat effect was observed in the differential thermal analysis measurements between 25°C and 700°C. The temperature at which the slope of the log σ vs. 1/T changes from a linear to a nonlinear dependence varies from about 350°C to 480°C.

(6) The vaporization of selenium and the absorption of copper at high temperatures were investigated. Two samples, numbers 211 (4) and 211 (5), with electrical conductivities of 10^{-7} mho/cm. were sealed in clean fused silica tubes. One tube contained 1/3 of an atmosphere of argon (99.995%) along with a control sample, number 211 (4), and the second tube contained a test sample, number 211 (5), along with a small piece of copper and the argon. The samples were heated simultaneously in a furnace to 530°C and held there for two hours. After cooling, the room temperature conductivity of the control sample, number 211 (4), had increased from 10^{-7} mho/cm. to 0.16 mho/cm. In the tube containing number 211 (5) and the piece of copper, there was a gray deposit on parts of the copper surface. This may have been selenium or copper selenide. The electrical conductivity of number 211 (5) was 7.2 mho/cm. which is typical of the values obtained after heating an electrical specimen in the measuring system.

The experiment suggests that a combination of selenium loss and copper pick-up may occur during the measurements at high tempera-

tures. Alternately, there may be no significant pick-up of copper, but the copper could act as a sink for the absorption of selenium. In the tube without copper, a smaller amount of selenium was lost and the compound was in equilibrium with selenium vapor. This would explain the difference in final conductivity, 0.16 vs. 7.2 mho/cm. In the electrical measuring system there never was any evidence of a selenium deposit on the copper parts. The larger volume of the measuring system would mean a higher loss of selenium is likely and possibly vapor transport to colder sections of the system.

An attempt was made to attribute the high conductivity (6 mho/cm.) after heating to impurities which were introduced during the heating. Sample number 215 (1C) had been measured in an argon atmosphere up to 527°C and showed the usual irreversible change in electrical conductivity (10^{-7} mho/cm to 6 mho/cm.). By placing the sample in direct contact with a small piece of lead in sealed quartz tube with an argon atmosphere, it was possible to lower the room temperature electrical conductivity from 6 mho/cm. to 0.004 mho/cm. after a heat treatment of 1-1/2 hours at 500°C.

A sample of high conductivity $Ag_2In_8Se_{13}$ was sealed in a tube with selenium to determine if the conductivity could be lowered. Sample number 211 (4) had an electrical conductivity of 0.16 mho/cm. after heating in a sealed tube with argon. Heating this sample to 530°C in a selenium atmosphere was sufficient to restore the electrical conductivity to a value of 4×10^{-6} mho/cm. at 20°C. The effect of heat treating a low conductivity sample in a selenium atmosphere was also investigated. Sample number 215 (3A) had a room temperature conductivity of 2×10^{-7} mho/cm. before being sealed in a tube with selenium and heated above 500°C. After cooling to room temperature, the conductivity was 4×10^{-6} mho/cm. These results strongly suggest that the irreversible change in electrical properties can be partly attributed to a loss of selenium from the compound $Ag_2In_8Se_{13}$.

A model which would explain the irreversible change in the electrical conductivity in $Ag_2In_8Se_{13}$ after heating is shown in Figure 38. In part (a), the compound is sealed under vacuum and given a number of zone refining passes which are insufficient to remove the excess silver and indium caused by the vaporization of selenium. This may have been the case with sample number 199 which had a room temperature conductivity of 5 mho/cm. Part (b) shows the results of adequate zone refining. Selenium is lost but the excess silver and indium are removed so that a low conductivity (10^{-7} mho/cm.) is obtained (samples 211, 215, and 225). In part (c), the process occurring near 500°C in the electrical measuring equipment is postulated: selenium loss and possibly copper absorption. After cooling, the room temperature conductivity is 5 mho/cm. Parts (d) and (e) describe the heat treatments carried out with and without copper present in a sealed quartz tube. The lead treatment which lowered the conductivity from 5 mho/cm. to 0.004 mho/cm. is shown in part (f). The recovery of the low electrical conductivity by heating a sample in a selenium atmosphere is illustrated in part (g).

Discussion of the Semiconducting Properties of $Ag_2In_8Se_{13}$.

The electrical conductivity, Hall effect, and Seebeck coefficient measurements on $Ag_2In_8Se_{13}$ indicated intrinsic behavior above 200°C and below 500°C. The energy gap of the compound at 0°K is 1.51 (± 0.05) eV on the basis of the electrical conductivity and Hall effect measurements, and the temperature dependence of the energy gap obtained from the Seebeck coefficient data is -6×10^{-4} eV/°C. The Hall mobility is 110 cm^2/volt-second at 190°C, and the value at 300°K is 180 cm^2/volt-second by extrapolation. The temperature dependence of the Hall mobility is $T^{-1.4}$. The mobility ratio (μ_n/μ_p) may be about 30 on the basis of the Seebeck coefficient data. The maximum thermal conductivity over the range 0°C to 310°C is 0.0125 watts/cm. °C at 310°C.

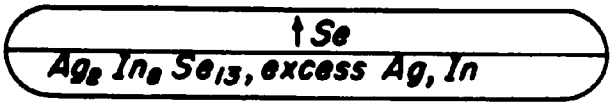
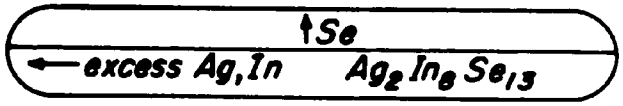
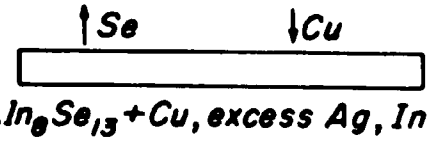
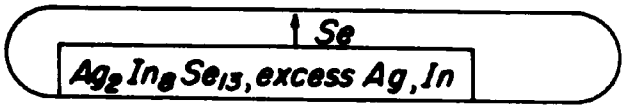
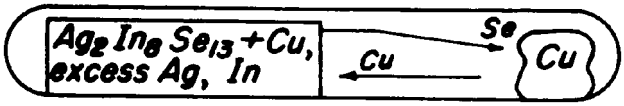
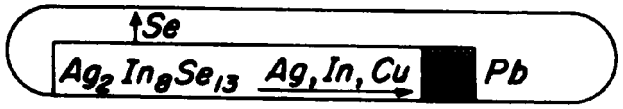
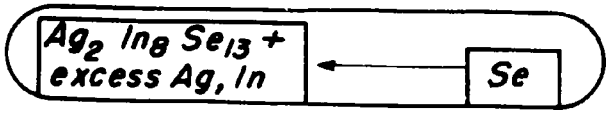
	EXPERIMENTAL CONDITIONS	Room temperature electrical conductivity, mho/cm
(a)	SEALED TUBE-NO PURIFICATION 	5.
(b)	SEALED TUBE-ZONE REFINED 	10^{-7}
(c)	HEATING OF ELECTRICAL SAMPLE IN MEASURING SYSTEM 	5
(d)	HEAT TREATMENT-SEALED TUBE 	0.16
(e)	HEAT TREATMENT-SEALED TUBE WITH COPPER 	7.
(f)	HEAT TREATMENT-SEALED TUBE WITH LEAD 	0.004
(g)	HEAT TREATMENT-SEALED TUBE WITH SELENIUM 	10^{-6}

Figure 38. Electrical Conductivity Changes in $Ag_2In_8Se_{13}$.

The electrical conductivity of $Ag_2In_8Se_{13}$ prepared by zone refining is about 10^{-7} mho/cm. at room temperature. The conductivity can be increased to about 10 mho/cm. by heating the compound above 500°C in an argon atmosphere. The principal cause of the large increase in electrical conductivity is believed to be the loss of selenium at high temperatures. As a result of this selenium loss, no data were obtained on the intrinsic properties of $Ag_2In_8Se_{13}$ above 500°C.

From the similarity of the crystal structures and chemical formulae, the properties of $Ag_2In_8Se_{13}$ ($Ag_6In_{24}Se_{39}$) might be expected to be closely related to those of In_2Se_3 ($In_{26}Se_{39}$). The data[39] available on In_2Se_3 show an optical energy gap of 1.2 eV and an electron mobility of 30 cm^2/volt-second, both at 300°K. The energy gap of $Ag_2In_8Se_{13}$ is about 1.2 eV at 300°K and the electron mobility is 180 cm^2/volt-second at 300°K. $Ag_2In_8Se_{13}$ does not have a transition near 200°C, such as that reported for In_2Se_3,[29] but both compounds have a high temperature transformation near 750°C. In the case of $Ag_2In_8Se_{13}$, this transformation results in a decrease in electrical conductivity from 7 mho/cm. to 2 mho/cm. The increase in electrical conductivity of $Ag_2In_8Se_{13}$ at 300°K as a result of an apparent deficiency of selenium may also occur in In_2Se_3.

THE PHASE DIAGRAM BEHAVIOR OF THE PSEUDO-BINARY SYSTEM OF ZnTe-In_2Te_3.

Introduction

Differential thermal analysis measurements were used to determine the characteristics of the phase diagram for the ZnTe-In_2Te_3 system. Before presenting the results of this investigation, a review will be given of the published literature on the ZnTe-In_2Te_3 system.

Literature Review

Hahn, et al.[2] reported lattice parameter values for the ZnTe-In_2Te_3 system. The 67 mole % ZnTe - 33 mole % In_2Te_3 composition was the only two phase material found by X-ray analysis. Woolley and Ray[8] also reported X-ray analysis measurements on this system. The high In_2Te_3 (100 mole % In_2Te_3 to 17 mole % ZnTe - 83 mole % In_2Te_3) and the high ZnTe (100 mole % ZnTe to 73 mole % ZnTe - 27 mole % In_2Te_3) regions of the phase diagram had disordered zinc blende structures. The compositions in the intermediate region had ordered chalcopyrite structures.

Results of Differential Thermal Analysis Measurements

Eighteen different compositions in the pseudo-binary phase diagram of ZnTe - In_2Te_3 were tested in the differential thermal analysis equipment. The compositions were: 100, 90, 80, 75, 70, 60, 50, 45, 40, 30, 25, 20, 15, 10, 7-1/2, 5, 2-1/2, and 0 mole % ZnTe. Heating and cooling curves for each sample are shown in Figure 39. All samples, with the exception of the 40 mole % ZnTe composition, were cooled from the liquid state, after fusion of the elements, by quenching the sample tube either rapidly in air or in a water bath. Prior to the differential thermal analysis (DTA) measurements, the samples were usually annealed for about one week near 600°C. Table XII shows the exact annealing conditions for each sample and some of the liquidus, solidus, and solid- solid trans-

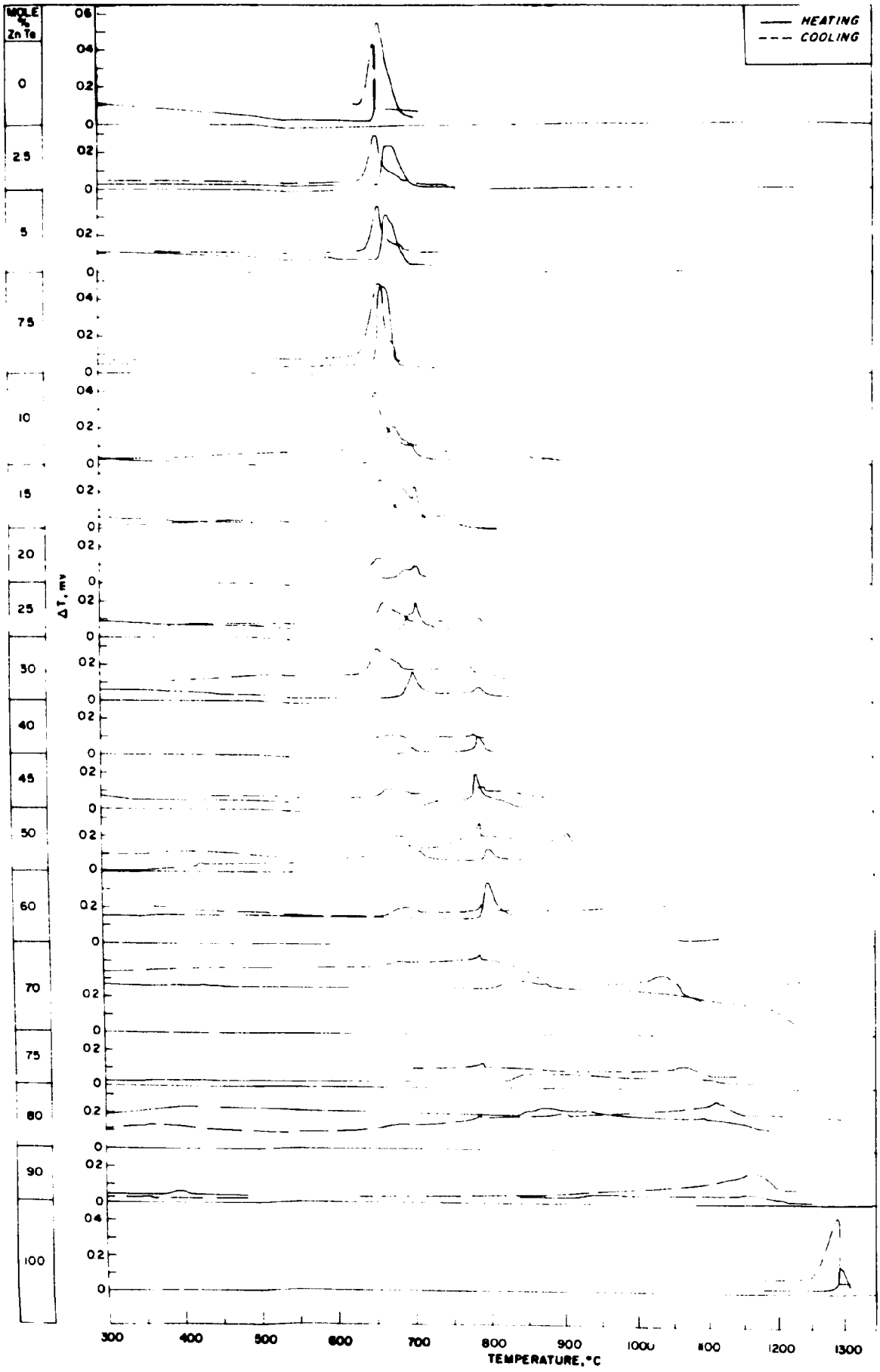


Figure 39. Differential Thermal Analysis Heating and Cooling Curves for the ZnTe-In_2Te_3 System.

TABLE XII

SUMMARY OF DIFFERENTIAL THERMAL ANALYSIS MEASUREMENTS

FOR THE PSEUDO-BINARY PHASE DIAGRAM OF Zn Te - In_2Te_3.

Sample Composition		Sample Number	Annealing Conditions	Differential Thermal Analysis Results			
				Heating		Cooling	
Mole % Zn Te	Mole % In_2Te_3			Liquidus Temp. °C	Transition Temp. °C	Liquidus Temp. °C	Transition Temp. °C
100	0	432	None	1290		1290	
90	10	668	6 days at 600° C	1210	914, 397	1197	361
80	20	664	5 days at 595° C	1164	837	1149	906, 788, 697
75	25	699	7 days at 640° C	1115	823	1094	792
70	30	667	5 days at 600° C		805, 427		792
60	40	635	4 days at 620° C	1044	795	1022	803, 723
50	50	687	2 days at 600° C		793, 428	917	791, 697
45	55	724	3 days at 600° C, 7 days at 375° C	842	783, 719	873	796, 700
40	60	634	None	800	700	795	695
30	70	666	10 days at 600° C	817	791, 704	817	787, 695
25	75	708	11 days at 590° C	820	710, 693	812	795, 702
20	80	649	None		717		688
15	85	697	7 days at 600° C	779	708, 691	768	701
10	90	665	10 days at 600° C	747	708, 679	739	696
7-1/2	92-1/2	723	7 days at 500° C	695	670	690	673
5	95	696	7 days at 600° C	710	669	715	
2-1/2	97-1/2	722	7 days at 500° C	715	671	719	
0	100	147	None	669		667	

formation temperatures obtained from the DTA data.

The pseudo-binary phase diagram for the ZnTe-In_2Te_3 system shown in Figure 40 was drawn on the basis of the DTA data. The liquidus line starting at the melting point of ZnTe, 1290°C, extends downward to about 22 mole % ZnTe and 795°C and then over to 100 mole % In_2Te_3 and 667°C. There appears to be three peritectic compounds in the system. The first is at 50 mole % ZnTe and decomposes at 795°C. The other two may be near 25 mole % ZnTe and 15 mole % ZnTe with decomposition temperatures of 708°C and 692°C, respectively. A two phase region of solid (δ-phase) and liquid may occur between 15 mole % ZnTe - 85 mole % In_2Te_3 and 100 mole % In_2Te_3.

A solid-solid transition occurs near 420°C in the 90, 70, and 50 mole % ZnTe compositions. The small heat effect associated with this transition may account for its absence on the DTA curves of the other samples between 100 and 50 mole % ZnTe. The change from α - phase to β - phase material should take place near 30 mole % ZnTe if the results of Woolley and Ray[8] are used as a guide. The β - phase and γ - phase materials are disordered chalcopyrite and the δ - phase material has a disordered zinc blende structure according to the X-ray results.[8]

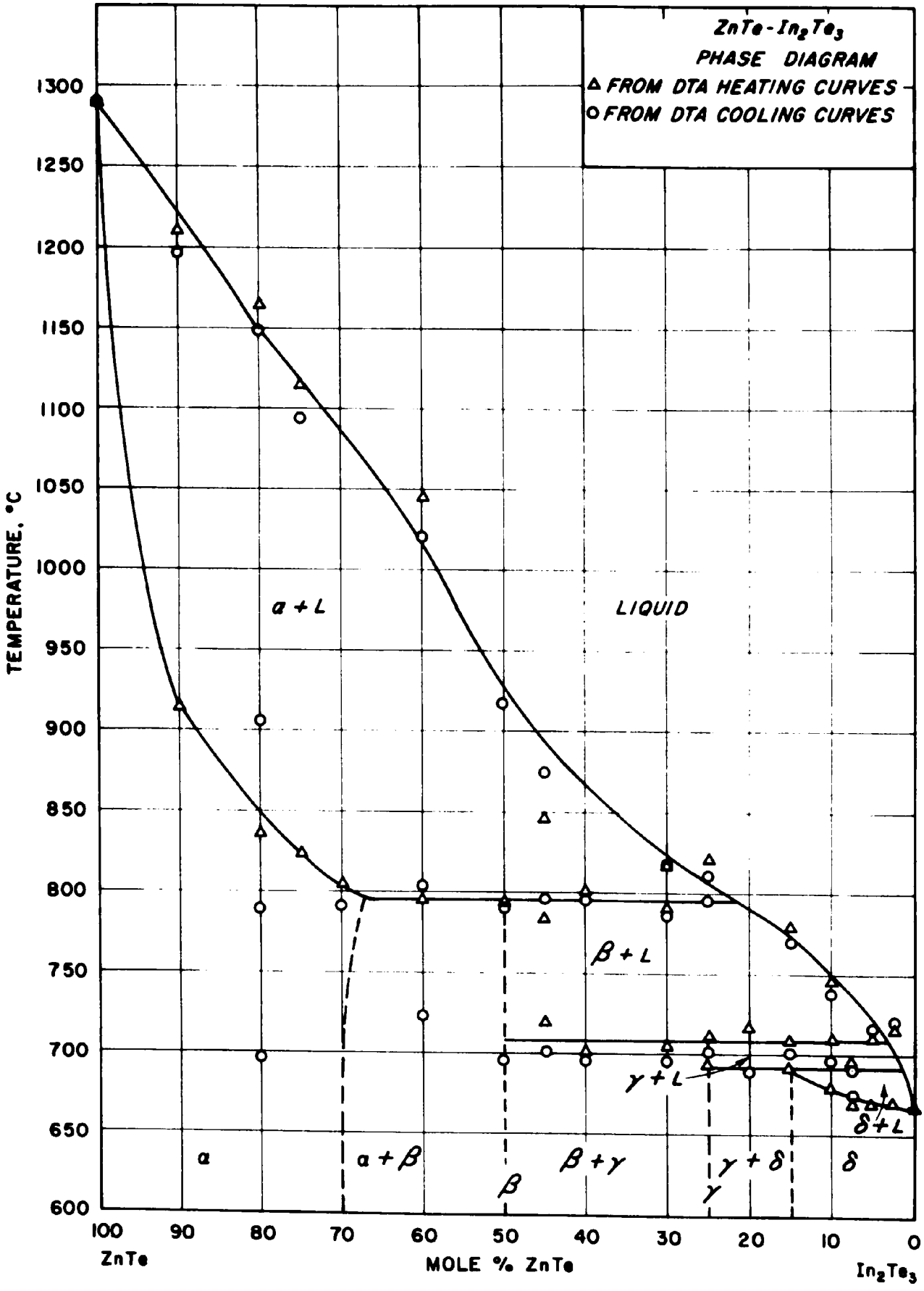


Figure 40. Phase Diagram for the ZnTe-In_2Te_3 System.

OTHER PSEUDO-BINARY SYSTEMS

Introduction

A limited study was made of the systems Cu_2Se-In_2Se_3, Cu_2Te-In_2Te_3, HgSe-In_2Se_3, HgTe-In_2Te_3 by differential thermal analysis. As a result of the complex series of transformations found in the copper systems, emphasis was shifted to the more promising pseudo-binary diagrams that have already been discussed. The HgSe-In_2Se_3 investigation was limited to two compositions because of the violent reactions which occur during the preparation from the elements. The effort on the HgTe-In_2Te_3 system consisted of attempts to prepare electrical samples of the congruently melting compound $HgIn_2Te_4$.

Literature Review

Hahn, et al.[1,2] reported X-ray analysis results on the Cu_2Se-In_2Se_3, Cu_2Te-In_2Te_3, HgTe-In_2Te_3 systems and $HgIn_2Se_4$. Woolley and Ray[8] also reported lattice parameter measurements on the HgTe-In_2Te_3 system.

Hansen[36] gives a partial phase diagram for the Cu-Se binary system. The melting point of Cu_2Se is listed as 1115°C, and there is a crystalline transformation in Cu_2Se near 100°C.

The phase diagram for the Cu-Te binary system is contained in Hansen.[36] Cu_2Te melts at 1125°C, and there are two peritectic compounds, which decompose at 630°C and 727°C, near Cu_2Te. At slightly higher copper concentrations there are solid-solid transitions at 305°C, 360°C, and 555°C.

The Cu_2Se-In_2Se_3 Pseudo-binary System

Differential thermal analysis measurements were obtained on the following compositions in the Cu_2Se-In_2Se_3 pseudo-binary system: 100, 80, 60, 50, 40, 20, and 0 mole % Cu_2Se. The samples were annealed under the conditions shown in Table XIII before making the DTA

TABLE XIII

SUMMARY OF DIFFERENTIAL THERMAL ANALYSIS MEASUREMENTS

FOR THE PSEUDO-BINARY PHASE DIAGRAM OF $Cu_2Se - In_2Se_3$.

Sample Composition		Sample Number	Annealing Conditions	Differential Thermal Analysis Results			
				Heating		Cooling	
Mole % Cu_2Se	Mole % In_2Se_3			Liquidus Temp. °C	Transition Temp. °C	Liquidus Temp. °C	Transition Temp. °C
100	0	628	None	1148	143	1144	134
80	20	673	6 days at 550° C, 1 day at 340° C	952	941, 918, 791, 142	935	912, 777, 138
60	40	651	7 days at 590° C	1000	933, 912, 787, 139	978	930, 911, 781, 139
50	50	1017	None	1018	820, 789	993	800, 787
40	60	652	6 days at 600° C, 4 days at 480° C	1016	464	987	
20	80	653	7 days at 590° C	968	899, 884, 751	943	896
0	100	676	5 days at 595° C	888	751, 210	885	731, 98

measurements. The liquidus, solidus, and solid-solid transformation temperature obtained from the DTA heating and cooling curves are listed in Table XIII.

Cu_2Se melts at 1148 (± 5) ^{o}C and has a solid-solid transition at 143^{o}C. This low temperature transition also occurs in the 80 and 60 mole % Cu_2Se compositions. The 80 and 60 mole % Cu_2Se have common transitions near 790^{o}C, 912^{o}C, and 930^{o}C. A number of possibilities exist for the phase diagram behavior in the high Cu_2Se side of the diagram. The heat effect near 790^{o}C could be a eutectic or a solid-solid transition. If the latter is the case, then the transition near 912^{o}C is likely to be a eutectic, and the 930^{o}C transition represents the decomposition of a peritectic compound.

The 50 mole % Cu_2Se composition has two transitions at about 810^{o}C and 788^{o}C which have small heat effects in comparison to the heat absorbed on melting just below 1000^{o}C. This is the only sample on which DTA measurements are lacking below 700^{o}C. The 40 mole % Cu_2Se melts near 987^{o}C, and there is a transition at 464^{o}C.

The 20 mole % Cu_2Se has a small transition near 751^{o}C on heating; this is probably related to the solid-solid transformation in In_2Se_3 near 740^{o}C. A number of overlapping transitions occurred between 870^{o}C and the liquidus temperature of 943^{o}C.

An outline of the Cu_2Se-In_2Se_3 phase diagram will have to await further DTA measurements.

The Cu_2Te-In_2Te_3 Pseudo-binary System

The liquidus, solidus, and solid-solid transformation temperatures for seven compositions, at 80, 60, 50, 40, 20, and 0, mole % Cu_2Te are shown in Table XIV for the Cu_2Te-In_2Te_3 system. The DTA results on sample number 737 are limited to the heating cycle because of an equipment failure near 750^{o}C. The results on the other samples represent the observed transitions between 25^{o}C and the liquid state of

TABLE XIV

SUMMARY OF DIFFERENTIAL THERMAL ANALYSIS MEASUREMENTS

FOR THE PSEUDO-BINARY PHASE DIAGRAM OF $Cu_2Te - In_2Te_3$.

Sample Composition		Sample Number	Annealing Conditions	Differential Thermal Analysis Results			
				Heating		Cooling	
Mole % Cu_2Te	Mole % In_2Te_3			Liquidus Temp. °C	Transition Temp. °C	Liquidus Temp. °C	Transition Temp. °C
80	20	637	6 days at 590° C		739, 654, 639, 583, 360, 320		
80	20	663	7 days at 600° C 1 day at 330° C	765	734, 650, 636, 575, 465, 360, 320	742	734, 637, 607, 558, 425, 357, 310
60	40	639	2 days at 580° C	803	743, 655, 641, 364	777	740, 647, 612, 558, 320
60	40	663	6 days at 550° C	803	738, 655, 638, 582	772	737, 643, 608, 554
50	50	731	None	801	780, 670, 654	783	667, 654
40	60	638	6 days at 590° C	810	782, 429	784	607
20	80	632	2 days at 580° C	772	672	760	660
0	100	147	None	669		667	

material. The heat effects from the transitions below 600°C were small for all the samples.

The only region of the pseudo-binary phase diagram of Cu_2Te-In_2Te_3 which might be explained on the basis of the DTA measurements is between the 60 and 100 mole % Cu_2Te. First, a review of the results reported by Hansen[36] for the Cu-Te phase diagram will help in the interpretation of the pseudo-binary data.

In the Cu_2Te-In_2Te_3 system, the higher liquidus temperature of the 60 mole % Cu_2Te compared to the 80 mole % Cu_2Te may mean the 734°C transition is a eutectic. If this is the case, then the liquidus line drops from 1125°C at 100 mole % Cu_2Te to 734°C near the 80 mole % Cu_2Te. This would account for the presence of the 650°C and 734°C transitions in both the 80 and 60 mole % Cu_2Te, but absent in the Cu_2Te.

The results on the remainder of the pseudo-binary system are too limited to predict the phase diagram characteristics.

Pseudo-binary Systems Containing Mercury

DTA measurements were obtained on the 40 and 50 mole % HgSe compositions in the HgSe-In_2Se_3 pseudo-binary phase diagram. The mole % HgSe composition melts near 825°C and the 50 mole % HgSe at 830°C. The latter composition has a small transition at 730°C on heating and at 696°C on cooling. Neither composition appears to melt congruently.

$HgIn_2Te_4$, the 50 mole % HgTe composition from the HgTe-In_2Te_3 system, appears to be a congruently melting compound (708°C) from the DTA results. The zone refining techniques available were not adequate for the preparation of samples free of microcracks in all but one case. The one sample proved to be multiphase, possibly as a result of a decomposition in the zone refiner.

SUMMARY OF RESULTS

The pseudo-binary phase diagrams for the $CdSe-In_2Se_3$ system and the $ZnTe-In_2Te_3$ system have been established. In addition, partial phase diagrams are given for the $Ag_2Se-In_2Se_3$ system and the $Ag_2Te-In_2Te_3$ system. Summaries of the transition temperatures observed by differential thermal analysis are given for the $Cu_2Te-In_2Te_3$ and $Cu_2Se-In_2Se_3$ systems.

Two congruently melting compounds, $Ag_2In_8Se_{13}$ and $AgIn_3Te_5$, were found as a result of the phase diagram studies. Polycrystalline samples of these compounds and the peritectic compound $CdIn_2Se_4$ were prepared by zone refining. Zone leveling was used to prepare the three peritectic compounds in the $CdTe-In_2Te_3$ pseudo-binary system.

Some of the semiconducting properties, such as electrical conductivity, Hall effect, Seebeck coefficient, and thermal conductivity, were determined for $CdIn_2Se_4$, the three peritectic compounds from the $CdTe-In_2Te_3$ system , $AgIn_3Te_5$, and $Ag_2In_8Se_{13}$. The energy gap values obtained from the electrical measurements were 1.1 eV for $AgIn_3Te_5$, 1.51 eV for $Ag_2In_8Se_{13}$, 1 02 eV for $CdIn_8Te_{13}$, and 1.38 eV for the β-phase (45 mole % CdTe - 55 mole % In_2Te_3) and 1.17 eV for the δ-phase (9 mole % CdTe - 91 mole % In_2Te_3) materials from the $CdTe-In_2Te_3$ system. The Hall electron mobilities of $CdIn_8Te_{13}$, $AgIn_3Te_5$, and $Ag_2In_8Se_{13}$ were near 200 cm^2/volt-second at 300° K. These results are shown in Table XV.

The electrical conductivity of $Ag_2In_8Se_{13}$ was about 10^{-7} mho/cm. at 300° K. This value could be increased to about 10 mho/cm. by heating the compound above 500° C in an inert atmosphere. The change could be partially reversed by heat treating $Ag_2In_8Se_{13}$ in a selenium atmosphere.

The thermal conductivities of the β-phase material (45 mole % CdTe - 55 mole % In_2Te_3), $AgIn_3Te_5$, and $Ag_2In_8Se_{13}$ were approximately 0.011 watts/cm. °C near 300° K.

TABLE XV

SUMMARY OF SEMICONDUCTING PROPERTIES FOR THE TERNARY COMPOUNDS

Compound	Energy Gap at 0° K, eV	Hall Electron Mobility at 300° K, cm^2/volt-sec.	Thermal Conductivity at 300° K, watts/cm. $^{\circ}$C	Melting Point, $^{\circ}$C
β-phase (45 mole % CdTe-55 mole % In_2Te_3)	1.38		0.011	785
$Cd\,In_8Te_{13}$ (20 mole % CdTe-80 mole % In_2Te_3)	1.02	240		702
δ-phase (9 mole % CdTe-91 mole % In_2Te_3)	1.17	80		695
$Ag\,In_3Te_5$ (25 mole % Ag_2Te-75 mole % In_2Te_3)	1.1	250	0.010	699
$Ag_2In_8Se_{13}$ (20 mole % Ag_2Se-80 mole % In_2Se_3)	1.51	180	0.011	815

CONCLUSIONS

Some knowledge of the binary phase diagrams is necessary for the interpretation of the transitions in the ternary system along the pseudo-binary tie line. This is demonstrated, particularly, by the complex behavior in the Cu_2Te-In_2Te_3 system at the high Cu_2Te side of the diagram.

The addition of either Ag_2Se or CdSe in amounts up to 20 mole % to In_2Se_3 tends to lower the melting point and produces a eutectic near the In_2Se_3 side of the pseudo-binary phase diagram. The addition of ZnTe or CdTe to In_2Te_3 causes an increase in melting point and the formation of peritectic compounds.

The ZnTe-In_2Te_3 pseudo-binary phase diagram has the same characteristics as the CdTe-In_2Te_3 diagram.

The substitution of small amounts of cadmium or silver for indium in the compound In_2Te_3 does not cause a significant change in energy gap. This is seen by comparing the energy gaps for $AgIn_3Te_5$ (1.1 eV) and $CdIn_8Te_{13}$ (1.02 eV) with In_2Te_3 (1.1 eV).[33]

For the ternary compounds containing indium and tellurium with similar crystal structures, which were studied in this investigation, the melting point provides some indication of the energy gap value.

There is no change in thermal conductivity in going from ordered In_2Te_3 to the ternary compound $AgIn_3Te_5$ (25 mole % Ag_2Te - 75 mole % In_2Te_3) and the β-phase (45 mole % CdTe - 55 mole % In_2Te_3) material from the CdTe-In_2Te_3 system.

A slight deficiency of selenium in the compound $Ag_2In_8Se_{13}$ can cause a large increase in the electrical conductivity and a change from intrinsic to extrinsic behavior.

The use of compounds in pseudo-binary systems serves as a means of altering the properties of the binary compounds which make up the system, and possibly improving on certain desirable properties.

APPENDIX I

PREPARATION OF SAMPLES

Introduction

This appendix describes in detail the procedures followed in obtaining high purity, polycrystalline samples for electrical and thermal measurements. The elements, which were of semiconductor grade purity and etched prior to using, were reacted in evacuated quartz tubes to form the appropriate compounds and mixtures. Subsequently, either differential thermal analysis measurements were made in special quartz tubes or the material was zone refined or zone leveled. Each compound was found to present special problems which required modifications in the preparational procedure. These are described along with the zone refining equipment used.

Raw Materials

All the samples were prepared from the elements with purities of either 99.99+% (or 99.999+%.) The selenium (99.999+%), tellurium (99.999+%), silver (99.99+%), and cadmium (99.99+%) were obtained from the American Smelting and Refining Corporation. The indium (99.999+%) was supplied by the Indium Corporation of America.

Etching Procedure

Three of the elements, silver, selenium, and mercury, were added directly to the sample tubes without etching. Indium was etched with dilute aqua regia, followed by concentrated nitric acid, and rinsed well with deionized water. Cadmium and zinc were treated with concentrated nitric acid and rinsed with deionized water. Tellurium was treated with dilute nitric acid and rinsed with deionized water. Concentrated nitric acid and deionized water were used on copper; this was followed by a solution of cupric ammonium chloride and ammonium hydroxide and then a rinse with deionized water.

Preparation of Samples for Differential Thermal Analysis and Zone Refining

Two general classes of samples were prepared: those for differential thermal analysis and those for zone refining. The differential thermal analysis samples were prepared by adding the stoichiometric quantities of the pure elements, usually a total of 18 grams, to a 10 mm. inside diameter quartz tube which was then sealed off at a pressure of 5×10^{-5} mm. Hg or lower. The mixture was heated using a programmed cycle that avoided explosions in most cases. The digital temperature programming unit used is described by Hozak, Cook, and Mason.[28] The compositions were heated about 200°C above the liquidus temperature and then water quenched. The material was removed from the sealed tube and ground to a powder before adding to a differential thermal analysis tube. This tube was made of 10 mm. quartz with a concentric well (4 mm. inside diameter) in the bottom to accommodate a thermocouple. The tube was sealed off at a pressure of 5×10^{-5} mm. Hg or lower with an over-all length of about 4 inches. The amount of free space above the sample was kept to a minimum. Before making the differential thermal analysis measurements, the sample was usually annealed one week in the region of 600°C, depending on the phase diagram being investigated.

Samples for zone refining were prepared in one of five ways. For compositions which had a low heat of reaction during the fusion of the elements, 70 grams of the elements were placed in a 10 mm. inside diameter quartz tube and sealed off at a pressure of 5×10^{-5} mm. Hg or below so that the length was approximately 12 inches. Heating was carried out at a rate of a few hundred degrees centigrade per hour until the material was about 200°C above the melting point of the compound. The tube was then transferred as a liquid to the zone refining furnace.

In the case of $AgIn_3Te_5$, two other methods of zone refining were tried. One consisted of sealing the compound in an evacuated

10 mm. inside diameter quartz tube which was then sealed in an evacuated 16 mm. inside diameter quartz tube. The other method used a carbon boat for a container during the zone refining. The spectroscopic grade carbon boat was baked at 1400°C under vacuum and then kept under an argon atmosphere prior to its use. The compound was added to the boat and placed inside a 16 mm. inside diameter quartz tube which was then sealed under vacuum.

For compositions which liberated a high heat of reaction during the fusion of the elements, such as $Ag_2In_8Se_{13}$, the sample size was reduced to 35 grams and two fusion samples were made using a slow heating rate. These were then combined to provide one zone refining sample. An alternate method which was useful for the preparation of 250 gram samples was the diffusion of selenium into a mixture of silver and indium. The stoichiometric quantities of the elements were sealed in an inverted Y-tube with selenium on one side and the silver and indium on the other. After heating rapidly to 400°C, the temperature was increased about 50°C per day and then held at 50°C above the melting point of the compound for one day. All the selenium diffused and reacted with the silver and indium.

Zone Refining

The zone refining furnaces, which resemble submarines in appearance, had six independently heated zones. The liquid zone of the sample could be observed through a pyrex window mounted six inches above the center region of the furnace. Before inserting the samples, the furnace was balanced so that the center zone was about 15°C above the melting point of the congruently melting compound. The solid sections of the ingot were usually 60°C below the melt point. The liquid zone moved at a rate of 3/4 inches per hour for normal zone refining by moving the sample tubes through the stationary furnaces. The liquid zone was usually 1-1/2 inches long and the length of the sample about 12 inches. Zone leveling of the peritectic compounds was

carried out at 0.3 inches per hour and in some cases at 0.16 inches per hour. The application of zone leveling to peritectic compounds is described by Mason and Cook.[6]

APPENDIX II

DIFFERENTIAL THERMAL ANALYSIS

Differential thermal analysis (DTA) measurements were made with a sample from the pseudo-binary system and a reference material, such as indium It was possible to detect solid-liquid transitions as well as solid-solid transformations which liberated sufficient heat to cause a temperature difference of about 0 5^{o}C between the sample and reference A continuous recording of the sample temperature and the differential temperature between the sample and the reference material could be obtained from room temperature up to as high as 1300^{o}C

The measuring system is shown schematically in figure 41 The thermocouple mounted in the bottom of the sample tube was connected through an ice-water reference junction to the Y scale of a Leeds and Northrup Model G Speedomax X-Y Recorder The differential temperature signal was amplified with a Leeds and Northrup D C amplifier and fed to the X-scale of the recorder The range was 0-10 mv in each direction on chart paper 10 inches wide The differential emf was shifted to read zero at mid-scale by providing a 5 mv auxiliary emf in series with the output from the D C amplifier

When the output from the sample temperature thermocouple reached 10 mv , a Leeds and Northrup precision portable potentiometer was used to buck out 10 mv At the same time the chart paper on the X-Y recorder was reset so that the next 10 mv of the temperature scale was recorded on a new section of chart paper With chromel-alumel thermocouples, a chart about 40 inches long would be obtained for measurements on a sample between 25^{o}C and 1000^{o}C The Kanthal resistance heated furnace which had an automatic program control, provided essentially linear heating rates of about 2-1/2^{o}C per minute

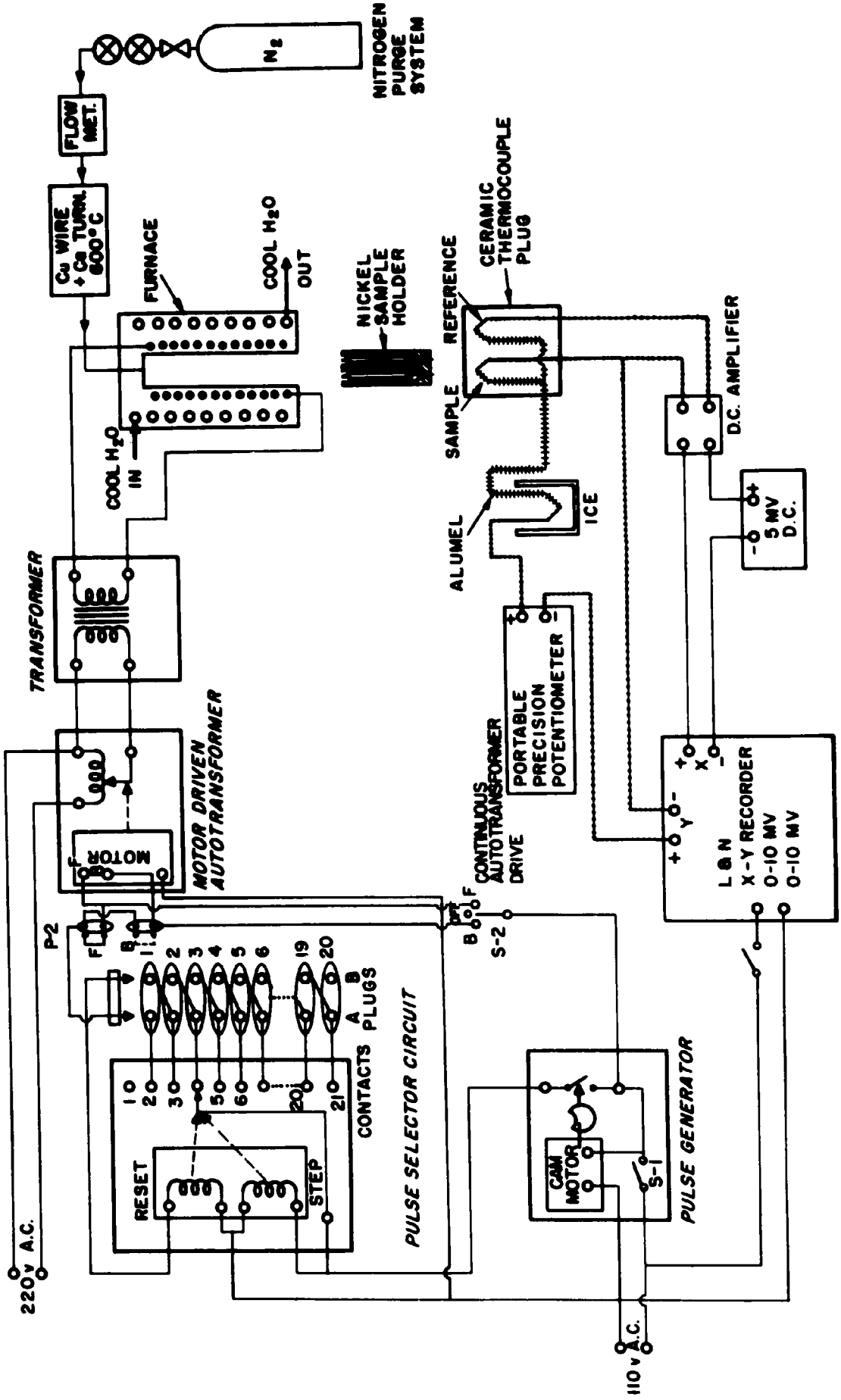


Figure 41. Differential Thermal Analysis Measuring System.

APPENDIX III

CHEMICAL ANALYSIS

The development of a quantitative chemical analysis scheme for ternary compounds containing silver, indium, and tellurium or cadmium, indium, and tellurium was complicated by co-precipitation of the elements and interference from the reagents used in the analysis.

The initial investigation was centered on the system Cd-In-Te, in particular, the composition $CdIn_2Te_4$. After dissolving the compound in nitric acid and removing the nitric acid with a hot water bath, the tellurium was slowly precipitated with sulfur dioxide over a period of about 2 days. The precipitate was washed with ether and dried in vacuum at $50^{\circ}C$. The use of hydrochloric acid to dissolve the tellurium-containing compound was avoided since the recovery of indium in subsequent steps would not have been possible.

Three methods for the analysis of indium were evaluated: titration with ethylenediaminetetraacetic acid, precipitation with a complex salt, and precipitation of the hydroxide Schwarzenbach[40] describes the direct titration of indium with ethylenediaminetetraacetic acid and Eriochrome Black T. In the presence of cadmium, a masking agent, such as KCN, must be added. After titration of the indium, the cadmium is demasked with formaldehyde and titrated. When the analysis was tried on a solution of indium and cadmium after removal of tellurium, there was difficulty in interpreting the color end point.

Hexa-amino-cobalt (III) chloride, $(Co(NH_3)\ Cl_3$, Ishimori,[41] was used to precipitate indium as $Co(NH_3)_6InCl_6$ from a solution containing cadmium, indium, and tellurium. Either because of the solubility of the complex salt or interference from the elements, cadmium or tellurium, the recovery was not quantitative.

The precipitation of $In(OH)_3$ with ammonia and drying of the precipitate at $600^{\circ}C$ in air to form In_2O_3 proved to be quantitative and compatible with the analysis methods for the cadmium and tellurium.

After the removal of tellurium with sulfur dioxide and indium with ammonia, the cadmium remaining in solution was precipitated with 8-hydroxyquinoline (oxine). The cadmium oxine precipitate was dried under vacuum at 40°C and weighed. This method of cadmium analysis is described by Willard and Diehl.[42]

In the case of the silver-indium-tellurium ternary system, it was found that the silver and tellurium co-precipitate from solution when treated with sulfur dioxide. The indium was then precipitated as $In(OH)_3$ with ammonia and weighed as In_2O_3 after air drying at 600°C. This single element analysis method proved adequate since the assumption was made that the composition analyzed was in the pseudo-binary system of Ag_2Te-In_2Te_3. Knowing the per cent of indium in the composition, the weight of In_2Te_3 is also known and the Ag_2Te can be obtained by difference.

APPENDIX IV

ELECTRICAL CONTACTS

Before any electrical measurements can be made on a semiconductor it is necessary to obtain ohmic contacts. This proved to be one of the most troublesome problems in the early work on the ternary compounds. Starting with room temperature measurements on $HgIn_2Te_4$, $CdIn_2Te_4$, and $CdIn_2Se_4$, a simple pressure contact device of phosphor bronze was tried for the current supply and point contacts of tungsten for resistivity probes. In some cases rectification was observed and there was uncertainty about contact potentials which could lead to erroneous results. Soldered contacts using an indium-tin alloy were next used. These contacts were adequate for room temperature measurements, but the low melting point of the solder limited the useful temperature range.

Since the intrinsic properties of these ternary compounds were of primary interest, it was necessary to obtain electrical measurements well above room temperature. Various nickel and gold platings were applied to the semiconductors and measurements were made with tungsten probes in a silicon oil bath. However, in some cases, on heating to 200° C it was found that the plating diffused into the sample and altered the electrical conductivity substantially.

A pressure contact device would have been sufficient for the high temperature measurements if the materials being investigated had electrical conductivities in the range of 0.1 mho/cm. at room temperature. This was not the case for most of the ternary compounds investigated, so that the use of platinum wires seemed to be the only choice. A short length of either 30 or 32 gauge platinum wire in the form of a hairpin was heated with an electric current and pressed against the surface of the semiconductor to form a bond. This worked very well for the compounds $AgIn_3Te_5$ and $Ag_2In_8Se_{13}$ with melting points of 698° C and 815° C, respectively. But, for the compound $CdIn_2Se_4$, which melts around 915° C, the thermal shock resulted in repeated fracturing of the contacts.

APPENDIX V

MEASUREMENTS OF HALL EFFECT, ELECTRICAL CONDUCTIVITY, AND SEEBECK COEFFICIENT

Electrical Circuit

Electrical conductivity and Hall effect measurements were carried out by the conventional direct current techniques described by Lindberg.[21] The direct current was supplied by a Lambda Model 65M power supply. The current was filtered to reduce ripple by use of an 8.5 henry choke in series with a 40 μf capacitor. The desired current level through the sample was attained by placing resistors in series with the sample and in parallel with the capacitor. Switches were available for reversing the polarity of the current, the Hall probes, and the electrical conductivity probes. The potential readings were taken with a Leeds and Northrup K-2 potentiometer. A schematic diagram of the above circuitry is given in Figure 42.

The magnetic field used in the Hall effect measurements was obtained from a 2100 gauss permanent magnet. This magnet had a pole face diameter of 2-1/2 inches and a 2-3/4 inch gap. To facilitate reversing the magnetic field, the magnet was mounted on a large roller bearing, and could be rotated exactly 180 degrees without moving the sample.

The Seebeck coefficient was obtained from the differential temperature across the ends of the sample and the Seebeck voltage between the same points. The signal from the chromel-alumel differential thermocouple was fed to a Leeds and Northrup DC amplifier and then to a Leeds and Northrup Speedomax Recorder. A switching circuit was used to record the amplified Seebeck voltage across the ends of the sample and the sample temperature immediately after the recording of the temperature differential.

Electrical Samples

Rectangular blocks with approximate dimensions of 0.7 x 0.2 x 0.1 inches were cut from the zone refined ingots. After polishing with Linde B

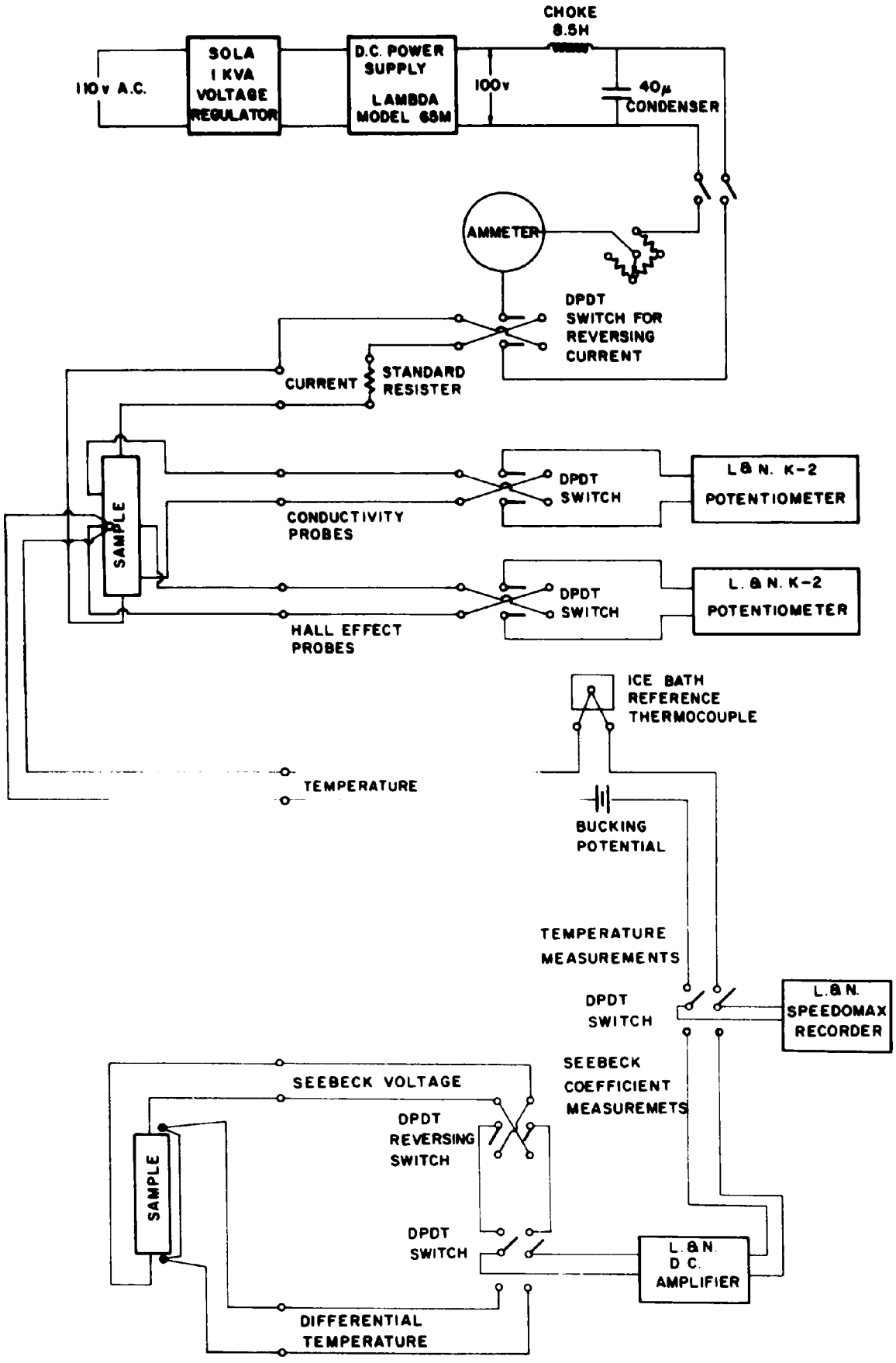


Figure 42. Electrical Circuit Used for Measuring the Electrical Conductivity, Hall Effect, and Seebeck Coefficient of the Semiconducting Compounds.

powder and etching,* the specimen was examined microscopically for the presence of a second phase. The single phase samples were then repolished and cleaned in an ultrasonic washer (Sonogen Ultrasonic Generator, Model AP10).

The dimensions of the polished electrical specimens were determined with a micrometer. The spacing of the platinum wires along the length of the sample was measured with a toolmaker's microscope. The shorting out of the Hall voltage by the current electrodes at the ends of the sample was neglected, primarily, because of the small area of the current contacts and the length-to-width ratio of the sample.

Sample Holder and Container

The sample holder and container shown in Figure 43 were used in the temperature range of 20°C to 850°C. The sample holder was machined from Lava (hydrous aluminum silicate, American Lava Corporation, Chattanooga 5, Tennessee) and baked at 1000°C. Electrical contact was made to the sample by fusing hot 30 or 32 gauge platinum wire to the surface, as discussed in Appendix IV. A 30 gauge chromel-alumel differential thermocouple was placed at the ends of the sample.

The sample holder was mounted on a fired Lava (lavite) platform with stainless steel screws. Directly over the center of the sample was a molybdenum tube containing a 30 gauge chromel-alumel thermocouple. This was used to provide a continuous recording of the sample temperature.

A 2-1/2 inch long copper shield was placed over the sample holder while a solid copper rod with a heater mounted on it was connected to the lower end of this shield. The heater was made of a threaded piece of lavite which was wrapped with 28 gauge chromel heating

*The etch was made by mixing the following ingredients: 33 ml. glacial acetic acid; 23 ml. concentrated hydrochloric acid; 5 ml. concentrated sulfuric acid; 3 ml. concentrated nitric acid; 7 ml. chromic acid solution (33 gm. CrO_3 per 100 ml. water); and 29 ml. of cupric chloride solution (15 gm. $CuCl_2$ per 100 ml. water).

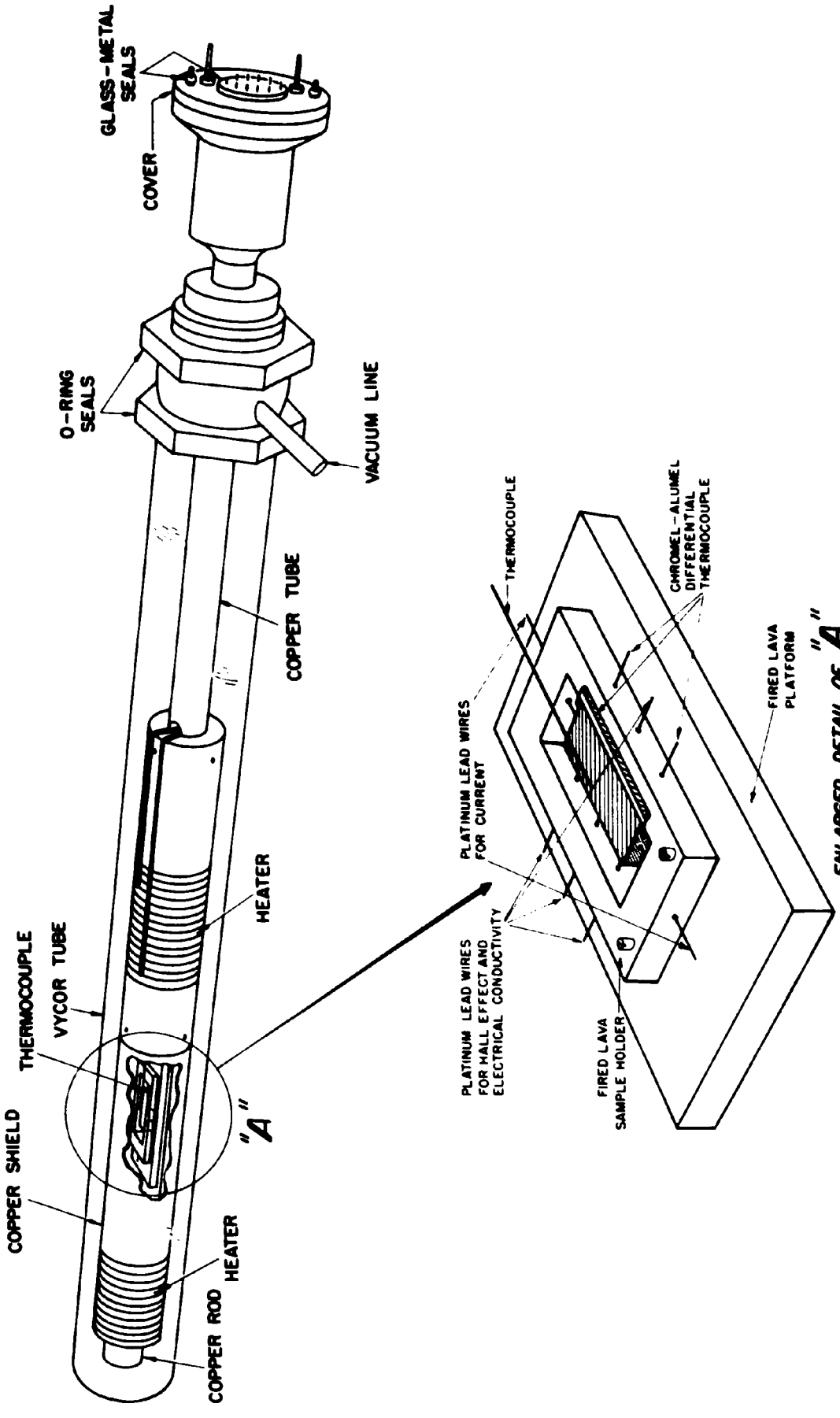


Figure 43. Sample Holder and Measuring System for the Determination of the Electrical Conductivity, Hall Effect, and Seebeck Coefficient of the Semiconducting Compounds.

wire. The large mass of copper as represented by the solid copper rod was used to damp out temperature fluctuations.

Connected to the top end of the copper shield was a 1/2-inch copper tube with a copper spacer and a lavite heater similar to the lower heater. A lavite spacer prevents heat conduction up the copper tube. A Vycor tube encloses the sample and supporting apparatus. This tube was wrapped with Pyrex wool to reduce heat losses. The open end of the Vycor tube was sealed by means of "O" ring seals to a mounting coupling. The 1/2-inch copper tube passes through this coupling by means of seals which allow the vertical positioning of the sample directly between the poles of the magnet. An outlet from the coupling leads to a pressure gauge, a vacuum system, and the hydrogen and argon supply. The samples were measured under either a hydrogen or argon (99.995%) atmosphere. Oxygen is removed from the hydrogen by passing it through a "Deoxo" catalyst. The water vapor in the hydrogen was removed with molecular sieves in the earlier measurements and with a liquid nitrogen cold trap for the later measurements. The argon is passed through a dry ice cold trap before entering the measuring system.

Measuring Procedures

Hall Effect

The direct current method of measuring the Hall effect requires four readings. The order of measurements is: (1) positive current and positive field directions; (2) negative current and positive field directions; (3) positive current and negative field directions; (4) negative current and negative field directions. The four readings usually required 90 seconds. The current was kept in the positive direction except for the short interval when readings (2) and (4) were taken. This stabilized the contribution from Peltier heating so that its effect can be eliminated in the calculations. A continuous reading of the sample temperature was obtained on a Speedomax recorder during the time the Hall data were taken. The temperature variation was less than 0.3° C.

If the voltage readings are designated as V(I+, H+), where the first term in the parentheses indicates the positive direction for the current and the second term is the magnetic field in the positive direction, then the Hall voltage is

$$V_H = \frac{V(I+, H+) - V(I+, H-) + V(I-, H-) - V(I-, H+)}{4}$$

Lindberg[21] shows that this method eliminates all the thermomagnetic effects except the Ettingshausen effect, which is usually small and can be neglected.

Electrical Conductivity and Seebeck Coefficient

The sample holder must be moved out of the magnetic field for the electrical conductivity and Seebeck coefficient readings. The electrical conductivity is measured in the positive and negative current directions at each temperature. By averaging the two values, the Seebeck potential caused by a temperature gradient along the sample is eliminated. The Seebeck coefficient is measured after stabilizing the temperature differential between the ends of the sample at about $2^{\circ}C$.

Type of Current Carrier

The carrier type of the semiconducting compounds was checked in at least one of three ways. For materials with an electrical conductivity greater than about 0.01 mho/cm., the standard hot probe method was used at room temperature. When thermoelectric measurements were made, the type of carriers was determined simultaneously. Hall effect measurements also provided information on the carrier type.

Sample Calculations

Calculation of the Hall Coefficient

The Hall coefficient is calculated from the formula

$$(40)\quad R_H = \frac{t}{10^{-8} I H}\left[\frac{V(I+, H+)-V(I+, H-)+V(I-, H-)-V(I-, H+)}{4}\right]$$

where R_H is the Hall coefficient in $cm.^3$/coulomb, t is the sample thickness in cm., I is the sample current in milliamperes, H is the magnetic field strength in gauss, and V(I+, H+), V(I+, H-), V(I-, H-), and V(I-, H+) are the Hall voltage readings in millivolts.

The calculation is illustrated with the data from $Ag_2In_8Se_{13}$, sample number 215(2B), at 358.0°C.

I = 8.01 ma.	V(I+, H+) = -8.132 mv.
t = 0.205 cm.	V(I+, H-) = -7.675 mv.
H = 2100 gauss	V(I-, H-) = +7.621 mv
	V(I-, H+) = +8.099 mv.

$$R_H = \frac{0.205 \text{ cm.}\left[-8.132-(-7.675)+(+7.621)-(8.099)\right]\text{mv.}}{10^{-8}\,(8.01 \text{ ma.})\,(2100 \text{ gauss})\,(4)}$$

$$R_H = 285 \text{ cm.}^3/\text{coulomb}$$

The IBM 709 computer was used to calculate the Hall coefficient, the reciprocal absolute temperature and $RT^{3/2}$. The energy gap obtained from the $RT^{3/2}$ vs. 1/T data was calculated by a least squares analysis.

Calculation of the Electrical Conductivity

The electrical conductivity σ was computed by means of the formula

$$(41)\quad \sigma = \frac{I\ell}{w\,t}\left[\frac{2}{V_+ + V_-}\right]$$

where I is the current in milliamperes, ℓ is the distance between the conductivity probes, w is the sample width t is the sample thickness, and V_+ and V_- are the potential drops in millivolts across the probes with the current in the positive and negative directions, respectively.

The calculation is illustrated with the data from $Ag_2In_8Se_{13}$

sample number 215 (2B), at 359.2°C.

$I = 0.970$ ma $\qquad V_+ = 80.40$ mv.

$w = 0.513$ cm. $\qquad V_- = 80.69$ mv.

$t = 0.205$ cm.

$\ell = 1.283$ cm.

$$\sigma = \frac{(0.970 \text{ ma.})\ (1.283 \text{ cm.})}{(0.513 \text{ cm.})\ (0.205 \text{ cm.})} \left[\frac{2}{80.40 + 80.69}\right] \frac{1}{\text{mv.}}$$

$$\sigma = 0.147 \text{ mho/cm.}$$

The IBM 709 computer was used to calculate the electrical conductivity, the natural logarithm of the electrical conductivity, and the reciprocal absolute temperature. These results were then used to plot the temperature dependence of the electrical conductivity and to determine the energy gap by a least squares analysis.

Calculation of the Seebeck Coefficient

The Seebeck coefficient, α, was calculated from the measurements of the potential difference across the ends of the sample and the temperature difference which was obtained with a chromel-alumel differential thermocouple.

The following measurements were made on $Ag_2In_8Se_{13}$, number 211 (1A), at 216.2°C:

temperature difference = 0.092 mv. = 2.30°C

potential difference = 2450 μv.

Seebeck coefficient = $\frac{2450\ \mu\text{v.}}{2.30^\circ\text{C}}$ = 1065 μv./°C

APPENDIX VI

THERMAL CONDUCTIVITY

A dynamic calorimeter described by LaBotz[23] was used to measure the thermal conductivity of the semiconducting compounds. This method uses a constant power source placed on one side of the sample and the energy which flows through the sample is collected by a sink on the opposite side of the sample block. Measurements of the heat flow into the copper sink and the temperature gradient across the sample permit the calculation of the sample thermal conductivity. The theory associated with the calculations has been explained by LaBotz.[23]

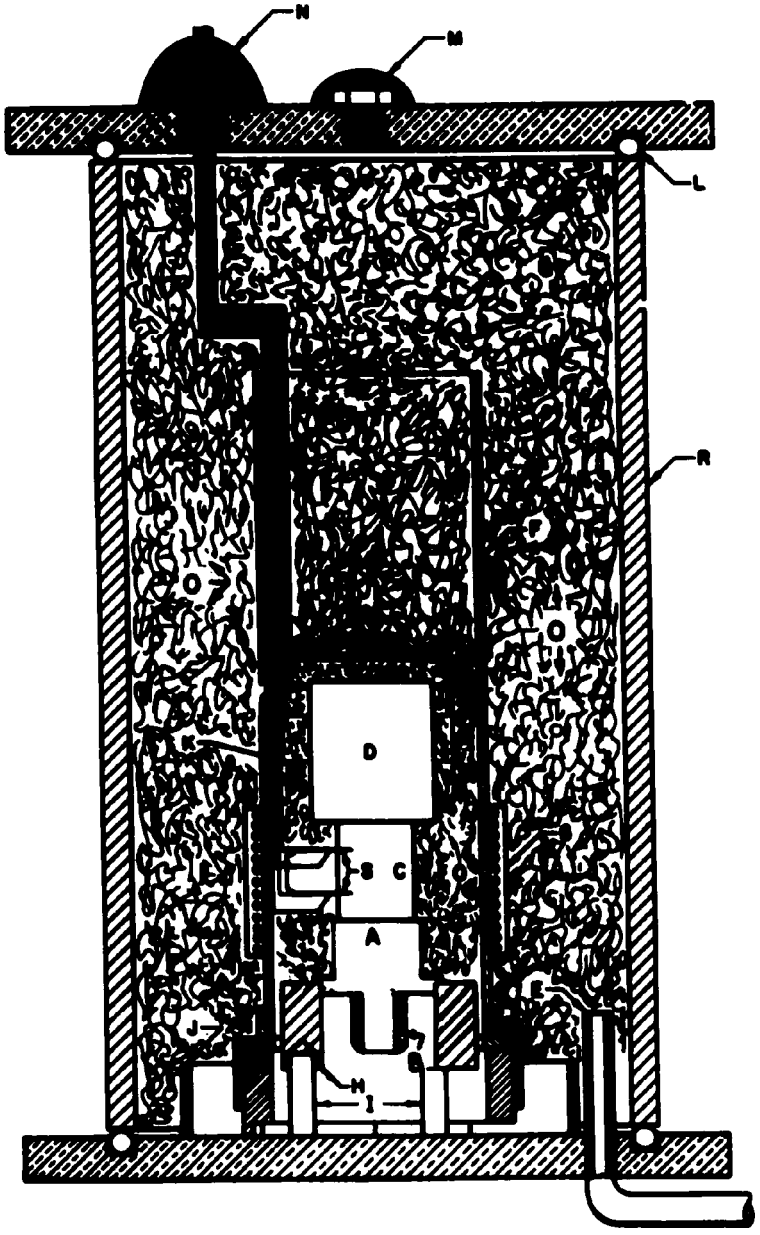
Description of Equipment

A sketch of the thermal conductivity apparatus is shown in Figure 44. The source rests on a lavite disc, which in turn rests loosely on three steel rods supported by the brass base. The sink, sample, and source are held tightly together by two 30 gauge (.010" dia.) chromel wires, which loop over the sink and under the lavite supporting disc. This insures good contact between the three elements and also removes the possibility that the sink may be jarred off the sample. The sample and sink are enclosed in Pyrex wool.

The source-sample-sink combination is enclosed in a radiation shield made from a 2" diameter copper tube. The tube fits into a silver-plated steel disc which in turn is kept from contacting the bottom brass plate by a lavite disc. The shield extends from slightly below the source to about 4 inches above the top of the sink. The shield is covered inside and out with aluminum foil.

The shield in turn is contained in a 4.5 inch diameter glass cylinder, which has "O" ring seals to both the bottom and top brass plates. The space between the glass cylinder and radiation shield is completely filled with Pyrex wool.

The power leads to the source and shield heaters pass through the bottom plate by means of hermetically sealed connectors. The



Key

A - Source block
B - Source heater
C - Sample
D - Sink
E - Vacuum Line
F - Shield
G - Shield heater
H - Lavite source support
I - Steel rods supporting "H"
J - Shield to prevent liquid N_2 from contacting glass
K - Shield control differential thermocouple
L - "O" ring seal
M - Port for pouring in liquid N_2 - sealed with Apiezon wax
N - Thermocouple port sealed with Apiezon wax
O - Pyrex wool

R - glass cylinder
S - Sample differential thermocouple and Seebeck probes

Figure 44. Equipment Used for Measuring Thermal Conductivity.

vacuum lead also passes through the bottom plate, and is located between the glass cylinder and the copper shield.

All thermocouple leads pass through the top plate where they are sealed by means of Apiezon sealing wax. Permanent hermetically sealed connectors were not used because the system must be dismantled each time the sample is changed. The large number of leads would make permanent hermetic seals impractical. In addition, the possibility of spurious thermal emfs arising as a result of the intermediate metal to metal contact is eliminated.

The measurement and control circuits are shown schematically in Figure 45. The temperature of the sink is measured using a 30 gauge chromel-alumel thermocouple with an ice-water reference junction. A Leeds and Northrup potentiometer is placed in series with the thermocouple output, such that a bucking potential can be placed in the circuit. The thermocouple output less the bucking potential is fed through a Leeds and Northrup D.C. amplifier into a Wheelco recorder with a 0-10 millivolt range. The use of the D.C. amplifier makes possible accurate slope determinations over a range of heating rates. In ordinary operation an amplification of 10 is used, but amplifications of 5 or 20 are also used rather frequently.

A 40 gauge (.003" dia.) chromel-alumel differential thermocouple is used to measure the temperature drop across the sample. The junction of the couple is placed in .020" diameter holes drilled into the sample by means of an ultrasonic cutter. The output of the couple is connected to a Leeds and Northrup D.C. amplifier. The amplifier output passes through a gold contact relay and into a Leeds and Northrup Speedomax Recorder. The Seebeck voltage is also passed through the relay and into the Speedomax. The input to the recorder is switched automatically from the Seebeck voltage to the differential thermocouple output and vice versa every 20 seconds by means of a timer which controls the gold contact relay.

The differential thermocouples are made from bare chromel and

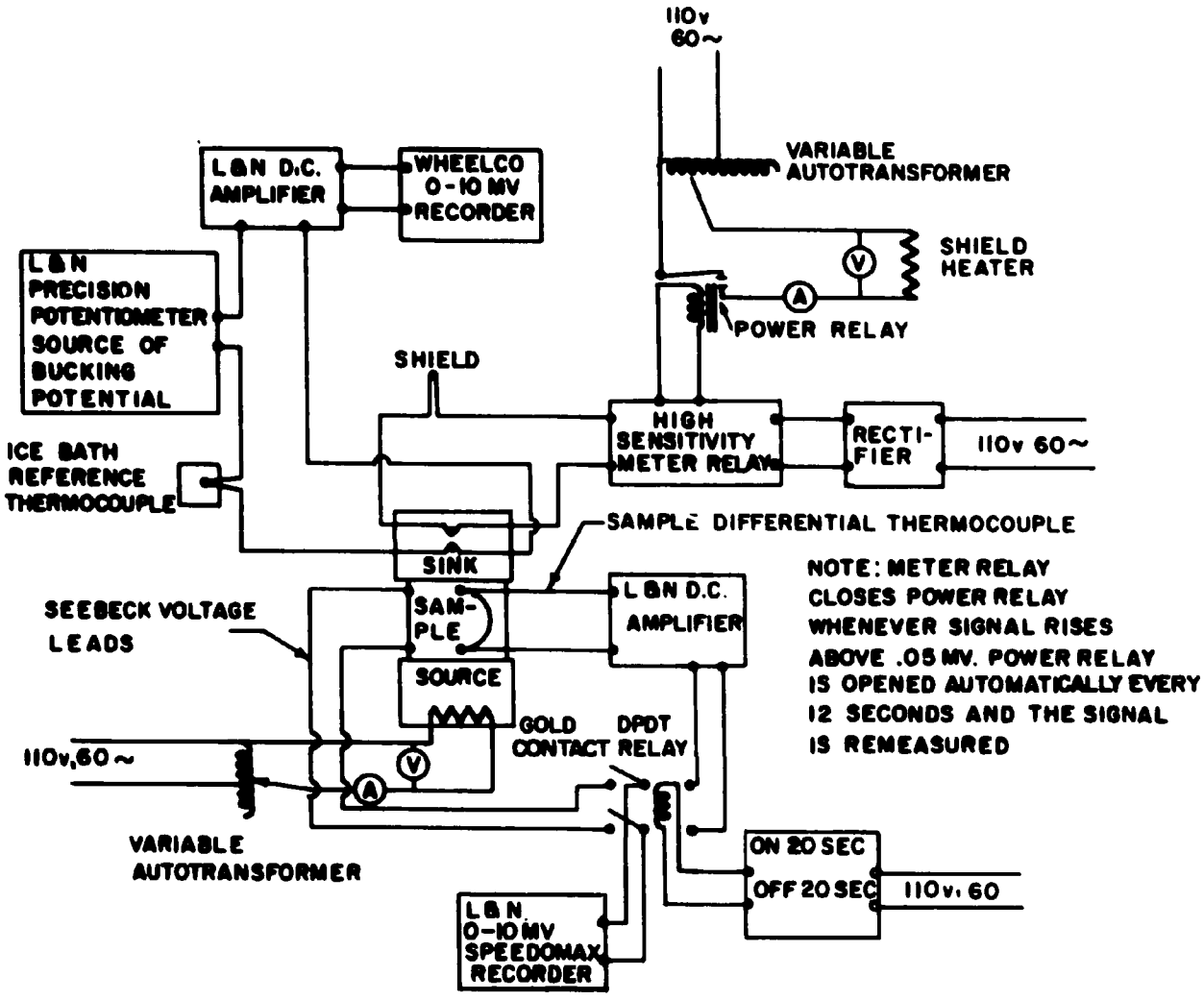


Figure 45. Measurement and Control Circuits for the Thermal Conductivity Apparatus.

alumel wire, calibrated by the manufacturer. As the junctions are inserted into holes in the sample the wires have to be insulated from the sample and from each other. By drawing the wire through a bead of molten borax glass ($Na_2B_4O_7$) and then quickly through a flame it is possible to deposit a thin, tough, high resistance film on the wires. When examined under a microscope this film appears to be approximately .0003" thick, has a brownish color, and does not break or crack when the wire is bent. The resistance of this coating is approximately 700,000 ohms at room temperature. If allowed to set in the air for several weeks a white powder forms on the coating, probably due to the formation of one of the hydrates of sodium tetraborate. Because of this the thermocouples are used immediately after they are made.

Thermocouples made in this way work rather well. Several of the thermocouples were checked using boiling water and ice water junctions and were on calibration. In addition to this they gave accurate results to above 400°C when used in checking the thermal conductivity of Inconel.

The temperature control on the radiation shield is achieved by means of 30 gauge copper-constantan differential thermocouple. One junction of the thermocouple is embedded in the sink and the other junction rests against the radiation shield directly adjacent to the sink. The output of this thermocouple activates a very highly sensitive meter relay. Whenever the output of this differential thermocouple rises above .05 mv (a Δ T of approximately 1°C) the shield heater is switched off by the meter relay. Whenever the signal drops below .05 mv the heater power is turned back on. The magnitude of the shield heater power is controlled by use of a powerstat.

Calibration and Operation

The instrument was checked by measuring the thermal conductivity of Armco iron, Inconel and fused SiO_2, the thermal conductivities of which have been rather firmly established by experimental

measurements and reported in the literature. The measured values cover a range from . 170 to . 0033 gm cal/cm sec ^{o}K, a range of a factor of 50.

Armco iron has a thermal conductivity which decreases with rising temperature, that of Inconel increases slowly with temperature, while that of fused SiO_2 is nearly constant. The instrument was able to detect all types of temperature dependence.

There is a two-fold limitation on the upper temperature which can be attained by the instrument. The actual value of this limit for any given sample depends upon the sample geometry and its thermal conductivity. As the rate of heat exchange between the sink and its surroundings increases with temperature due to increased radiation effects, the error introduced by this heat leak also usually increases with rising temperature. The temperature at which this spurious heat leak becomes sizeable relative to the total amount of heat passing from the sample to the sink is a function of the cross section, length, and thermal conductivity of the sample. In other words, when a large amount of heat is passing from the sample into the sink, the amount of heat exchanged between the sink and the surroundings does not reach significant proportions until a high measuring temperature is reached.

A second limitation on the maximum temperature is placed by the vacuum seals. The sealing method employed is satisfactory until the temperature of the seals reaches about 100-150^{o}C. When a sample with a low thermal conductivity or small cross section is measured, a heating rate of 1 to 2^{o}C/minute is generally used. With this low heating rate the seal temperature reaches its limit when the sample temperature is slightly above 300^{o}C. However, for material with a high thermal conductivity or samples with a large cross section heating rates to 3 to 4^{o}C/minute can be used. Under these conditions the sample temperature may be over 400^{o}C before the vacuum seals reach their limiting temperature.

In order to make measurements from $0^{\circ}C$, it was necessary to cool the instrument far enough below $0^{\circ}C$ so that "steady state" conditions could be attained by the time the sample had reached $0^{\circ}C$. This precooling was performed simply by pouring liquid nitrogen into an open port in the top cover plate. In a few instances it appeared as though there was frost formation within the instrument. This was indicated by a rise in the temperature gradient across the sample and a drop in the sink heating rate from slightly below to slightly above $0^{\circ}C$. The apparent cause of this was the melting of frost on the sink.

Good thermal contact between the sink, sample and source was achieved by placing a thin layer of silicone grease impregnated with copper between the contacting surfaces. * This material had both a high thermal conductivity and a high electrical resistivity.

The samples of $Ag_2In_8Se_{13}$ and $AgIn_5Te_8$ were run under the same conditions as the fused silica. The heating rate varied from about $1.2^{\circ}C$ to $2.4^{\circ}C$ per minute, while the temperature drop across the sample ranged from about $10^{\circ}C$ to $20^{\circ}C$. The vacuum obtained was generally about 1 mm. of mercury or better. Measurements were made up to $310^{\circ}C$, which was felt to be a conservative estimate of the upper limit of reliability for the samples being measured.

Seebeck coefficient data was taken on only one sample and was found to be in general agreement with the values obtained in the electrical measuring system. The high resistivity of the silver ternary compounds made it necessary to fuse hot platinum wires to the samples in order to measure the Seebeck potential. Since the wires were easily broken and significant Seebeck data could only be obtained above about $200^{\circ}C$ where contact resistance problems are no longer present, the Seebeck coefficient was measured on only one sample ($Ag_2In_8Se_{13}$) in the thermal conductivity apparatus.

---

*"Thermocopper Grease, "obtained from I. T. T. Laboratories, 3700 East Pontiac Street, Fort Wayne, Indiana.

Sample Calculation of Thermal Conductivity

The thermal conductivity, λ_{th}, is given by the equation

$$(42) \quad \lambda_{th} = \frac{LR}{A\Delta T}\left\{m_c C_{p_c} + (m_s C_{p_s}/2)\right\}$$

where L = distance between thermocouple junctions in the test sample, cm.

A = cross sectional area of the test sample, $cm.^2$

R = rate of temperature rise of the test sample, $^{\circ}C/sec.$

T = temperature difference between the thermocouples in the test sample, $^{\circ}C$

m_c = mass of the heat sink, gm.

C_{p_c} = specific heat of the copper heat sink, $gm.\,cal./^{\circ}C$

m_s = sample mass, gm.

C_{p_s} = specific heat of the sample, $gm.\,cal./^{\circ}C$

In the case of $AgIn_3Te_5$, sample number 206, the following data was taken on test run number 1 when the sample temperature was between $99^{\circ}C$ and $120^{\circ}C$:

$L = 0.975$ cm

$R = 0.0307^{\circ}C/sec.$

$A = 1.80\ cm.^2$

$\Delta T = 15.6^{\circ}C$

$m_c = 17.29$ gm.

$C_{p_c} = 0.0963\ gm.\,cal./^{\circ}C$

$m_s = 15.05$ gm.

$C_{p_s} = 0.0495\ gm.\,cal./^{\circ}C$

$$\lambda_{th} = \frac{0.975(0.0307)}{1.80(15.6)}\left\{17.29(0.0963) + 15.05(0.0495)/2\right\}$$

$$\lambda_{th} = 0.00216\ gm.\,cal./cm.\,sec.\ ^{\circ}C$$

$$\lambda_{th} = 0.00905\ watts/cm.\ ^{\circ}C$$

BIBLIOGRAPHY

1. Hahn, H., Frank, G., Klingler, W., Meyer, A. D., Storger, G., Z. Anorg. u. allgem. chem., 271, 153-170 (1953).
2. Hahn, H., Frank, G., Klingler, W., Storger, A-D., Storger, G., Z. Anorg. u. allgem. chem., 279, 241-250 (1955).
3. Mooser, E. and Pearson, W., J. Electronics, 1, 629-645 (1956).
4. Rhines, F. N., Phase Diagrams in Metallurgy. McGraw-Hill Book Company, New York, 193-203 (1956).
5. Pfann, W. G., Zone Melting. John Wiley and Company, New York (1958).
6. Mason, D. R. and Cook, J. S., J. Appl. Physics, 32, 475-477 (1961).
7. Simon, R., Symposium on Thermoelectric Power Conversion, Dallas, Texas (January 1961).
8. Woolley, J. C., Ray, B., J. Phys. Chem. Solids, 15, 27-32 (1960).
9. Woolley, J. C., Private Communication to D. R. Mason.
10. Thomassen, L., Mason, D. R., J. Electrochem. Soc., 106, 206c, (Abstract), (1959).
11. Busch, G., Mooser, E., Pearson, W., Helv. Phys. Acta, 29, 192-193 (1956).
12. Busch, G., Junod P., Mooser, E., Schade, H., in Halbleiter und Phosphore, edited by M. Schon and H. Welker, Friedr. Vieweg, Braunschweig, 470-473 (1958).
13. Peters, C. W., Private Communication Reported by Mason and O'Kane.[20]
14. Edwards, D. F., O'Kane, D. F., Bull. Am. Phys. Soc., Series II, 5, 78 (1960).
15. Hall, R. N., Private Communication Reported by Mason and O'Kane.[20]
16. Newman, R., Private Communication Reported by Mason and O'Kane.[20]
17. Kolomiets, B. T., Mal'Kova, A. A., Soviet Physics, Solid State, Suppl. II, 32-38 (1959).
18. Austin, I., Goodman, C., Pengelly, A., J. Electrochem. Soc., 103, 609-610 (1956).

19. Zhuze, V. P., Sergeeva, V. M., Shtrum, E. L., Soviet Physics-Technical Physics, 3, 1925-1938 (1958).

20. Mason, D. R., O'Kane, D. F., Proceedings of the International Conference on Semiconductor Physics, Prague (1960), Publishing House of the Czechoslovak Academy of Sciences, Prague (1961), pp. 1026-1031.

21. Lindberg, O., Proc. I. R. E., 40, 1414-1419 (1952).

22. Putley, E. H., The Hall Effect and Related Phenomena, Butterworths and Company, London (1960).

23. LaBotz, R. J., Thermoelectric Properties of the Pseudo-binary System Mg_2Si-Mg_2Ge, Ph. D. Thesis, University of Michigan (1961).

24. Smith, R. A., Semiconductors, Cambridge University Press, London (1959).

25. Johnson, V. A., Lark-Horovitz, K., Physical Review, 92, 226-232 (1953).

26. Ioffe, A. F., Semiconductor Thermoelements and Thermoelectric Cooling, Infosearch, Ltd., London (1957).

27. Ioffe, A. V., Ioffe, A. F., Izv. Akad. Nauk. SSSR, 20, 65 (1956).

28. Hozak, N. L., Cook, J. S., Mason, D. R., J. Electrochem. Soc., 108, 105-106 (1961).

29. Miyazawa, H., Sugaike, S., J. Phys. Soc. Japan, 12, 312 (1957).

30. Hahn, H., Angew. Chemie, 65, 538 (1953).

31. Semiletov, S. A., Soviet Physics-Solid State, 3, 544-548 (1961).

32. Woolley, J. C., Pamplin, B. R., J. Electrochem. Soc., 108, 874-879 (1961).

33. Zhuze, V. P., Sergeeva, V. M., Shelykh, A. I., Soviet Physics-Solid State, 2, 2545-2555 (1961).

34. Davis, P., Shilliday, T., Physical Review, 118 (1960), 1020-1022.

35. Zaslavskii, A. I., Sergeeva, V. M., Smirnov, I. A., Soviet Physics - Solid State, 2, 2565-2572 (1961).

36. Hansen, M., Constitution of Binary Alloys, McGraw-Hill Book Company, New York (1958).

37. Grochowski, E. G., Mason, D. R., Electrochem. Soc., Electronics Division Abstracts, 10, 100 (1961).

38. Denning, R. M., Private Communication to D. R. Mason.

39. Brice, J. C., Newman, P. C., Wright, H. C., Brit. J. Appl. Physics, 9, 110-111 (1958).

40. Schwarzenbach, G., Complexometric Titrations, Interscience Publishers, New York (1957).

41. Ishimori, T., Ueno, K., Jap. Analyst, 5, 329-331 (1956).

42. Willard, H., Diehl, H., Advanced Quantitative Analysis, D. Van Nostrand Company (1943).